AD-A214 296

Oxygen and Other Atmospheric Gases

W. A. Chupka
S. D. Colson
E. E. Eyler

Yale University
Department of Chemistry
New Haven, CT 06511

27 February 1989

Final Report
15 September 1986-30 September 1988

APPROVED FOR PUBLIC RELEASE; DISTRIBUTION UNLIMITED

AIR FORCE GEOPHYSICS LABORATORY
AIR FORCE SYSTEMS COMMAND
UNITED STATES AIR FORCE
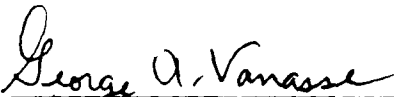HANSCOM AIR FORCE BASE, MASSACHUSETTS 01731-5000

DTIC
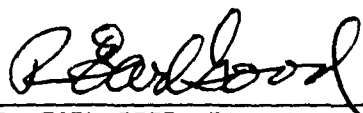ELECTE
NOV 13 1989
S
B
D

89 11 09 015

"This technical report has been reviewed and is approved for publication"

Laila Dzelzkalns
LAILA S. DZELZKALNS
Contract Manager
Infrared Physics Branch
Optical/Infrared Technology Div.

George A. Vanasse
GEORGE A. VANASSE, Chief
Infrared Physics Branch
Optical/Infrared Technology Div.

R. Earl Good
R. EARL GOOD, Director
Optical/Infrared Technology Division

REPORT DOCUMENTATION PAGE

1a. REPORT SECURITY CLASSIFICATION			1b. RESTRICTIVE MARKINGS		
Unclassified					

2a. SECURITY CLASSIFICATION AUTHORITY		3. DISTRIBUTION/AVAILABILITY OF REPORT
2b. DECLASSIFICATION/DOWNGRADING SCHEDULE		Approved for public release; Distribution unlimited

4. PERFORMING ORGANIZATION REPORT NUMBER(S)	5. MONITORING ORGANIZATION REPORT NUMBER(S)
	AFGL-TR-89-0064

6a. NAME OF PERFORMING ORGANIZATION	6b. OFFICE SYMBOL (If applicable)	7a. NAME OF MONITORING ORGANIZATION
Yale University		Air Force Geophysics Laboratory

6c. ADDRESS (City, State, and ZIP Code)	7b. ADDRESS (City, State, and ZIP Code)
Department of Chemistry New Haven, CT 06511	Hanscom AFB Massachusetts 01731-5000

8a. NAME OF FUNDING/SPONSORING ORGANIZATION	8b. OFFICE SYMBOL (If applicable)	9. PROCUREMENT INSTRUMENT IDENTIFICATION NUMBER
		F19628-86-C-0214

8c. ADDRESS (City, State, and ZIP Code)	10. SOURCE OF FUNDING NUMBERS			
	PROGRAM ELEMENT NO.	PROJECT NO.	TASK NO.	WORK UNIT ACCESSION NO.
	61102F	2310	G4	BQ

11. TITLE (Include Security Classification)

Oxygen and Other Atmospheric Gases

12. PERSONAL AUTHOR(S)
W. A. Chupka; S. D. Colson; E.E. Eyler

13a. TYPE OF REPORT	13b. TIME COVERED	14. DATE OF REPORT (Year, Month, Day)	15. PAGE COUNT
FINAL	FROM 9/15/86 TO 9/30/88	1989 February 27	128

16. SUPPLEMENTARY NOTATION

17. COSATI CODES			18. SUBJECT TERMS (Continue on reverse if necessary and identify by block number)
FIELD	GROUP	SUB-GROUP	Oxygen Multiphoton Spectroscopy
			Rydberg States Photoelectron Spectroscopy
			Laser Spectroscopy Photoionization Shape Resonances

19. ABSTRACT (Continue on reverse if necessary and identify by block number)

Laser multiphoton, mass and photoelectron spectroscopy has been used to investigate the energy level structure and photophysics of oxygen and other atmospheric gases. Particular emphasis was placed on determining the location, predissociation and photoionization processes of the previously unknown lower ns and nd gerade Rydberg states and their interactions with valence states. A shape resonance in the ionization continuum near threshold was found to play a large role in inducing non-Franck-Condon transitions. Optimum transitions for production of vibrationally state-selected O_2^+ ions were found. The effects of dissociation continua and strongly mixed Rydberg-valence states as intermediates in multiphoton processes were demonstrated and explored.

20. DISTRIBUTION/AVAILABILITY OF ABSTRACT		21. ABSTRACT SECURITY CLASSIFICATION	
☐ UNCLASSIFIED/UNLIMITED ☐ SAME AS RPT. ☐ DTIC USERS		Unclassified	
22a. NAME OF RESPONSIBLE INDIVIDUAL		22b. TELEPHONE (Include Area Code)	22c. OFFICE SYMBOL
Laila Dzelzkalns		(617) 377-3671	AFGL/OPI

DD FORM 1473, 84 MAR

83 APR edition may be used until exhausted.
All other editions are obsolete.

CONTENT

Oxygen and Other Atmospheric Gases

W.A. Chupka, S.D. Colson and E.E. Eyler

Yale University

Final Report (May 15, 1989)

I. Introduction

The purpose of the work done under this contract can be broadly described as follows: (1) to locate and characterize previous ly unknown or very poorly known excited states of diatomic oxygen (and other important atmospheric gases), (2) to explore and elucidate the spectroscopic, photophysical and other dynamical characteristics of molecules in those states and (3) to develop methods for preparing the molecular ions as purely as possible in selected vibronic states (for subsequent studies of their reactivities as a function of internal excitation).

In spite of nearly a century of countless studies of the spectroscopy of O_2, there exist glaring gaps of understanding of its excited states as may be seen from the many questionable and even total lack of assignments in the most recent compilation of diatomic spectral data[1]. This gap is especially prominent and important below the ionization limit, and expecially above the onset of the Schumann-Runge continuum at 175nm. Thus, in contrast to the case of most common diatomic molecules, there is no spectroscopic determination of its first ionization potential, no assignment of any Rydberg series converging to that limit and even the identification of the lowest ($3s\sigma$) member of the energetically lowest Rydberg series converging to the first ionization limit was

1

inaccurate, having been done by inelastic electron scattering. This situation is due in large part to the fact that from two oxygen atoms in their lowest electron configurations, a total of 62 valence states are formed. A few of the lowest states are bound but most are repulsive, with potential curves which intersect those of the Rydberg states and interact with them to varying degrees. Some interactions are so strong as to result in adiabatic curves of mixed Rydberg-Valence character which are not readily recognizable spectroscopically. Other interactions which are weaker nevertheless produce such strong predissociation of the Rydberg state that rotational analysis is impossible and hence useless in characterizing the state. Still weaker interactions produce predissociation that severely suppresses photon emission and eliminates emission spectroscopy as a useful tool except in a very few cases. Since Rydberg-Valence interaction strength decreases as $(n*)^{-3}$, where $n*$ is the effective principal quantum number, the higher Rydberg states might seem to provide useful data. However at the necessary high values of $n*$ the absorption spectrum (for instance) is hopelessly congested by the rapidly converging and overlapping bands.

Modern techniques including the use of multiphoton ionization and multi-laser spectroscopy coupled with mass and photoelectron spectroscopy have made it possible to do experiments which can evade many of the difficulties which have thwarted classical spectroscopists. This report, together with the attached appendices, records the progress we have made in the course of this contract.

The work on O_2 in this laboratory began even before the

2

initiation date of this contract. The initial result[2,3] was the first location of the lowest Rydberg states of the O_2 molecule by an optical spectroscopic technique. These states were the v=0-4 vibrational levels of the $^3\Pi_g$ and $^1\Pi_g$ (3sσ) states which are optically forbidden by one-photon excitation from the ground $^3\Sigma_g^-$ state of O_2. Since these states were optically forbidden by classical absorption they had previously been located only by theoretical calculation[4] and by inelastic electron scattering[4,5] with some error. The electron scattering data were far too crude to provide information on the lifetime of these states. However, the spectroscopic data showed (from line width measurements and application of the uncertainty principle) that all levels were predissociated to greatly varying degrees.

Under this contract, the study of the (3sσ) Rydberg states has continued and has been extended to Rydberg states which had never been previously detected by any method, namely the 4s-3d and 5s-4d Rydberg complexes. Before continuing, we explain why, if these states are optically forbidden from the ground state of O_2 and hence do not contribute to its conventional absorption spectrum, these states are important. Firstly, these states can play a decisive role in non-optical processes such as dissociative electron-ion recombination and other physical processes occuring in the upper atmosphere and in plasmas. In fact the (3sσ) Rydberg states have been shown in recent work[6] to play the dominant role in dissociative charge exchange reactions of O_2^+ ions. This latter work depended heavily on our previous work[2,3]. An excellent review which details both theoretical and experimental approaches to the problem of dissociative recombination has been written by Bardsley

3

and Biondi[7]. A more recent theoretical treatment applied specifically to O_2 has been given by Guberman[8]. Secondly, the strength of the interaction of these Rydberg states with the repulsive valence states which are responsible for their predissociation yields a general parameter which characterizes the strength of interaction with all ns and nd Rydberg states. This latter parameter can be obtained from our linewidth measurements and the necessary analysis has been in progress. Thirdly, while these states do not contribute to ordinary optical absorption, they play a large part in the interaction of O_2 with electrons (as shown by scattering experiments[4,5]) and other particles and in the increasingly important area of non-linear interaction with intense light beams. In fact, the way we observe these states is by a two-photon resonant, three-photon ionization experiment using an intense focused laser beam.

The facts that 1) predissociation is so pervasive throughout all the excited states of O_2 and that 2) dissociative continua are so prominent in the ordinary ultra-violet absorption spectrum make it essential, for an adequate fundamental understanding of the photophysics and chemistry of O_2, that the valence states responsible for these effects be identified and the amounts of the various atomic products of these dissociative processes be determined. While the lowest energy ordinary absorption continuum(the intense Schumann-Runge continuum) has been well characterized and its products(^3P and ^1D oxygen atoms) reliably identified for sometime, very little is reliably known for optically allowed states at higher energies and nothing (until the recent charge exchange work[6] which supplemented our work) is

known experimentally of the dissociative behaviour of optically forbidden states and continua. In the course of this work, we have developed, in part, techniques to detect and identify products of dissociative processes.

A further very brief digression into the reasons for the general importance for the study of Rydberg states, especially those converging to the first ionization limit, will be useful at this point. The class of molecular states which are most intractable to both theoretical and experimental investigations are continuum states, i.e. both dissociative and ionization continua and yet these states play very important roles in the behavior of molecules at high energies (5eV) and in media where ionization occurs such as discharges, plasmas, etc. Our investigations deal with both types of continuum problems in both direct and indirect ways. We now focus on ionization continua. The onset of ionization at threshold is really a continuation of Rydberg excitations beyond $n=\infty$ (i.e. the "same channel"). The very successful Quantum Defect Theory of Seaton[9] makes explicit use of this connection, whereby the quantum defect parameter δ of bound Rydberg states [determined by fitting Rydberg state energies referred to the ionization potential to the expression $E=-Ry/(n-\delta)^2$] becomes π^{-1} times the phase shift, δ, which characterizes continuum functions. Thus the study of Rydberg states is the best and most detailed way to characterize an ionization continuum for energies within several or more eV of the ionization limit. The greater detail results from the fact that angular momenta are readily characterized for Rydberg states from the rotational structure while nearly the only way such characterization can be done from measurement of ionization

5

continua is by measuring the electron angular distribution, and even the only gives information about the superposition of several angular momentum amplitudes (a few other rarely useful techniques exist, such as polarization studies of fluorescence from excited ions and rotationally resolved photoelectron spectra). Thus Rydberg state information can be used to predict photoelectron angular distributions but the reverse cannot be done.

Similarly, one of best ways of experimentally determining the position of dissociative (repulsive) valence states, (practically the only way if the state is not optically allowed from the ground state) is by detecting its effect of predissociating Rydberg states. Again the strength of its interaction with Rydberg states can be extrapolated into the ionization continuum to give its autoionization width, but again with more information since one can say into which continua it is autoionizing. This is illustrated in figure 1.

Furthermore, the most useful and successful theoretical framework for understanding the many interactions among Rydberg states, between Rydbergs and various continua, and the continuation of these interactions into the ionization continuum in order to predict e.g. autoionization, etc. is the Multichannel Quantum Defect Theory (MQDT) developed by Fano[10] and co-workers. Again the parameters required are best obtained by the study of Rydberg states.

Thus, far from being a more-or-less routine activity of simply adding new states to molecular energy level compilations, the study of Rydberg states and their interactions with valence states is absolutely essential to understanding the behavior of atomic

6
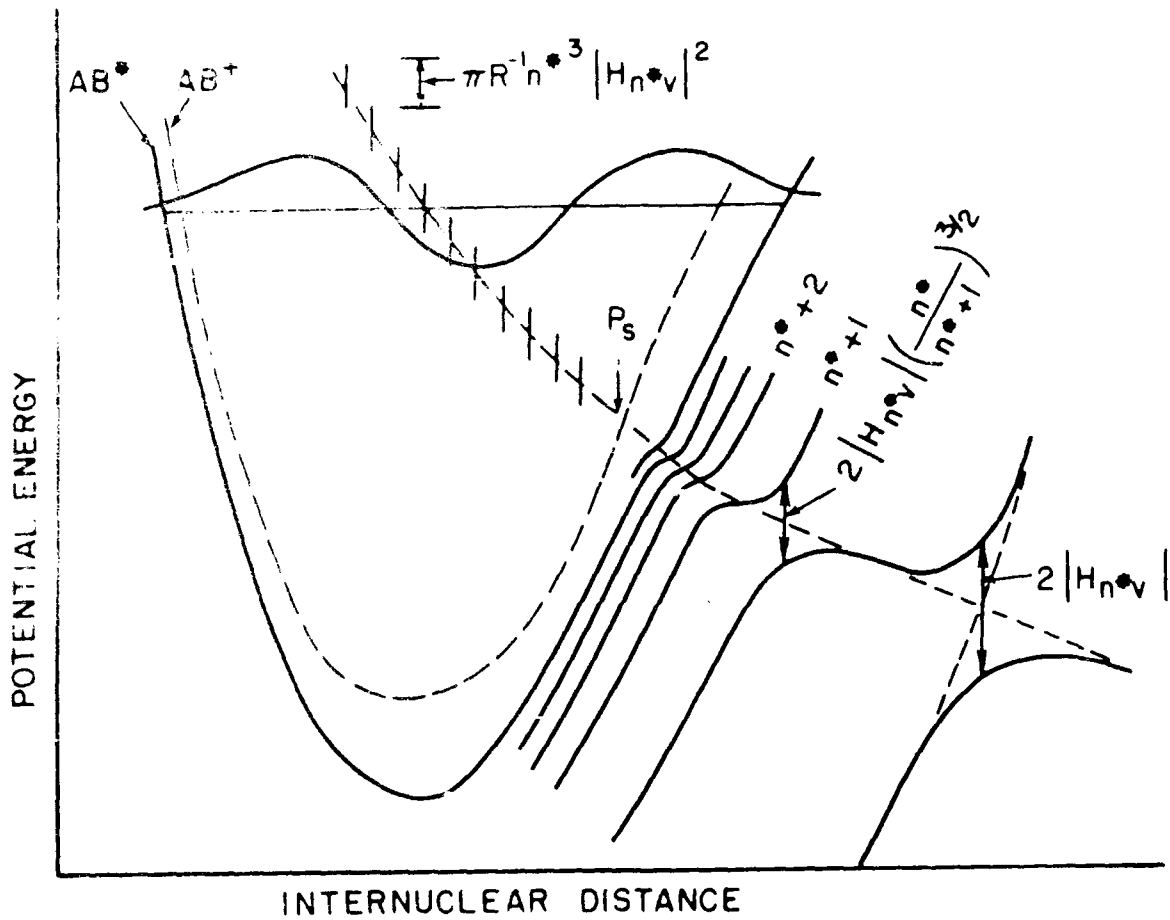
FIGURE 1. Schematic potential curves belonging to an ion and one of its converging Rydberg series labeled by the effective principle quantum numbers n^*, $n^* + 1$, etc., illustrating the interaction of a valance state with the Rydberg series and with its adjoining ionization continuum. The "fixed-nuclei" autoionization width and the stabilization point, P_s, are also shown.

and molecular systems at higher energies below and above their ionization limits.

II. Experimental Methods

A number of state-of-the-art experimental techniques used in this work are briefly described as follows.

a) Resonantly-Enhanced Multiphoton Ionization (REMPI) (single color): By using a wavelength-tunable, focused and pulsed laser beam, excited states of molecules (and atoms) can be formed and ionized by a process which can be schematically indicated as:

IONIZATION LIMIT

RESONANT STATE

GROUND STATE
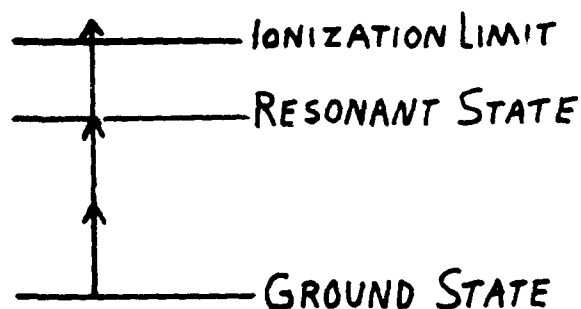
where the resonant state is usually reached by two or three photons. (The above sketch illustrates what will be called a 2+1 REMPI process) Since the ionization intensity is enormously enhanced when the photons are energetically resonant with one of the states of the molecule, a plot of ion intensity versus laser wavelength resembles a conventional spectrum. (see fig 2. which shows the spectrum of the $3d\pi$ $^1\Sigma_g^+$ state produced from the metastable $^1\Delta_g$ state of O_2). One advantage of the multiphoton resonant excitation is that it can provide excitation of states which are forbidden in conventional one-photon spectroscopy. Thus for molecules with a center of symmetry (such as O_2), $g \leftrightarrow g$ and

8

$(3d\pi)\ {}^1\Sigma_g^+ \leftarrow \leftarrow\ {}^1\Delta_g$

FIGURE 2

9
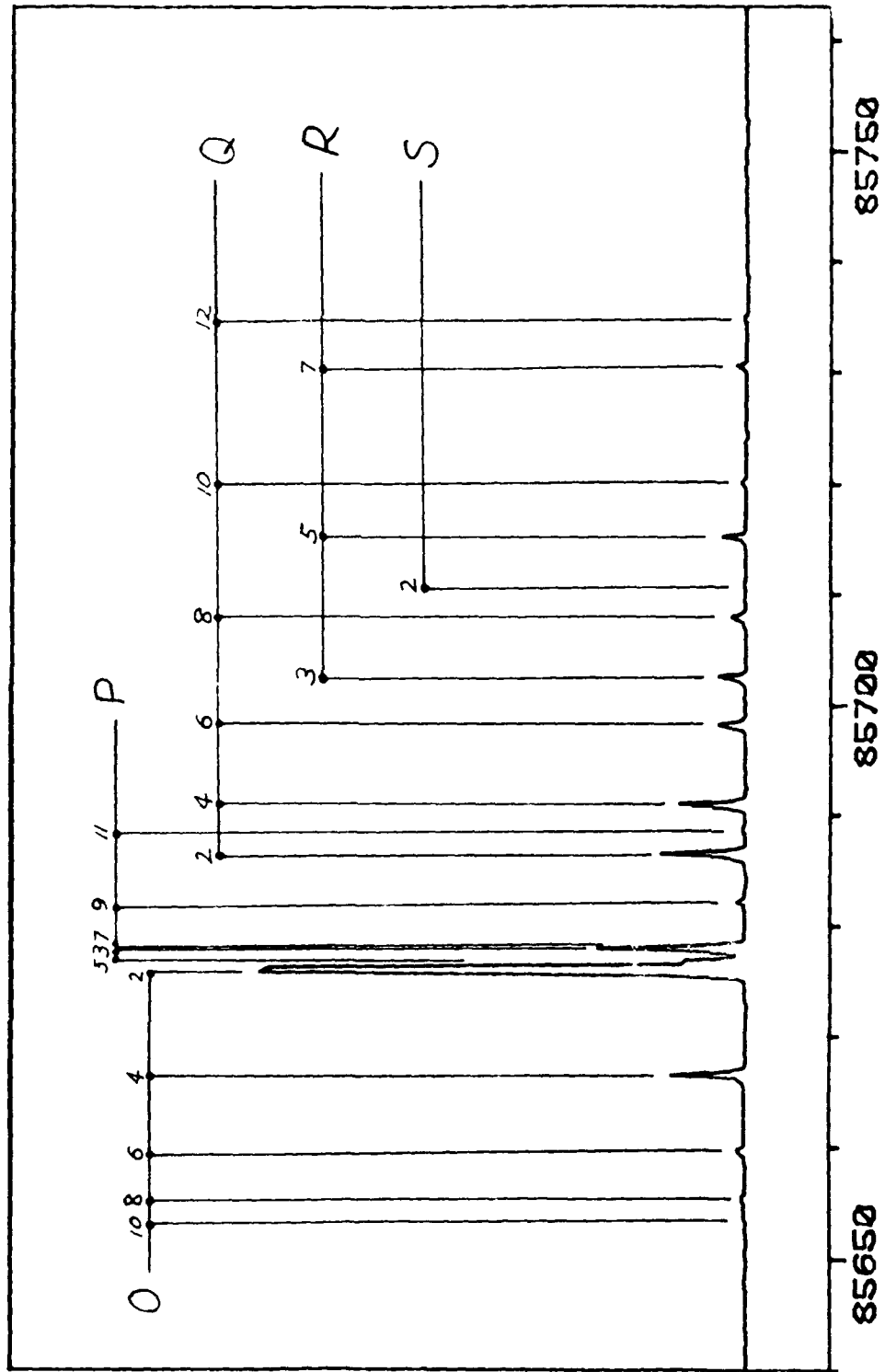
u↔u transitions are forbidden for one-photon excitation but are allowed for even numbers of photons absorbed. Also many other kinds of experiments become feasible due to the high concentrations of excited states and of photons that can be attained with pulsed lasers.

b) Optical-Optical Double Resonance (OODR): Because of the high spatial and temporal concentrations of excited species and photons attainable with pulsed lasers, it becomes possible to perform such an OODR experiment as:
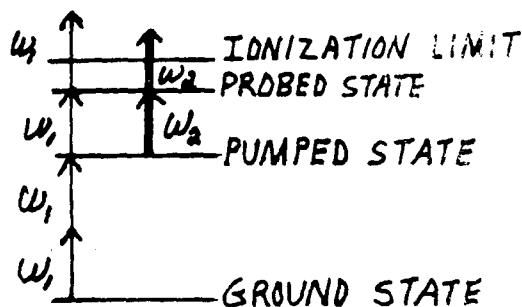
FIGURE 3

In this experiment ω_1 is kept fixed and ω_2 is scanned. Thus the spectrum generated originates from a single rovibronic excited state, providing a spectrum of state B which is enormously simplified and more easily analyzed. However, not all "pumped" states are suitable for this technique. For instance, it must sufficiently long-lived with respect to predissociation and with respect to photoionization by ω_1. Part of the effort of this contract has been directed to finding such a suitable state(s) for O_2 or to devising techniques to otherwise circumvent unsuitable circumstances.

10

c) Time-of-flight Mass Spectrometry: The short time of ion formation by a ≈ 10 nsec laser pulse lends itself to ion mass analysis by acceleration by a constant voltage and then a simple measurement of the time-of-flight to a charged-particle detector. The mass analysis provides nearly perfect assurance that the recorded spectrum is that of the molecule of interest rather than that of some readily ionizable impurity. Thus NO, which has a readily detectable spectrum at the part-per-million level, is distinguished by production of a mass 30 ion, easily separated from the mass 32 ion O_2^+. The apparatus also has the ability not only to detect and identify fragment ions (such as O^+), but also to measure the kinetic energy released on formation, from a measurement of the time-of-flight peak width. This is one method used to determine the state of excitation of product atoms and ions since kinetic energy is the only form of external energy release in the case of a diatomic molecule.

d) Time-of-flight Photoelectron Spectrometry: Again, the short time of photoelectron formation lends itself to the time-of-flight method for electron kinetic energy analysis. We use a recently-developed technique of magnetic collimation whereby essentially all the photoelectrons emitted in a 2π solid angle are magnetically collimated with minimum flight-time deterioration before entering the flight tube region. This near 50 percent detection efficiency makes it possible to energy analyze photoelectrons from relatively weak transitions. Such measurements are very valuable in several ways: (1) they provide a method for identifying resonant states and distinguishing between badly overlapped transitions; (2) they provide the only certain

11

measurement of the internal energy distribution of the ions produced, and (3) they provide valuable information about the details of the process of photoionization of the resonantly excited states.

e) Supersonic Molecular Beams: Wherever possible we have used the *phenomenon of rotational cooling* by supersonic jet formation in order to collapse the extensive rotational distribution characteristic of a room-temperature gas to that of the gas at temperatures of the order of 10K. This cooling is accomplished by expanding the gas at *the highest practical pressure* through an orifice which is very much smaller than the molecular mean free path. We have used a pulsed gas valve where possible, in order to minimize the pumping speed, and also continuously emitting nozzles where necessary. The narrower rotational distribution results in spectral simplification, although not to as high a degree as the OODR technique.

f) Microwave Discharge Excitation Source: In addition to using the ground $^3\Sigma_g^-$ state of O_2 as the initial state of our experiments, we have used a microwave discharge in O_2 at low pressures (≈ 10 Torr) to generate the long-lived metastable $^1\Delta_g$ state of O_2 and inject it into the photoionization region of our time-of-flight mass spectrometer. This technique has been used by an earlier worker in this field but we have improved it to obtain much superior spectra. As will be explained later, this enabled us to obtain extensive spectra of singlet 3d Rydberg states which were readily analyzable and will be of great help in the interpretation of the much more intractable triplet spectra.

III. Results

Since in any one experiment we often investigated several aspects of the contracted research, and since major results became clear only after several different experiments, it is probably clearer for the reader to have the results gathered under several main topic headings. Otherwise, while a reading of the attached appendices would constitute the most comprehensive and detailed final report, it would tend to obscure the most important accomplishments in a mass of detail. Therefore we present the research results in a distilled form as follows.

A. Detection, analysis and assignment of the 4s-3d and 5s-4d Rydberg complexes of O_2

1) The Triplet System

The v=0-3 levels of the 4s-3d levels of the 5s-4d Rydberg complexes have been identified by a (2+1) REMPI process (appendices 5 and 8). The electronic states are g (gerade) states and are accessed from the $^3\Sigma_g^-$ ground state of O_2. The reason for the description as a "complex" is due to the fact that ns and (n-1)d Rydberg electrons have approximately the same effective principal quantum number (i.e. binding energy), and hence have about the same energy. Since the nsσ orbital and (n-1)dσ orbital have the same symmetry, the resulting states can interact and perturb each other yielding "mixed" states which complicates analysis and assignment. These states have not been detected previously by any method although a theoretical calculation exists.[4] Vibrational analysis (and rotational analysis of two bands) shows that the states are very nearly pure Rydbergs in character, with no detectable perturbation. Line widths are laser band-width limited (≈ 1 cm^{-1})

13

indicating little or no predissociation. However, only one band system, $3d\delta^3\Pi_g$ could be identified reliably by rotational analysis and the theoretical calculations are of limited reliability in band assignment. In fact, one of the major goals of this part of the research is to assess the accuracy of these calculations. Since publication of appendices 5 and 8, better spectra of higher resolution and improved signal/noise ratio have been obtained and are in the process of analysis with good prospect of success in additional assignments.

2) The Singlet System

Since the analysis of these data is still proceeding and no paper can yet be written, these experiments and their results will be described in somewhat more detail than those for which reprints and manuscripts are available and are appended here. Using the $^1\Delta_g$ metastable state of O_2 prepared in a microwave discharge, the energy region of the 4s-3d Rydberg complex was explored and a number of states identified by a 2+1 REMPI process. Due to improved laser resolution and somewhat less band complexity and overlap compared with the triplet system, it has been possible to identify positively every band of significant intensity. This analysis is now nearly complete, and has yielded positive identification of $(3d\pi)^1\Delta_g$, $(3d\pi)^1\Sigma_g^+$, $(3d\delta)^1\Phi_g$ and $(3d\delta)^3\Phi_g$ states in the v=0-3 vibrational levels (see appendix 15). Nearly all line widths are laser-bandwidth limited ($\leq$ 0.1 cm^{-1}) and therefore nearly all lifetimes are > 10^{-10} sec. Relative rotational line intensities of most of the bands follow theoretical values given by generalized Honl-London line strength formulas for 2-photon transitions (Note that such line strength formulas depend only on

14

geometry as expressed by Wigner 3-j symbols and hence do not require knowledge of the physics of the transition). However, in a number of cases, measured rotational line intensities decrease with increasing rotation compared with theoretical values, indicating the existence of heterogeneous predissociation, i.e. predissociation by valence states with values of Λ (or Ω) differing from that of the Rydberg states, hence requiring significant coupling between electronic and rotational degrees of freedom. In some of these cases, e.g. the $(3d\pi)^1\Delta_g$ state, linewidths at higher rotational quantum number (J 4 or 5) become larger than the laser bandwidth and the widths and hence decay rates become measurable. In these cases the linewidths increase with rotational quantum number as expected for the proposed heterogeneous predissociation. Quantitative analysis of these effects is still in progress. Successful analysis may lead to the identification of the valence states responsible for the predissociation and, at least in some cases such as the $^1\Delta_g$ state, will give parameters characterizing the particular Rydberg-Valence interaction.

The success in characterizing in detail many (not yet all) of the 3d Rydberg states is important in many ways.

a) These are the first gerade Rydberg states of O_2 to yield spectra with so many bands which are rotationally analyzable in such detail. (The earlier work on the 3sσ states provided only two bands which were rotationally analyzable to some degree and there is some question about one of them). In fact, in the detail of analyzable rotational structure, these spectra are superior to those of any (u or g) Rydberg states of O_2. For instance, band origins are so accurately located for all vibrational levels v=0-3

15

that there is a very good probability that they represent more accurate values for the vibrational spacings of the O_2^+ ion, the core of the Rydberg state, than the values obtained from band <u>head</u> positions of the spectrum of the bare O_2^+ ion itself. Certainly this will be the case if we succeed in obtaining similar spectra for the 4d Rydbergs, since the very small bonding or anti-bonding effect of the 4d Rydberg will be completely negligible at least for the $^1\Delta_g$ and $^1\Sigma_g^+$ states.

Table I gives the energies of the band origins determined from our data for the singlet 3d $^1\Phi_g$, $^1\Delta_g$ and $^1\Sigma_g^+$ states which we have observed. The vibrational spacings are compared to literature values[11] obtained from extensive analysis of many bands of the A → X transition of the O_2^+ ion and correspond to the RKR potential curve which best explains both band positions and intensities. It should be noted that from molecular orbital correlation diagrams ndδ Rydberg orbitals are expected to be very slightly bonding while ndπ orbitals are expected to be very slightly antibonding for small displacements from the equilibrium internuclear separation. Comparisons among the data of Table I agree with this expectation. Extension of those data to the 4d Rydbergs should give very accurate and reliable vibrational spacings for the O_2^+ ion.

b) We have with certainty located the $(3d\delta)^1\Phi_g$ and all three components ($\Omega=2,3$ and 4) of the $(3d\delta)^3\Phi$ states (for v=0-3). The positions of none of the $(3d\delta)$ Rydberg states were calculated in the earlier theoretical work[4] and hence this is the first determination of their energies by any method. Furthermore, the intensity of the formally-spin-forbidden transition $^3\Phi_g(\Omega=3) \leftarrow \leftarrow ^1\Delta_g$ is

16

Table I. Energies and Vibrational Spacings (in cm^{-1}) of Some 3d
Singlet Rydberg States of Oxygen

v	$^1\Sigma_g{}^+$	$^1\Delta_g$	$^1\Phi_3$	$^3\Phi_3$	$\Delta v(O_2{}^+)$
0	85684.5	85506.3	85035.2	84832.2	
	(1871.1)	(1872.1)	(1866.9)	(1880.6)	(1872.6)
1	87555.6	87378.4	86902.1	86712.8	
	(1840.3)	(1839.4)			(1840.0)
2	89395.9	89217.8			
	(1804.5)	(1804.3)			(1807.4)
3	91200.4	91022.1			

nearly the same as that of the allowed $^1\Phi_g(\Omega=3)\leftarrow\leftarrow^1\Delta_g$ transition. This fact and the relative energies of all three Ω-components of the $^3\Phi$ state give a very clear indication of the breakdown of the usual LS-type coupling scheme which is only semi-quantitatively alluded to in the theoretical paper[4]. Upon further analysis our experimental spectra should address this problem quantitatively and be very helpful in treating the general problem of transition between coupling cases in the Rydberg states of O_2, a problem which very often complicates analysis of Rydberg spectra.

c) The reliable determination of the energies of assigned electronic states in the 3d singlet Rydberg manifold will be of great assistance in reliably assigning states in the triplet manifold. This is due to the fact that, in general, the energy ordering is expected to be the same (as indicated by the theoretical calculations), with the triplet states lying below the singlets by $\approx0.01-0.04$ eV. The ongoing re-analysis of improved triplet spectra is proceeding with this in mind.

d) In the rotational analysis of three of the electronic excitations, namely excitations to the $(3d\delta)^1\Phi_g(\Omega=3)$, $(3d\delta)^3\Phi_g(\Omega=3)$, $(3d\delta)^1\Delta_g(\Omega=2)$ states, certain aspects of line-strength theory have been used which apparently have not been appreciated before, although they are implicitly contained in well-known theory for two-photon excitation. Namely for $\Omega=3 \leftarrow\leftarrow \Omega=2$ transitions the R(4) line strength is identically zero while all other R's are not. While a very few comparisons of multiphoton line-strength theory with experiment have been made, they have never dealt with either of the types of transitions given above and, given the commonly large fluctuations in pulsed laser intensity, state assignment

based on line strengths is not usually very trustworthy. However in this case, the <u>complete absence</u> of the R(4) line in the $(3d\delta)^1\Phi_g \leftarrow\leftarrow {}^1\Delta_g$ spectrum provides strong support for our assignment. Similarly for the excitation of the $(3d\pi)^1\Delta_g$ state (an $\Omega=2 \leftarrow\leftarrow \Omega=2$ transition), the line strength is composed of two different transition tensor components for linearly polarized li.ht while one of these components becomes exactly zero for circularly polarized light. In the excitation to $(3d\pi)^1\Delta_g$ the component which becomes zero for circularly polarized light is responsible for over 90% of the intensity for linearly polarized light and the dramatic difference between the two spectra (see fig.4) is additional proof of the electronic assignment. Differences between spectra taken with linearly and circularly polarized light have been used before in the case of (polyatomic) symmetric top molecules, but this is the first case of such a strong difference for a diatomic molecule.

e) There remain some important questions brought out by this research and which remain to be answered (an example of the trite but true description of a good piece of research as one which raises more questions than it answers). Only a few will be mentioned here. In the singlet system we have found only the $(3d\pi)^1\Sigma_g^+$, $(3d\pi)^1\Delta_g$ and $(3d\delta)^1\Phi_g$ states. The $(3d\sigma)^1\Pi_g$, $(4s\sigma)^1\Pi_g$ and $(3d\delta)^1\Pi_g$ states are formally allowed by 2-photon selection rules but we have not been able to detect these states. At our very highest laser powers we have seen some very weak peaks which may belong to one of these states but we cannot exclude other possibilities, since not enough lines to permit analysis were seen. This is especially disturbing in the case of the $(4s\sigma)^1\Pi_g$ state

FIGURE 4

20
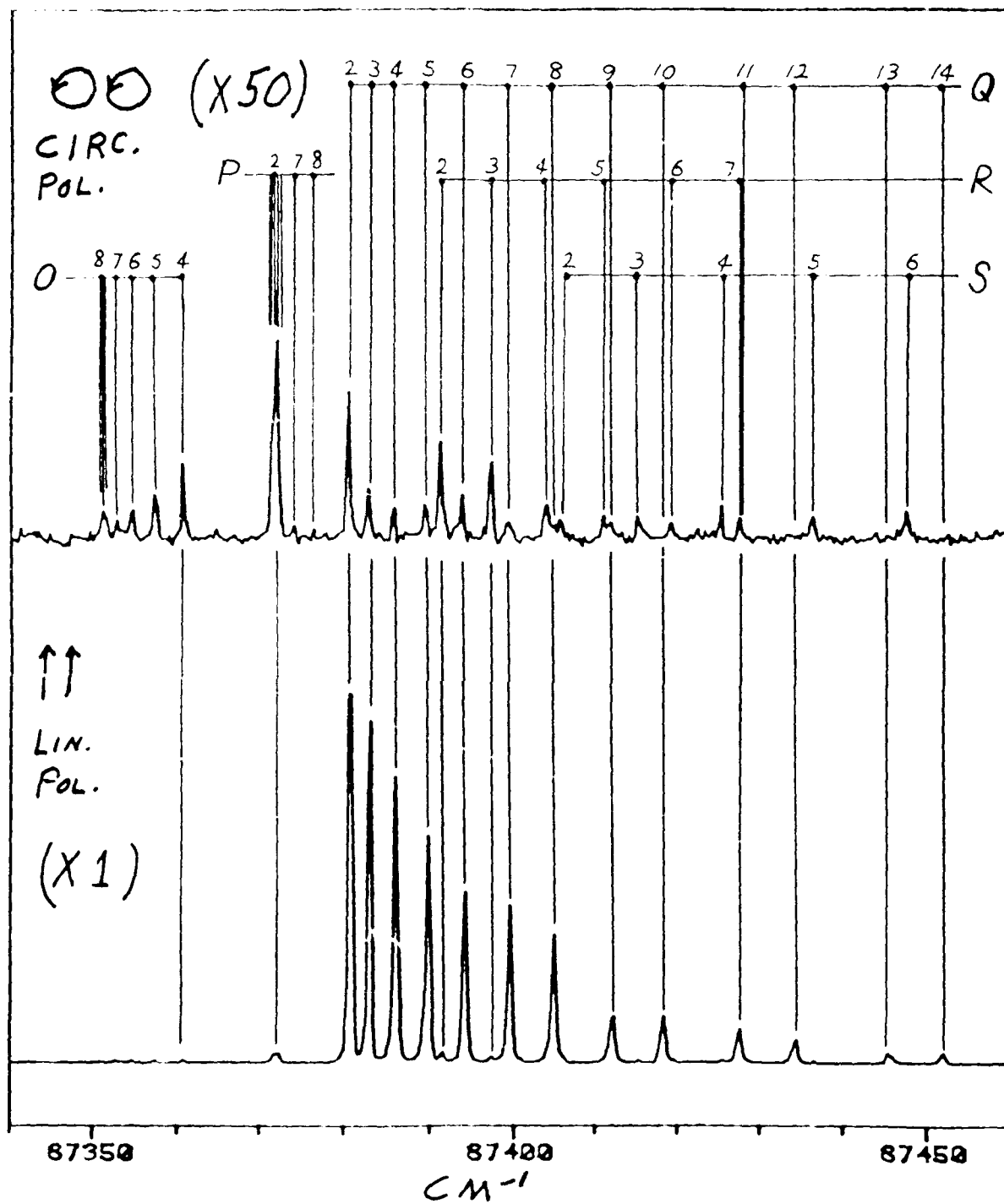
since the $(3s\sigma)^1\Pi_g$ state appears very strongly in the 2-photon spectrum, even though these latter states are mostly strongly predissociated while the $(4s\sigma)$ state should be less predissociated and hence easier to detect by REMPI. In single photon spectroscopy one expects (and finds) Rydberg intensities to decrease as $(n*)^{-3}$ where $n*$ is the effective principle quantum number. "All else being equal" one expects the same decrease (by ≈3.5 in this case) for the $4s\sigma$ state in 2-photons in which case the state would be very readily detectable. However, the 2-photon amplitude involves a complicated sum over many states and also the $(4s\sigma)$ state differs from the $(3s\sigma)$ state in having considerable admixture of $(3d\sigma)$ so that a rationalization is possible, although a reliable explanation is not readily apparent at present. Another unanswered question is the following. We have seen $\underline{very}$ strong transitions from the $\underline{singlet}$ $^1\Delta_g$ metastable state to the $\Omega=3$ spin-orbit component of the $\underline{triplet}$ $^3\Phi_g$ state and this formally spin-forbidden transition is obviously (from the spectrum) due to strong interaction with the $\Omega=3$ component of the singlet $^1\Phi_g$ state. Why don't interactions of comparable magnitude occur between other singlet and triplet states of the same value of Ω, for instance between $(3d\pi)^3\Delta_g(\Omega=2)$ and $(3d\pi)^1\Delta_g(\Omega=2)$? From the absence of resulting spectra we infer that such interactions must be at least about two orders of magnitude weaker than that for the $^3\Phi_g - {}^1\Phi_g$ case. The explanation is not readily apparent but should come from a detailed understanding of angular momentum coupling strengths in the molecule.

3)General Overview of (gerade) Rydberg States

We have made very great progress in locating and characterizing the s (ℓ=0) and d (ℓ=2) Rydberg states. We can eliminate, for all but the most esoteric processes, the g (meaning ℓ=4, not meaning gerade here) Rydberg states as being unimportant. Thus, when we have located all members of the 4s-3d complex, (both singlets and triplets) and characterized their interactions with each other and with valence states, the major part of the level structure of the gerade Rydbergs converging to the ground state of the ion will be well understood. Doing the same for the 5s-4d and higher Rydbergs will be less important since well known and reliable scaling laws can predict the most important properties of all higher Rydbergs. One exception is the characterization of certain vibronic interactions which can produce the phenomenon of vibrational autoionization above the ionization limit.

The most important remaining block of information necessary for an overall understanding of the entire gerade structure and spectrum of O_2 below its ionization limit is the set of repulsive gerade valence potential curves in this region and the strength of their interaction with the Rydberg states. The only information presently available on this subject, (other than the inferences that can be drawn from the predissociation widths of our data) is the set of theoretical calculations made by a number of groups[8,12,13]. All these groups calculate their valence state potential curves using molecular orbital basis functions which are spatially compact, so that they are not suitable for describing Rydberg states with their far more extended (or diffuse) orbitals. Thus they calculate diabatic potential curves which exclude the possibility of describing the interaction of a Valence state with a

22

Rydberg state. Calculations employing basis sets suitable for describing both Rydberg and valence states are difficult and have only rarely been done in high quality calculation. A few such calculations involving a few u (ungerade) Rydberg states of O_2 have been done and will be discussed later. While we cannot, from our data alone, extract experimental curves for the valence states which are predissociating our Rydberg states, we can often use the theoretically calculated curves to identify a single plausible predissociating valence state and then vary its position and interaction strength in an attempt to reproduce our experimentally measured predissociating rates. For instance for the $(3d\pi)^1\Delta_g$ Rydberg state *we have four vibrational levels*, v=0-3, for which we have linewidth data and we have identified the lowest energy $^1\Pi_g$ valence state from the theoretical calculations as seemingly the only plausible predissociating state. Therefore we expect to be able to extract the interaction energy and optimize the position of the valence state potential curve to give agreement with our data.

B. The E $(3p\pi)^3\Sigma_u^-$ state of O_2. Demonstration of its mixed Rydberg-Valence character.

Only two states of the u (ungerade) Rydberg system of O_2 have been identified up to the present. They are the E$(3p\pi)^3\Sigma_u^-$ and the F $(3p\sigma)^3\Pi_u$ states. While absorption features corresponding to these states have long been known, only recently have they been assigned with any confidence based on a theoretical calculation[14] showing that both states are really strongly mixed Rydberg-Valence states. The calculated potential curves, shown in Fig.5(a) and (b) result from one of the very few accurate calculations of Rydberg-Valence

23

interaction. They also demonstrate why the Rydberg states optically allowed from the ground state are essentially unknown except for the E and F states, since the higher u Rydbergs will be similarly perturbed and difficult to identify.

We have confirmed the mixed Rydberg-Valence character of the E state directly by measuring the photoelectron spectrum produced by (2+1) REMPI via the v=0 level of the E state as the resonant intermediate and shown in Fig.5(c). If the E state were a "normal" unperturbed Rydberg state, the photoelectron peak corresponding to producing the ion in the v=0 state should be the most intense, whereas it is one of the least intense. In Appendix 2, a more quantitative discussion of the photoelectron spectrum is given in terms of the Rydberg-Valence potential curve of Fig.5(a). More recently Wang et al[15], using improved potential curves very similar to those of Fig.5(a) have calculated a photoelectron spectrum which gives even better agreement with our data, but which we believe is not appropriate to our experiment. Briefly, we prefer a calculational method which assumes that the process of formation of the E state is not coupled coherently to the subsequent photoionization of the E state, while their method assumes that the overall (2+1) REMPI process is completely coherent. The arguments for our point of view are given in the preprint Appendix 12. This disagreement is not simply academic, since it concerns a very important aspect of the general REMPI process including the validity of many conclusions regarding lifetimes of intermediate states drawn by other researchers in this field.[16] As detailed in the preprint of Appendix 12, each procedure is correct in two different limits of laser conditions

24

E (eV)

ION $^2\pi_g$

120

$^3\Sigma_u^-$ π_g 3pπ (E)

100

$^3\Sigma_u^-$ π_u $^3\pi_g$ ^{3}

80

60

188   228 248   288   328
R(bohr)
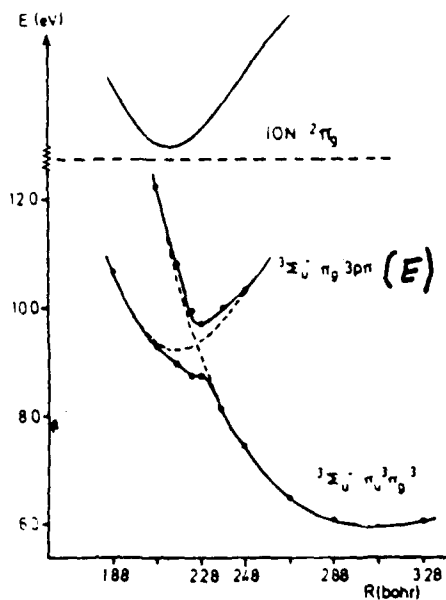
(a) Calculated CI potential curves for the lowest two $^3\Sigma_u^-$ states of O_2 (energy values in eV taken relative to the $^3\Sigma_g^-$ ground state, distances in bohr). Results for the corresponding pure Rydberg and valence states are also estimated in the figure (dashed lines); the latter Rydberg curve should be nearly parallel to that of the $^2\pi_g$ ground state of O_2^+ also included.

E (eV)

140

$^3\pi_u$ π_g 3pσ (F)

120

100

80

$^3\pi_u$ π_g 3σ_u

60

188   228 248   288   328
R(bohr)
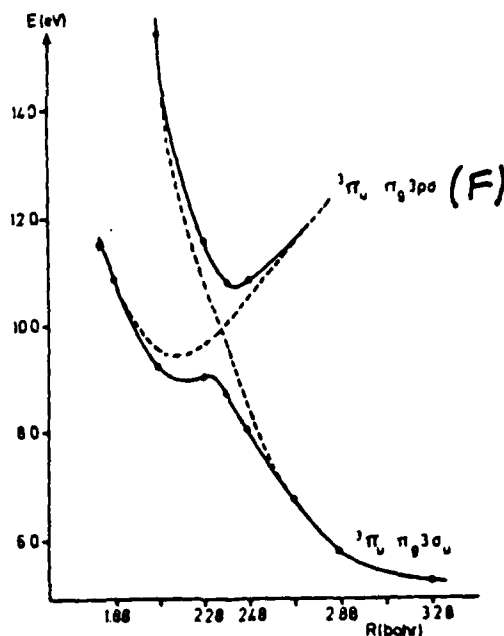
(b) Calculated CI potential curves for the lowest two $^3\pi_u$ states of O_2. Results for the corresponding pure Rydberg and valence states are also estimated in the figure (dashed lines).

Electron Intensity (arb. unit)

v"=3

v"=2

v"=1

v"=4

v"=0

.2   .4   .6   .8   1   1.2   1.4   1.6   1.8
ELECTRON KINETIC ENERGY (eV)
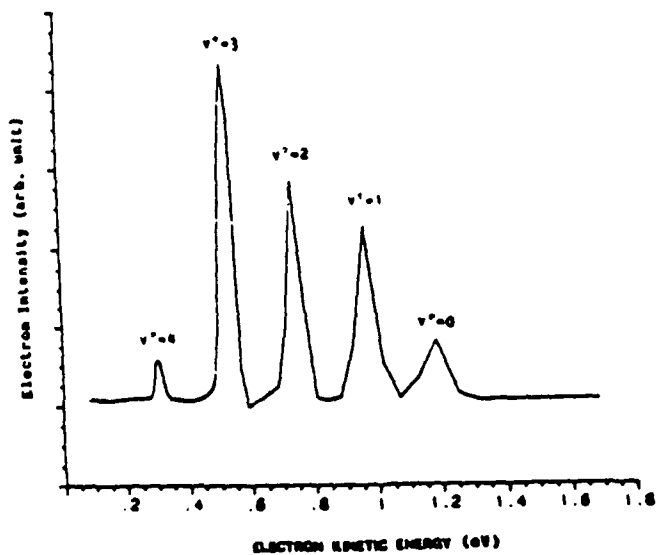
(c) The three-photon resonance enhanced one-photon ionization photoelectron spectrum of the longest band of O_2 at 373.12 nm. In the present one color experiment, the highest energetically accessible vibrational quantum number of O_2^+ in its $X^2\pi_g$ state is 4. Partial photoelectron spectra taken at higher resolution clearly resolve the spin-orbit splitting of the O_2^+ ground state (≈ 200 cm^{-1}) for each vibrational level.

FIGURE 5

25

and intermediate state lifetime. The correct treatment *f*or conditions far from these two different limits remains to be developed, although we present arguments to show that most cases for which REMPI is used correspond to our "incoherent process" limit.

C. Photoionization and Photoelectron Spectroscopy of ns and nd Rydberg States (Appendices 5,6,7 and 8)

Until the last several years it was generally thought that photoionization of a Rydberg state was a very simple and well understood process. Since the Rydberg orbital is very nearly hydrogenic, except for being shifted inward by an amount determined by the quantum defect, the photoionization cross section versus photon energy was thought to be hydrogenic. Indeed if the ionization continuum is also assumed to be hydrogenic, theory shows that the cross section would be hydrogen-like, i.e. having a finite value at threshold and decreasing slowly with energy such as:

26
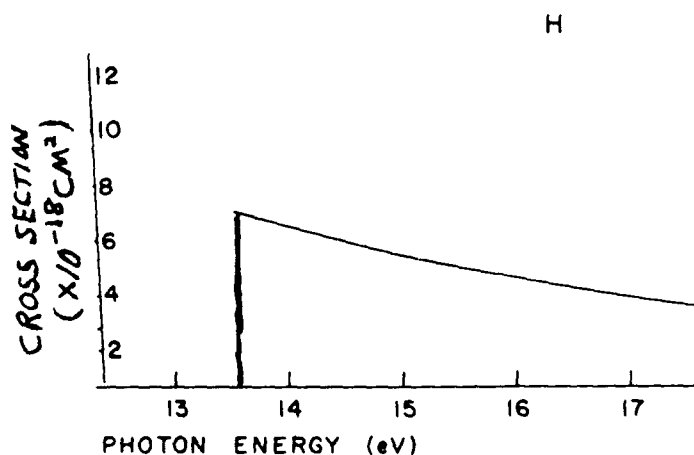
For instance a calculation of the photoionization cross section by Cohn[17] has precisely such behavior.

If the photoionization cross-section has such behavior and if the Born-Oppenheimer separation of electronic and nuclear motions was valid, it is easy to show by the Franck-Condon principle that photoionization of a true unperturbed Rydberg state should leave the vibrational quantum number of the ion core unchanged, i.e. that a $\Delta v=0$ selection rule should hold for photoionization. Such a $\Delta v=0$ selection rule is indeed shown to hold very well in a large number of cases and forms the basis of the best current method for preparing molecular ions in selected vibrational states as has been done by a number of workers.[18]

However, an increasing number of strong deviations from the $\Delta v=0$ selection rule has been observed and a general consideration of possible reasons for these deviations has been given.[19] In that analysis, the example of flagrant violation of the $\Delta v=0$ rule in the photoionization of the C $(2p\pi)^1\Pi_u$ state of H_2 was attributed to photon absorption by the ion core of the Rydberg state to produce an electronically doubly excited state which was repulsive (i.e. purely dissociative potential curve) but autoionized as it dissociated. This process has since been confirmed by more accurate theoretical calculations.[20]

In that paper[19], two other general phenomena were mentioned as potentially very effective in causing $\Delta v\neq0$ transitions. These were: (1) shape resonances in the ionization continuum, and (2) Cooper minima in the ionization continuum. At the time that paper[19] was written there were no examples of either.

In the course of our work on this contract we measured the

27

photoelectron spectrum produced by (2+1) REMPI via the $3s\sigma$ states in an attempt to see whether that process afforded a satisfactory method for production of vibrationally state-selected O_2^+ ions. The photoelectron spectra showed very significant deviations from the $\Delta v=0$ rules, especially for $v=1$ and 3 (see appendix 6). In this case, enough is known about the absorption spectrum of the O_2^+ ion core to eliminate core-absorption as the mechanism for the $\Delta v \neq 0$ transitions. However, an examination of theoretically calculated potential curves for excited valence states of O_2 led us to believe that a shape resonance might be responsible in this case. A shape resonance is an electronically excited state, lying above the ionization potential, and in which the electron is temporarily bound by virtue of some potential barrier (i.e. by the "shape" of the potential) in this case due to an angular momentum (i.e. centrifugal) barrier. It can also be thought of as a valence state lying above the ionization limit and which differs from the ionization continuum by only one orbital. In fact, the shape resonance in question is actually formed by the repulsive $3\sigma_u$ valence state of Fig.5(b) when it goes above the potential curve of O_2^+ shown in fig.5(a). The strong interaction (energy splitting of $\approx 2eV$) shown in Fig.5(b) is a semi-quantitative indication of the width of the resulting shape resonance. (It would be quantitative except that this width changes rapidly with internuclear distance, and in fact it is just this change of width and energy position of the resonance with internuclear distance which makes the Franck-Condon approximation invalid and causes $\Delta v \neq 0$ transitions.)

This explanation of strong $\Delta v \neq 0$ transitions as due at least in great part to the effects of a shape resonance were verified by

28

theoretical calculations and both our results (appendix 6) and the calculations of McKoy and co-workers[21] were published together as Communications to the Editor. The effect of a shape resonance was further confirmed by measuring the angular distribution of the photoelectrons ejected in ionization of the $(3s\sigma)$ $v=0-3$ Rydberg states (appendix 7). The measured angular distributions were in very good agreement (see Table 1 of appendix 7) with calculations of McKoy and co-workers (also given in appendix 7). The measured angular distributions for the $\Delta v \neq 0$ transitions were much more nearly isotropic than those for the v-conserving transitions (see Fig.1 of appendix 7). This can be explained by the (somewhat simplified) picture that while v-conserving transitions consist in large part of transitions "directly" into the continuum, the $\Delta v \neq 0$ transitions result predominantly from transitions in which the emerging electron is trapped briefly by the angular momentum barrier and "rattles around" a few times before escaping, hence producing a more nearly isotropic angular distribution.

Photoelectron spectra were also taken for the (2+1) REMPI process via the triplet 4s-3d complex states as described in appendix 8. These photoelectron spectra also show very considerable intensities for $\Delta v \neq 0$ transitions for ionization via most of the resonant levels as can be seen in Fig.3 of appendix 8. This observation is important for the following reason. The $(3s\sigma)$ Rydberg states are rather strongly predissociated and this factor apart from the shape resonance, can contribute somewhat to $\Delta v \neq 0$ transitions by an amount which is not readily calculated accurately. However, the members of the 4s-3d complex are so weakly predissociated (if at all) that this factor cannot make any

29

significant contribution to $\Delta v \neq 0$ transitions and yet we find them to occur. Therefore it is certain that the reason for $\Delta v \neq 0$ transitions does not lie in distortions (perturbations) of the Rydberg state but must be attributed to unusual features in the ionization continuum. From calculated potential curves (see Fig.9 of appendix 8) it can be seen that the situation in the continuum is more complex than that for ionization via the $3s\sigma$ Rydbergs. Not only does the shape resonance still play a role (although diminished compared to the $3s\sigma$ case) but other valence states which do not form shape resonances (because they differ in electron configuration from the continuum by more than one orbital) can become important because they can autoionize by configuration interaction. That is, they autoionize by exchanging energy between two electrons rather than by an electron tunneling through a potential barrier as in the case of a shape resonance (These latter states are sometimes called "core-excited" or "Feschbach" resonances).

The importance of these investigations of shape and other resonances lies in the following. Firstly there is the intrinsic interest in a fundamental phenomenon. Shape resonances in such diatomic molecules as N_2 and NO have drawn considerable scientific interest in the past decade or so. An excellent review is given by Dehmer et al[22]. All previous experimental work on shape resonances accessed them by ionization of inner core electrons from the ground vibrational and electronic state of the molecule. In our case, we were able to vary both vibrational and electronic states and hence probe a larger range of internuclear distance which, as detailed earlier, changes both position and width of the shape

resonance. Also our method circumvents certain problems of autoionization structure which plagued earlier investigations of shape resonances by the excitation from the ground state of O_2.

In a very apt analogy we have just begun to make use of a technique which allows us to look at ionization (and dissociation) continua from many angles and many distances (i.e. from many states of different energy spanning a wide range of internuclear distances) instead of from one viewing point (the ground electronic and vibrational state of the molecule). While a continuum, for instance the σ_u continuum of $O_2^+ + e^-$ in which our shape resonance (as well as core-excited resonances, etc) is embedded, is unchanging no matter how one accesses it, what the experiment sees of it depends on the initial state. This technique of using various Rydberg states (as well as valence states where possible), especially if two-color experiments are practical, promises enormous advances in the understanding of continua.

D. Ion State Preparation

One of the goals of this contract was to find a method for preparing O_2^+ ions as purely as possible in selected vibrational levels. Initially it was hoped that ionization via the various vibrational levels of $3s\sigma$ Rydberg state would result in adequate preparations, but this was not the case as discussed earlier. However, in the investigation of the 3d Rydberg states, ionization via one of the states, tentatively identified as $(3d\delta)^3\Pi_g$, did produce fairly pure ($>80\%$) preparations of O_2^+ ions in the vibrational levels $v=0-3$ as detailed in appendices 5 and 8. See especially Figure 4 of appendix 8. This should be a very useful

31

technique in investigating the effects of vibrational excitation of the O_2^+ ion on its reactions with neutral molecules. It may even be possible to study the effect of vibrational energy in other processes such as dissociative recombination in which theoretical calculations predict the effect can be very large[7,8].

E. Detection of O atoms (appendix 14)

Oxygen atoms in the three fine-structure components of the ground ^3P state were detected by a (2+1) REMPI process as described in appendix 14. The atoms were formed by dissociation of ground state O_2 by the same laser pulse which was used for detection. The detection sensitivity was estimated crudely to be of the order of 10^6 atoms/cm^3 and the REMPI spectrum readily distinguishes among the fine structure levels (Fig.1 of appendix 14). This detection method should be especially useful in identification of the state of O atoms produced by various pulsed methods. It was developed here as a tool in determining the states of oxygen atoms produced in the many predissociating states observed in this study, but has not yet been successfully applied to this problem.

The process of multiphoton photodissociation of O_2 which produced the O atoms is of considerable interest. It is tentatively determined to be a 2-photon dissociation producing two ground state atoms statistically distributed among the fine-structure components. This process may be useful in producing ground state O atoms with controlled and variable kinetic energy for further experiments.

F. Pump-Probe (OODR) Studies

The feasibility of pump-probe methods has been extensively investigated and serious difficulties have been found. The $3s\sigma$ Rydberg states provide very poor pump states because of the very short lifetime of most levels. However, experiments indicate that an intense effort using photoelectron spectra may very well be successful. The $4s$-$3d$ and $5s$-$4d$ levels would provide excellent pump states but would require infrared probe lasers which we do not have at present. The energies and other characteristics of those levels which would serve as good pump states to be probed by a second laser are given in appendix 8.

A perhaps more promising set of possibilities have resulted from the work using the $^1\Delta_g$ metastable state of O_2. One of the $(3s\sigma)^1\Pi_g$ levels (apparently near $v=2$) has fairly sharp rotational structure and may serve well as a pumped state. In addition most of the $3d$ singlet Rydbergs referred to in section A(2) have very sharp rotational structure indicating long lifetime, but again infrared probe lasers would be required for upward excitation.

Other possibilities using resonant "bleaching" methods exist and have been considered but not yet tried experimentally.

G. Excitation of (and via) repulsive states

As a test system for developing methods for studying dissociation and other dynamical processes of O_2, studies were carried out on Cl_2. The excited states and potential energy curves of Cl_2 have many qualitative similarities to those of O_2 but the energies are lower making transitions more easily accessible with our lasers. We demonstrated the feasibility and certain advantages of carrying

33

out multiphoton transitions via repulsive intermediate states. This demonstration illustrated for the first time a new method for following the time-evolution of rapidly decaying states which has considerable promise. We also investigated a case of very strong Rydberg-valence interaction producing an adiabatic potential curve with two minima. Details are given in appendices 1 and 3. In addition the identification of specific atomic states produced in photofragmentation is demonstrated in appendix 4. This latter process of photodissociation is also potentially useful in providing a source of Cl atoms of precisely known and variable kinetic energy and in a specific electronic state, the $^2P_{3/2}$ ground level, for kinetic studies of Cl atomic reactions.

H. Anomalous Lineshape Studies

The potential utility of certain lineshape phenomena in determining decay rates of excited states was demonstrated for N_2 (see appendix 9) and applied to the v=2 level of the $p\pi$ $K^2\Pi$ Rydberg state of NO. Neither the lifetime nor the mode of decay of this state was known previously. We have determined that its lifetime is < 2 nsec and the decay is predominantly by predissociation. The details are given in appendix 10.

References

1) K.F. Huber and G. Herzberg, <u>Molecular Spectra and Molecular Structure IV. Constants of Diatomic Molecules</u> (Van Nostrand Reinhold Co., N.Y. 1979).

2) A. Sur, C.V. Ramana and S.D. Colson, J. Chem. Phys. <u>83</u>, 904(1985).

3) A. Sur, C.V. Ramana, W.A. Chupka and S.D. Colson, J. Chem. Phys. <u>84</u>, 69(1986).

4) D.C. Cartwright, W.J. Hunt, W. Williams, S. Trajmar and W.A. Goddard, III Phys. Rev. A <u>8</u>, 2436(1973).

5) S. Trajmar, D.C. Cartwright and R.I. Hall, J. Chem. Phys. <u>65</u>, 5275(1976).

6) W.J. van der Zande, W. Koot, J.R. Peterson and J. Los, Chem. Phys. Letters <u>140</u>, 175(1987) and references therein.

7) J.N. Bardsley and M.A. Biondi, Adv. At. Mol. Phys. <u>6</u>, 1(1970).

8) S.L. Guberman, in <u>Physics of Ion-Ion and Electron-Ion Collisions</u>, (ed. by F. Brouillard, Plenum, New York, 1983), p167.

9) M.J. Seaton, Proc. Phys. Soc. (London) <u>88</u>, 801(1966) and references therein.

10) U. Fano, J. Opt. Soc. Am. <u>65</u>, 979(1975) and references therein.

11) P.H. Krupenie, J. Phys. Chem. Ref. Data, <u>1</u>, 423(1972).

12) R.P. Saxon and B. Liu, J. Chem. Phys. <u>67</u>, 5432(1977); <u>73</u>, 870(1980); <u>73</u>, 876(1980).

13) H.H. Michels, in Advances in Chemical Physics, ed. by J. Wm. McGowan (Wiley, New York, 1981). Vol. XLV.

14) R.J. Buenker and S.D. Peyerimhoff, Chem. Phys. Letters <u>34</u>, 225(1975).

15) J. Wang, A.J. Blake and L. Torop, J. Chem. Phys. 39, 4654(1988).

16) For instance M.N.R. Ashfold, J.M. Bayley and R.N. Dixon, Chem. Phys. 84, 35(1984); Ber. Bunsenges. Phys. Chem. 89, 254(1985), and references therein.

17) A. Cohn, J. Chem. Phys. 57, 2456(1976).

18) For example: W.E. Conaway, R.J.S. Morrison and R.N. Zare, Chem. Phys. Lett. 113, 429(1985).

19) W.A. Chupka, J. Chem. Phys. 87, 1488(1987).

20) V. McKoy, (to be published).

21) J.A. Stephens, M. Braunstein and V. McKoy, J. Chem. Phys. 89, 3023(1988).

22) J.L. Dehmer, D. Dill and A.C. Parr, in Photophysics and Photochemistry in the Vacuum Ultraviolet ed. by S. Mc Glynn, G. Findley and R. Huebner (D. Reidel Publ Co., Dordrecht, Holland, 1983).

Dynamics and spectroscopic manifestations of two-photon bound–bound absorption through a repulsive intermediate state

Leping Li, Robert J. Lipert, Haiyoon Park, William A. Chupka, and Steven D. Colson

Sterling Chemistry Laboratory, Yale University, New Haven, Connecticut 06511

The work by Heller et al.[1] on the time-dependent theory of Raman scattering provides a simple physical picture which separates the static effect due to the coordinate dependence of the electronic transition dipole, from the dynamic effects that arise from wave packet propagation on the Born–Oppenheimer surfaces. These concepts have been aptly applied by Kinsey and his co-workers to the study of emission spectroscopy of dissociating molecules as a means of probing details of dynamics in extremely short-lived species.[2]

Both the theory and experiment can be extended to two-photon absorption between two bound states through a repulsive intermediate state, since Raman scattering is just a special case of a two-photon process. In this extension, the wave packet dynamics on the repulsive potential surface will be probed by projection of the evolving wave packet into the discrete levels of an excited, instead of ground, state. At the

same time, the wave packet propagation on the repulsive potential surface will enable us to obtain information about excited bound states in regions which are normally inaccessible due to unfavorable Franck–Condon factors.

To apply this idea we have recently carried out an experiment on the Cl_2 molecule by a $2 + 1$ multiphoton ionization process in which the first photon falls into a fairly strong repulsive continuum but far from any effective bound transfer state. A detailed spectroscopic analysis will be given in a separate paper.[3] Here we focus on the role of the repulsive state as an intermediate in a two-photon, bound–bound transition, and illustrate a conceptually intuitive connection between the spectroscopic features and the underlying wave packet dynamics on the repulsive potential surface.

The experiment was performed in a time-of-flight mass spectrometer under collision-free conditions in a cw free jet of a 1% Cl_2/He gas mixture. The molecular beam was
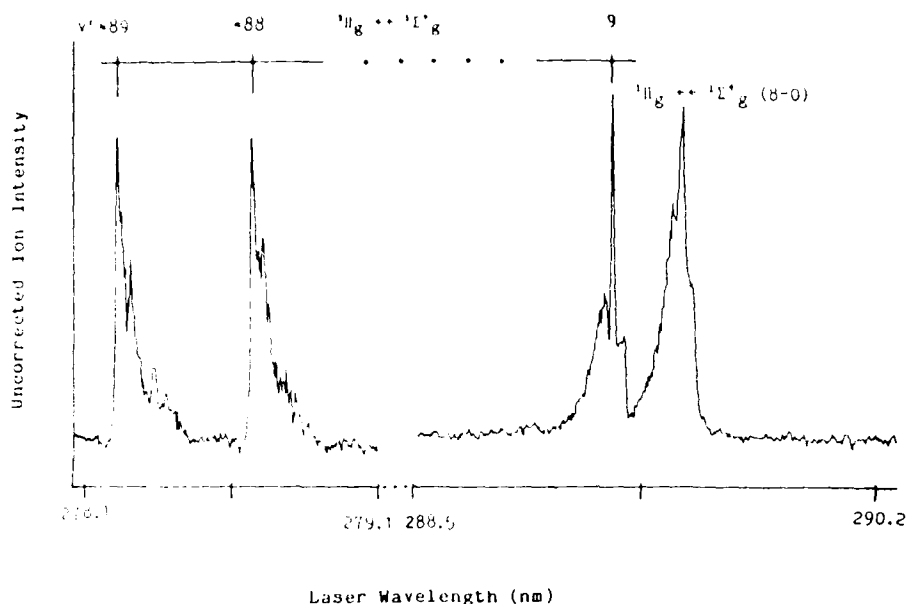
FIG. 1. $2 + 1$ multiphoton ionization spectrum of $^{72}Cl_2$ molecule to vibronic levels below and above the double-well barrier of the $^3\Pi_g$ state. Notice that the red (blue) shaded bands correspond to transitions to above (below) barrier levels. The observation of the highly excited vibronic states is made possible through a repulsive state at the one photon energy.

crossed by the tunable doubled output of a YAG-pumped dye laser of 8 ns pulse width, and approximately 1 cm^{-1} bandwidth.

The MPI spectra of chlorine exhibit two very long vibronic progressions. One of them is assigned to the $^1\Pi_g \leftarrow \leftarrow X\,^1\Sigma_g^+$, and the other to the $^3\Pi_g \leftarrow \leftarrow X\,^1\Sigma_g^+$ two-photon transitions. In the limited wavelength region scanned at present, the observed singlet progression extends from $v' = 0$ to $v' = 15$ with only moderately decreasing intensity and the triplet progression extends to $u' > 100$ since the top of the double well barrier of $^3\Pi_g$ lies near $v' = 75$.[4] The appearance of these astonishingly long progressions is obviously due to the presence of a repulsive state at the one-photon energy since 100 eV inelastic electron scattering data,[5] which should represent the Franck–Condon factors between the ground and excited states, show a very strong decrease in relative intensity from a maximum at $v' = 2$ to undetectable values for $v' > 6$.

For the long $^3\Pi_g \leftarrow \leftarrow X\,^1\Sigma_g^+$ progression, one expects to see a dramatic change of the spectral profiles for levels below and above the barrier due to the change of rotational constant from a value somewhat larger to one much smaller than that of the ground state. Thus transitions to (inner well) levels below the barrier should give blue shaded profiles while levels above the barrier ought to yield strongly red shaded profiles. This is exactly what we have observed. As shown in Fig. 1, the blue shaded profile corresponding to $v' = 9$ is in marked contrast to the red shaded profiles for $v' \approx 88$ and 89 of the $^3\Pi_g \leftarrow \leftarrow X\,^1\Sigma_g^+$ progression. The essential physical features of this two-photon, bound–repulsive–bound absorption process can be viewed in the spirit of the established time-dependent semiclassical quantum theory.[1,2] At $t = 0$, the wave packet on the repulsive potential is the initial ground state vibrationless wave function prepared by one-photon excitation. It has vanishingly small Franck–Condon overlap with the excited bound state beyond the

vertical region. No longer in the stationary state, it evolves in time and moves on the excited repulsive surface. Along the direction of motion, the wave packet will sequentially develop significant overlap with higher and higher stationary eigenfunctions in the upper bound states. The time evolution is determined by the shape of the potential and the position of the wave packet at $t = 0$. Typically, short-time behavior is dominated by forces $(\partial V/\partial R)$, and the spreading of the packet is governed by second derivatives $(\partial^2 V/\partial R^2)$.[2] Since the second photon absorption into the excited bound state depends critically upon the local Franck–Condon overlap, two-photon absorption through a repulsive intermediate state is a very sensitive probe of the change of the wave packet position and shape due to its evolution on the repulsive potential. At the same time, this enables us to probe highly excited vibronic levels which are otherwise inaccessible due to the very small Franck–Condon overlap. Thus, the observation of the two unusually long progressions is merely a spectroscopic manifestation of the wave packet dynamics on the repulsive potential and its subsequent excitation by the second photon absorption into the discrete levels of the excited bound state that have the correct energy and right Franck–Condon overlap at a given time during the laser pulse.

Although our interpretation parallels that given by Kinsey et al.[2] the spectroscopic information obtained in the two sets of experiments are quite different. In our case the wave packet is projected onto an excited bound state by absorption of the second photon and detected by subsequent one-photon ionization. This has the advantage that spectroscopic information can be obtained on numerous excited states in regions far from the ground state equilibrium position (rather than just the ground state). A further advantage of this method stems from the very high detection efficiency of mass-selected ion signals, in contrast with the difficulty of detecting the small number of photons emitted by a very

38

short-lived ($\ll$ 1 ps) molecule. In addition, the bound–repulsive–bound, two-photon excitations can be made to compete more effectively with photodissociation by increasing the probe laser intensity, an advantage similar to that of the stimulated emission pumping.[6] However, the vibronic intensities observed in emission are simpler to analyse than those in MPI. The latter result from a convolution of absorption and ionization cross sections.

In conclusion, we have demonstrated experimentally that the study of two-photon, bound–bound transitions through an intermediate continuum is an effective way to obtain spectroscopic information on highly excited states in normally inaccessible regions, and in principle can provide an alternative method for probing the dynamics of dissociating molecules. Also the potential surface of the ground state is usually better known than those of excited states.

[1] S. Y. Lee and E. J. Heller, J. Chem. Phys. **71**, 4777 (1979).

[2] D. Imre, J. L. Kinsey, A. Sinha, and J. Krenos, J. Phys. Chem. **88**, 3954 (1984), and references therein.

[3] L. Li, R. J. Lipert, W. A. Chupka, and S. D. Colson (in preparation).

[4] J. Fournier, F. Salama, and R. J. LeRoy, J. Phys. Chem. **89**, 3530 (1985).

[5] R. J. Stubbs, T. A. York, and J. Comer, J. Phys. B **18**, 3229 (1985).

[6] C. E. Hamilton, J. L. Kinsey, and R. W. Field, Annu. Rev. Phys. Chem. **37**, 493 (1986).

Observation of strong Rydberg–valence mixing in the $E\,{}^3\Sigma_u^-$ state of O_2 by 3+1 MPI photoelectron spectroscopy

Paul J. Miller, Leping Li, William A. Chupka, and Steven D. Colson

Sterling Chemistry Laboratory, Yale University, New Haven, Connecticut 06511

The photoelectron spectrum (PES) of the $E\,{}^3\Sigma_u^-$ state of O_2 has been measured with 3 + 1 multiphoton ionization (MPI). The observed vibrational progression in the *PE* spectrum is interpreted as due to ionization from a $(3p\pi)^3\Sigma_u^-$ Rydberg state which is strongly mixed with the $(\pi_u\,{}^3\pi_g^3)B\,{}^3\Sigma_u^-$ valence state. The observation of this mixing is in near agreement with the calculation by Buenker *et al.*

I. INTRODUCTION

In recent studies, the lowest two Rydberg states of oxygen, $(3s\sigma)^1\Pi_g$ and ${}^3\Pi_g$, have been identified and some molecular parameters measured by two-photon resonant three-photon ionization.[1,2] These two states are well behaved, predominantly single-configuration Rydberg states, and by far the strongest peak in the respective photoelectron spectra corresponds to $\Delta v = 0$ in the ionization step. More recently, we have extended our investigation to states of higher energy. In this region of energy the spectroscopy, level structure, configuration description, and state assignments become more complicated and difficult. The major cause of this state of affairs is the extensive occurrence of Rydberg–valence interactions of widely varying strengths, often resulting in such strongly avoided crossings as to yield drastically distorted adiabatic potential curves. The resulting rotational and vibrational level structures are quite different from those of the ion and the corresponding photoelectron spectra cannot be analyzed in terms of a simple diabatic description of the potential curves. One of these examples is the so-called "longest band," whose upper state was initially assigned to the $v' = 1$ level of the $(3p\pi)E\,{}^3\Sigma_u^-$ Rydberg state by Ogawa *et al.*[3] on the basis of its isotopic shift. Subsequent theoretical calculations[4,5] have shown that the E state potential curve is formed by a very strongly avoided crossing, yielding an unusually shaped potential curve and an anomalous isotope shift. These calculations strongly support the assignment of the "longest band" to the $E \leftarrow X(0-0)$ transition.

In this paper, we report the measurement of the photoelectron spectrum of the $E\,{}^3\Sigma_u^-$ state which was resonantly populated by three-photon excitation, and probed by a fourth photon ionization at a wavelength of 373.12 nm. The photoelectron spectrum of the $(3p\pi)E\,{}^3\Sigma_u^-$ Rydberg state shows strong evidence for mixed Rydberg–valence character. Our observation and analysis agree well with the identification of the upper state of the longest band as a strongly mixed Rydberg–valence state as predicted by Buenker *et al.*[4,5] The relative band intensities of the photoelectron spectrum can also be rationalized in terms of their calculation.

II. EXPERIMENTAL

The 3 + 1 resonance enhanced multiphoton ionization (REMPI) experiment was performed using a XeCl excimer

pumped dye laser (Questek 2240, Lambda Physik FL2002) with a pulse width of approximately 8 ns and a repetition rate of 11 Hz. The photoelectron spectrum of the E state at 80 404.01 cm^{-1} was obtained through three-photon excitation using QUI dye. The output of the dye laser had a pulse energy of 1 mJ and was focused with a 3 in. lens into the ionization region (about 5 mm from an effusive nozzle) in a "magnetic bottle" time-of-flight photoelectron spectrometer.[6] The electrons were detected and amplified by multichannel plates mounted at the end of a 50 cm flight tube and fed into a transient digitizer (Tektronix 7612D) interfaced to an LSI11/23 computer for electron kinetic energy analysis and signal averaging. The resulting PE spectrum contained an average of 10 000 laser shots and had an experimental resolution of ≈ 15 meV for the lowest energy peak.

III. RESULTS AND DISCUSSION

The measured photoelectron spectrum, seen in Fig. 1, shows increasing electron intensities from $v^+ = 0$ to 3, and very much lower intensity for $v^+ = 4$ (see Table I). This result contrasts sharply with the photoelectron spectra of the $3s\sigma$ Rydberg states which are only slightly perturbed and conform strongly to the $\Delta v = 0$ selection rule expected for unperturbed Rydberg states.[7] This expectation is based on the fact that an ion in a specific electronic state and the well-described Rydberg state with that specific ion core have nearly identical potential curves in the region of small nuclear displacements. The Franck–Condon principle then leads to an intensity maximum at $\Delta v = 0$ for all vibrations in one-photon ionization. However, according to the large scale *ab initio* calculations on the $E\,{}^3\Sigma_u^-$ state of molecular oxygen (which include extensive configuration interaction), one expects to see departures from v-conserving photoionization from this state. This is the case since the diabatic $(3p\pi)^3\Sigma_u^-$ Rydberg and the $(\pi_u\,{}^3\pi_g^3)^3\Sigma_u^-$ valence states undergo strong configuration interaction (0.98 eV minimal splitting at ≈ 2.28 bohr) resulting in two adiabatic potential curves. The equilibrium internuclear distance of the bound potential curve ($r_e = 1.206$ Å) is considerably greater than that of the $X\,{}^2\Pi_g$ state of O_2^+ ($r_e = 1.1164$ Å), giving rise to intense peaks corresponding to $\Delta v \neq 0$ transitions.

However, it has been shown[8] that anomalous photoelectron spectra of unperturbed Rydberg states can sometimes
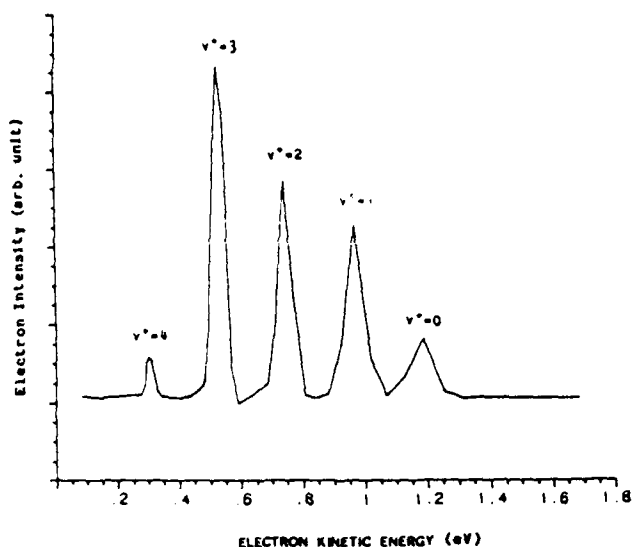
FIG. 1. The three-photon resonance enhanced one-photon ionization photoelectron spectrum of the longest band of O_2 at 373.12 nm. In the present one color experiment, the highest energetically accessible vibrational quantum number of O_2^+ in its $X^2\Pi_g$ state is 4. Partial photoelectron spectra taken at higher resolution clearly resolve the spin–orbit splitting of the O_2^+ ground state (≈ 200 cm^{-1}) for each vibrational level.

TABLE I. Relative Franck–Condon factors.

$v^+ - v'$	Experimental
0–0	1
1–0	2.11
2–0	2.26
3–0	3.16
4–0	0.38

result from photoexcitation of the ion core followed by autoionization of the doubly excited state produced. This situation is extremely unlikely in the present case, since the nearest allowed absorption by the bare ion core is about 13 730 cm^{-1} above the photon energy (26 337 cm^{-1}) used in this experiment. While the position of the doubly excited state is only crudely estimated by this procedure, the error (at the internuclear distance of concern here) is very unlikely to be of the magnitude to invalidate our qualitative analysis.

The gross features of the observed photoelectron spectra can be discussed by reference to Fig. 2. This figure shows the potential curves calculated by Buenker et al. together with the relevant vibrational wave functions. The energy levels are taken from Huber and Herzberg.[9] For the present semiquantitative purpose, harmonic oscillator wave functions are used for O_2^+. An approximate wave function for the $v = 0$ level of the E state was calculated by a perturbation technique. The Franck–Condon region is shown by vertical lines. The center line indicates the position of the maximum of the wave function. It should be noted that this maximum is shifted from the potential minimum to a larger value of the internuclear distance, due to the very asymmetric shape of the potential curve. A careful examination of the figure shows that the Franck–Condon factor will increase from $v^+ = 0$ to a maximum at either $v^+ = 2$ or 3 then decrease considerably for $v^+ = 4$.

In order to make a quantitative comparison with the experimental data, a detailed calculation is necessary making full use of both experimental parameters and the ab initio vibrational wave functions computed by Buenker et al. In addition it is important to take into account the variation of the transition moment to the ionization continuum with internuclear distance. This factor is normally negligible for a

pure Rydberg state. However, the E state is a mixture of the $\pi_u^3\,\pi_g^3$ and the $\pi_u^4\,\pi_g\,3p\pi_u$ configurations in which the coefficients of the valence and the Rydberg components vary rapidly with internuclear distance, especially near the potential minimum. Furthermore, the photoelectron spectrum mainly arises from the photoionization of the Rydberg component, since the formation of the $\pi_u^4\,\pi_g\,X^2\Pi_g$ state of O_2^+ by direct ionization would require a two electron jump from the $\pi_u^3\,\pi_g^3$ configuration of the valence component. Therefore, an accurate calculation of the photoelectron intensities must take account of this factor. The semiquantitative behavior of the Rydberg character of the E state as a function of internuclear distance is shown in Fig. 2(F). (The calculation used a two-level model[10] with the calculated[4] interaction matrix element $W_{12} = 0.49$ eV. Separations of the unperturbed levels were estimated from Fig. 1 of Ref. 4.) The consequence of the introduction of this factor is equivalent to a further outward shift and distortion of the $v' = 0$ wave function of the E state.

We note that according to Buenker et al. this valence state also contains a considerable amount of the secondary configuration $(3\sigma_g\,1\pi_u^4\,1\pi_g^2\,3\sigma_u)$. This configuration still requires a two-electron jump for ionization. High photoionization probability for such configurations could only occur by one-electron excitation to a still higher autoionizing valence state. An examination of the calculations of Michels[11] shows no such optically allowed state in this energy region.

We also note that if the original assignment by Ogawa of the longest band to the (1–0) transition is correct, then the Franck–Condon factors calculated for ionization of $v' = 1$ of the E state will be very different from those calculated for $v' = 0$. A cursory examination of the Franck–Condon overlaps indicates that the maximum will likely occur at $v^+ = 3$. However, the Franck–Condon factors for the other values of v^+ will deviate significantly from our experimental data. Also, this possibility seems unlikely in light of the high quality of the ab initio calculations by Buenker et al.

In this experiment we only see transitions from the $v' = 0$ of E state to levels of $^2\Pi_g$ state with v^+ less than or equal to 4 since our four-photon energy is only 685 cm^{-1} above the $v^+ = 4\,^2\Pi_g$ threshold. However, it is possible to produce ions with v^+'s larger than 4 in a two-color experiment where part of the photoionization can be carried out by photons of higher energy.

We have also carried out wavelength scans of the "longest band" in a supersonically cooled beam with both linearly and circularly polarized light. While the spectra were rotationally collapsed compared to room temperature, no
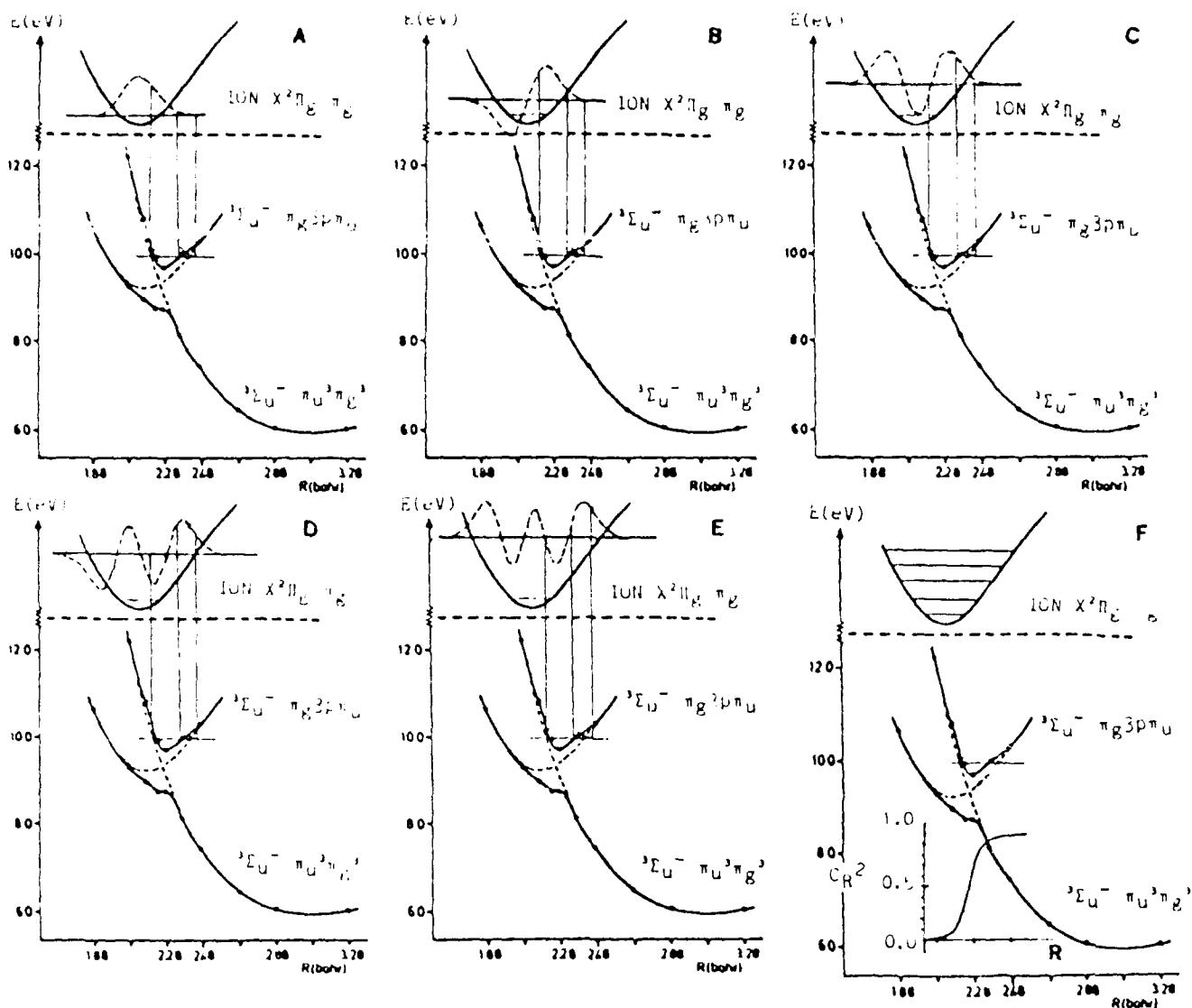
J. Chem. Phys., Vol. 88, No. 5, 1 March 1988

41

FIG. 2 Adiabatic potential curves calculated by Buenker *et al.*, together with vibrational wave functions of O_2^+ for $v'' = 0-4$. The outer vertical lines show the Franck-Condon region. The center line indicates the position of the effective maximum of the $E\,v' = 0$ wave function corrected for the variation of Rydberg character with internuclear distance. This variation is shown in (F) and discussed in the text.

distinct rotational structure was resolved and no discernible difference was observed between the spectra obtained using the two polarizations. In addition, wavelength scans were also carried out in the photoelectron spectrometer by monitoring simultaneously each of the photoelectron bands of Fig. 1. Again all scans yielded identical band shapes and energy positions within experimental error. From these observations, it seems virtually impossible that the observed band might be a composite[13] of more than one transition to closely lying intermediate states, each with its own characteristic photoelectron spectrum.

IV. CONCLUSION

3 + 1 resonance enhanced MPI-PES via $E\,^3\Sigma_u^-$ state shows all vibrational excitations of the ground state of O_2^+ that are accessible by the ionizing photon energy. This ob-

served spectral behavior in the PES is shown to arise via one particular intermediate Rydberg state with strongly mixed valence character, the upper state of the so-called longest band. At internuclear distances relevant for optical absorption, the extensive mixing manifests itself in the photoelectron spectrum. Our data clearly show that as calculated by Buenker *et al.*, the potential curve of the E state is very strongly distorted from that of an unperturbed $3p\pi\,^3\Sigma_u^-$ Rydberg state and that an adiabatic description of its potential curve is more appropriate in the spectroscopic analysis of this state.

ACKNOWLEDGMENTS

A. Sur, C. V. Ramana, and S. D. Colson, J. Chem. Phys. **83**, 904 (1985).

A. Sur, C. V. Ramana, W. A. Chupka, and S. D. Colson, J. Chem. Phys. **84**, 69 (1986).

M. Ogawa, K. R. Yamawaki, A. Hashizume, and Y. Tanaka, J. Mol. Spectrosc. **55**, 425 (1975).

R. J. Buenker and S. D. Peyerimhoff, Chem. Phys. Lett. **34**, 225 (1975).

R. J. Buenker, S. D. Peyerimhoff, and M. Perić, Chem. Phys. Lett. **42**, 383 (1976).

P. Kruit and F. H. Read, J. Phys. E **16**, 313 (1983).

S. Katsumata, K. Sato, Y. Achiba, and K. Kimura, J. Electron Spectrosc. Relat. Phenom. **41**, 325 (1986).

W. A. Chupka, J. Chem. Phys. **87**, 1488 (1987).

K. P. Huber and G. Herzberg, *Molecular Spectra and Molecular Structure, Vol. IV. Constants of Diatomic Molecules* (Van Nostrand Reinhold, New York, 1979).

G. Herzberg, *Molecular Spectra and Molecular Structure I. Spectra of Diatomic Molecules* (Van Nostrand Reinhold, Princeton, NJ, 1950), pp. 282–4.

H. H. Michels, in *Advances in Chemical Physics*, edited by J. Wm. McGowan (Wiley, New York, 1981), Vol. XLV.

J. B. Pallix, P. Chen, W. A. Chupka, and S. D. Colson, J. Chem. Phys. **84**, 5208 (1986).

43

Spectroscopy and photophysics of $^1\Pi_g$ and $^3\Pi_g$ Rydberg, ion-pair states of Cl₂, revealed by multiphoton ionization

Leping Li, Robert J. Lipert, Haiyoon Park, William A. Chupka, and Steven D. Colson

Sterling Chemistry Laboratory, Yale University, New Haven, Connecticut 06511

Mass-resolved, two-photon resonant, three-photon ionization of jet-cooled Cl₂ has been used to study the spectroscopy and photophysics of the lowest energy, double-well $^1\Pi_g$ and $^3\Pi_g$ states of mixed Rydberg ($4s\sigma$) and ion-pair character. Inner well levels from $v' = 0$ ($64\,027$ cm^{-1}) to $v' = 15$ ($73\,343$ cm^{-1}) have been observed for $^1\Pi_g$ of the mass 70 molecular chlorine isotope. Inner well levels for $^3\Pi_g$ have been observed from $v' = 0$ at $63\,472$ cm^{-1} to the top of the barrier, and well beyond that to levels spanning both wells. Observation of these long progressions is attributed to excitation via a repulsive continuum at a well-phonon level. The photophysics of this latter process as well as the mechanism for copious atomic ion formation are discussed. Variation of linewidth with vibrational quantum number due to the predissociation of inner well levels is observed and attributed to repulsive valence states. The data are in good agreement with the theoretical calculations of Peyerimhoff and Buenker, and Tuckett and Peyerimhoff.

I. INTRODUCTION

Although a large number of conventional spectroscopic investigations have been carried out on molecular chlorine,[1–7] characterization of the electronically excited gerade states remains very limited and poor. This situation is primarily due to the fact that excitation of these states by single-photon absorption from the ground state is forbidden but also partly due to the complication resulting from strong Rydberg-valence and ion-pair state interactions, and the difficulty of working with such a corrosive gas. While conventional spectroscopy has produced significant information on the optically allowed ungerade states, only recently has multiphoton spectroscopy and inelastic electron scattering yielded some useful information on the g states. The outer well of the lowest bound g states, the $E(0_g^+)$ and $f(0_g^+)$ states, have been investigated by stepwise (two-color) two-photon excitation.[8–10] However, the inner well (with $4s\sigma$ Rydberg character) of the state, $^3\Pi_g$ in Hund's case (a) notation, and that of the related $^1\Pi_g$ state, have been investigated only by the relatively low resolution technique of inelastic electron scattering,[11–13] in which isotope effects require isotopically pure samples or can barely be measured due to inadequate resolution.

All recent studies of Cl₂ have benefited enormously from the high quality *ab initio* calculations of Peyerimhoff and Buenker.[3] Their calcualtions have convincingly demonstrated the importance of Rydberg-valence interactions, which often result in double-well potential curves with apparently anomalous vibrational frequencies, and vibrational level-dependent predissociations and Franck–Condon factors. Of particular relevance to the present study is the detailed shape of the $^1\Pi_g$ potential curve and the strength of the interaction of the Rydberg potential curve with that of the repulsive $\pi_u \rightarrow \sigma_u$ valence state in the inner well. The appearance of the multiphoton ionization (MPI) spectrum will depend very sensitively on the strength of this interaction which will determine whether an adiabatic or diabatic approximation is more appropriate.

Part of the purpose of this experiment was to measure accurately the energies of the vibrational levels with amplitudes predominantly in the inner wells of the $^1\Pi_g$ and $^3\Pi_g$ states, to determine the barrier height for the $^3\Pi_g$ state, and to study the photophysics of the atomic ion production in the multiphoton process.

II. EXPERIMENTAL

A mixture of 1.0% Cl₂ (with natural isotopic abundance) in He (CryoDyne Specialty Gases) was expanded cw through a 25 μm nozzle at a backing pressure of 3 atm into a vacuum chamber maintained at 1.0×10^{-4} Torr. Approximately 1 mm from the nozzle the gas jet produced by free expansion intersected a laser beam from the frequency doubled UV output of a Nd:YAG pumped dye laser (Quanta-Ray DCR-2, PDL) focused with a 6 in. lens. The laser bandwidth was around 0.3 cm^{-1}. The resulting photoions were accelerated into a time-of-flight mass spectrometer by a repelling field of 300 V/cm. The ion signals in mass channels 35, 37, 70, 72, and 74 were monitored as a function of wavelength. The resulting mass spectra varied greatly with wavelength according to the identity of the two-photon resonant state. A typical set of mass spectra at different wavelengths is shown in Fig. 1. The resulting MPI spectra (not corrected for variations in laser output across the dye tuning curves) are shown in Fig. 2. The data of Fig. 2 were taken with the nozzle at room temperature. In order to identify vibratio al "hot bands", the spectrum from 308.1 to 318.3 nm was also taken with nozzle heated to about 1000 °C.

III. RESULTS AND DISCUSSION

The mass spectra in Fig. 1 are recorded at three different wavelengths, each corresponding to a resonance of one isotope of Cl₂. It is obvious that the atomic ion signal in mass channels 35 and 37 are well correlated with their precursors in the molecular channel. Indeed the MPI spectra of both atomic ions are superpositions of those of their precursors.
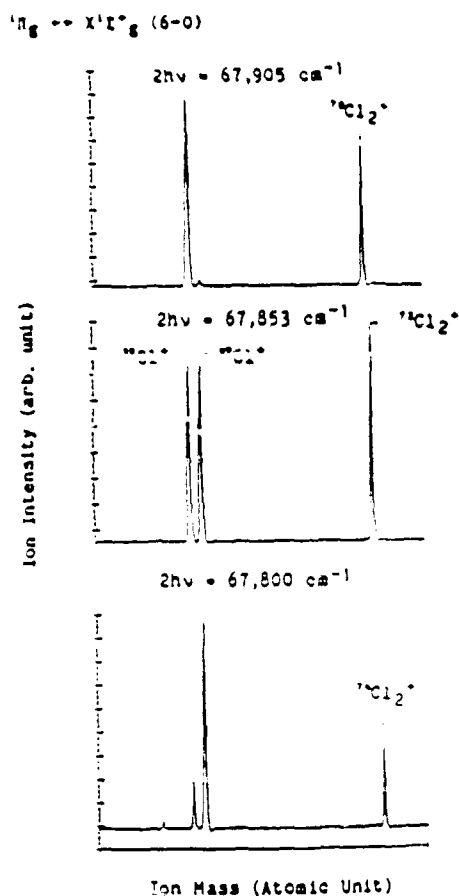
$^1\Pi_g \leftarrow X^1\Sigma^+_g$ (6-0)

FIG. 1. Time-of-flight mass spectra of chlorine. From the top to the bottom, the two-photon excitation energies corespond to the resonances of $^{70}Cl_2$, $^{72}Cl_2$, and $^{74}Cl_2$, respectively. The atomic chlorine ions of masses 35 and 37 are attributed to the one-photon dissociation of the ground state molecular ions of various chlorine isotopes (see the text for detailed discussions).

FIG. 2. MPI spectra of molecular($^{70}Cl_2$) and atomic(^{35}Cl) chlorine. The long progressions of transitions to both singlet and triplet Π states are due to the one-photon excitation of ground state wave packet to the repulsive state and its subsequent evolution on that potential curve. The bands which have very small vibrational frequencies (≈ 120 cm^{-1}) and are shaded towards the red are attributed to the two-photon excitations to the levels above the double well barrier of the $^3\Pi_g$ state.

demonstrating clearly the power of the MPI mass spectrometry technique for separating the isotope effects and observing photodissociation, the physics of which will be discussed later.

As pointed out before, the MPI spectra, in Fig. 2 were recorded simultaneously for ion mass 35, 37, 70, 72, and 74. In the mass 70 MPI spectrum, the most intense feature is a regular vibrational progression which is readily assigned to the inner well of the two-photon allowed ($4s\sigma$) $^1\Pi_g$ Rydberg state since the measured excited state vibrational frequency (≈ 654 cm^{-1} for lowest v) is very close to that of the $X\,^2\Pi_g$ state of the Cl$_2^+$ ion (≈ 645 cm^{-1}). The high degree of regularity of this progression and the near equality of its frequency with that of the ion provide strong evidence that a diabatic description is more appropriate than an adiabatic one for the inner well Rydberg-valence interaction calculated by Peyerimhoff and Buenker.[3]

Another interesting feature in the spectrum, especially apparent in the atomic ion channel, is a nice progression with very low vibrational spacings (≈ 120 cm^{-1}), with bands all shaded very strongly to the red and imbedded in the more intense high frequency progression assigned to the inner well ($4s\sigma$)$^1\Pi_g$. The very low vibrational frequency and very
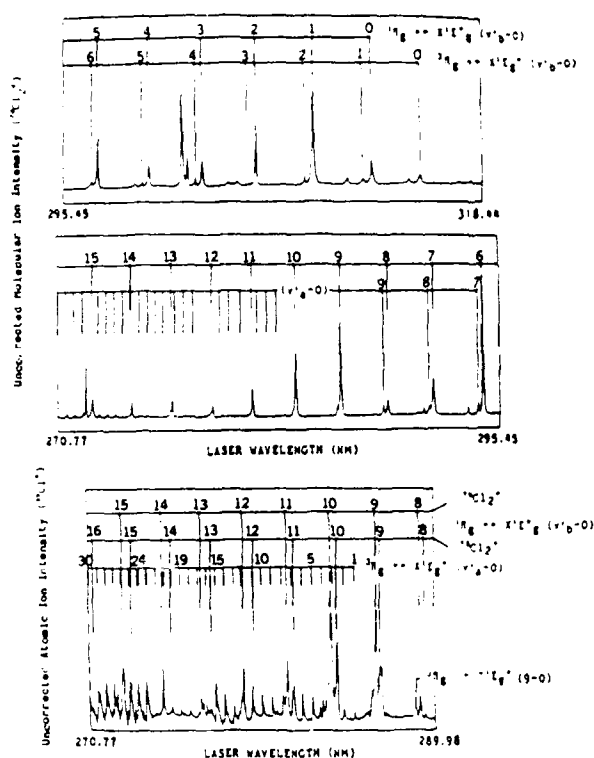
small rotational constant strongly suggest that the two-photon excited vibrational levels lie above the barrier of the double well associated with the $^3\Pi_g$ potential curve.

Although the rotational lines are not resolved in this work, we do expect some variation in the linewidth since all these levels are crossed by a repulsive curve, and will be predissociated to some extent. The spectra in Fig. 3 correspond to a certain portion of the spectrum in Fig. 2, but were taken at reduced laser intensity and in the lower molecular beam density region. It is clear that considerable rotational cooling has been attained, and ac Stark broadening has been minimized. From the spectra, we can establish an upper limit to the width due to predissociation, and locate the vibrational levels where predissociation is most strong due to the favorable Franck–Condon overlap between the bound ($4s\sigma$) Rydberg state and the repulsive ($\pi_u \to \sigma_u$) valence state. Other features in the spectra of Fig. 3 are also valuable in our overall spectral analysis and will be discussed later in this paper.

A. $^{1,3}\Pi_g$

According to Peyerimhoff and Buenker,[3] the unperturbed ($\pi_g \to 4s$)Π_g Rydberg state interacts with the repulsive 1 $^1\Pi_g$($\pi_u + \sigma_u$) valence state at very small internuclear distances and with the ion-pair valence state at large internuclear distance (see Figs. 3, 10, and 12 of Ref. 3), resulting in
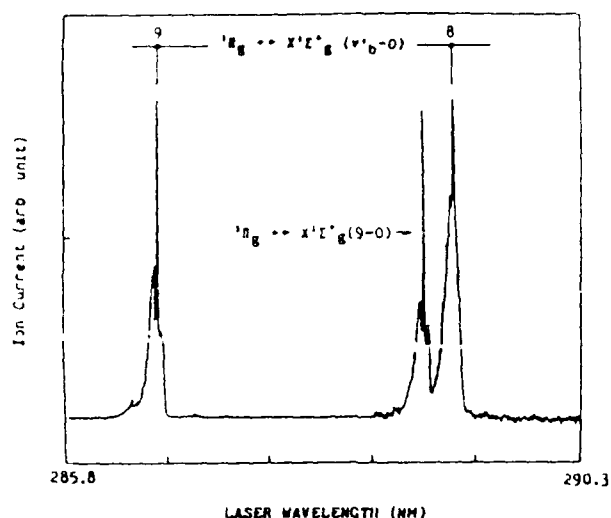
FIG 3 Part of the spectrum of ⁷⁰Cl₂ isotope taken at low laser power and in the most expanded region of the molecular beam The spectrum clearly exhibits the change of width due to the predissociation as a function of vibrational quantum number It also reveals the close similarity of the band contours of the transitions ³Π_g ← X ¹Σ_g⁺ and the ¹Π_g ← X ¹Σ_g⁺ The intense Q branch observed at low temperature is characteristic of two-photon Ω = 0 → Ω = 1 transitions of diatomic molecules.

TABLE I. Observed two-photon transition energies of the inner-well levels of the ¹Π_g and ³Π_g ion-pair states.

v'_i	Progression I (cm⁻¹) $^1\Pi_g \leftarrow X\,^1\Sigma_g^- (v'' = 0)$			Progression II (cm⁻¹) $^3\Pi_g \leftarrow X\,^1\Sigma_g^- (v'' = 0)$
	⁷⁰Cl₂	⁷²Cl₂	⁷⁴Cl₂	⁷⁰Cl₂
0	64 027	64 021	64 021	63 472
1	64 681	64 673	64 659	64 126
2	65 332	65 312	65 294	64 785
3	65 986	65 958	65 929	65 430
4	66 640	66 601	66 562	66 074
5	67 270	67 234	67 184	66 723
6	67 905	67 853	67 800	67 354
7	68 534	68 474	68 412	67 979
8	69 220	69 149	69 082	68 650
9	69 779	69 702	69 624	69 220
10	70 392	70 307	70 223	
11	70 998	70 906	70 812	
12	71 600	71 501		
13	72 187	72 081	71 970	
14	72 771	72 658	72 546	
15	73 343	73 227	73 106	

a rather complex asymmetric double well potential. In the energy region covered by this MPI experiment, the vibrational levels of the outer well have very unfavorable Franck–Condon factors directly with the ground state, as well as extremely low photoionization efficiencies. However we note that the first photon of the two-photon resonant process actually falls in a continuum primarily due to the repulsive $C\,^1\Pi_u$ state. This situation could result in significant excitation to outer-well levels which could best be detected by fluorescence. Nevertheless no such detection was attempted in our present experiment.

The origin of the $^1\Pi_g$ state has been determined crudely by Spence et al. (7.939 eV)[12] and by Stubbs et al. (7.946 eV)[13] by inelastic electron scattering. An earlier work by Jureta et al.[11] was reinterpreted by Spence et al. to give a value of 7.95 eV. Only Stubbs et al. had sufficient resolution (18 meV FWHM) to resolve bands well enough to give fairly good vibrational intervals. We assign the origin to the band at 64 027 cm⁻¹ (7.9384 eV) for the ³⁵Cl³⁵Cl isotope. Tables I and II give the energies for all the observed vibronic levels of inner well $^1\Pi_g$ and $^3\Pi_g$ states, and levels above the double-well barrier of the $^3\Pi_g$ state.

One problem associated with identification of the origin is the possibility that some of the bands in the region of origin may be hot bands. In fact, the reinterpretation by Spence et al.[12] involved reassignment of the origin band of Jureta et al.[11] as a hot band. We find the assignment of Spence et al. to be correct. We also identify hot bands, not only by precise position measurement, but also from the results of the heated-nozzle experiment.

At room temperature about 3% of Cl₂ is the $v'' = 1$ state, and one might expect very weak hot bands, especially with supersonic jet cooling. Nevertheless, a series of weak bands is observed and assigned to transitions originating

from $v'' = 1$ level because they show a constant frequency shift from the corresponding series built upon the origin. Although we have strong rotational cooling, apparently we have little vibrational cooling, as is very often the case. However the observed hot bands are more intense than expected from 3% population of $v' = 1$ level. Consideration of the potential curves of Cl₂ in the ground state ($r_e = 1.8915$ Å)

TABLE II. Observed energies of the above barrier levels of the double-well, $^3\Pi_g$ ion-pair state of chlorine molecules.

v'_u	$^3\Pi_g \leftarrow X\,^1\Sigma_g^- (v'' = 0)$ (cm⁻¹)
1	70 074
2	70 219
3	70 366
4	70 510
5	70 648
6	70 788
7	70 929
8	...
9	71 211
10	71 347
11	71 493
12	71 629
13	71 759
14	71 875
15	72 007
16	72 136
17	72 263
18	72 394
19	72 518
20	72 645
21	...
22	72 888
23	73 016
24	73 140
25	73 259
26	...
27	73 492
28	73 617
29	73 733
30	73 851

and in the 4s Rydberg state (r_e) of the $Cl_2^+ = 1.988$ A) indicates that the Franck–Condon factor for the 1–0 hot band is considerably larger than that for the 0–0 transition. Analysis of high temperature data taken from 308.1 to 318.3 nm leads to positive identification of hot bands in Fig. 2. This identification is further supported by the measured isotope shifts which are slightly to the red for the origin band but to the blue for the 1–0 hot band. Higher hot bands originating from $v'' = 2$ are also prominent at the temperature of 1000 °C but undetectable at room temperature (Fig. 2).

The measurement of isotope shifts is very valuable not only in the identification of origin bands, but also in confirming assignments of higher vibrational levels and characterization of the few unassigned bands of Fig. 2. Also evident is the importance of isotopically pure spectra since the isotope shifts for the highest observed values of $v' = 15$ are about 116 cm^{-1} for masses 70–72, and about 237 cm^{-1} for masses 70–74. Such shifts will result in serious degradation of resolution in nonisotopically selective experiments carried out on chlorine with natural isotopic abundance.

It has been noted earlier that the relative intensities of the bands of Fig. 2 have not been corrected for laser power. Moreover, the $v' = 2$ band in Fig. 2 was found to be so intense that the laser intensity was deliberately attenuated in scanning the band in order to avoid instrumental saturation effects. This band is actually observed to be the most intense one of the whole progression, a fact which is consistent with the data of Stubbs *et al.*[13]

B. $^3\Pi_g$

An optical–optical double resonance technique has been applied by Shinzawa *et al.*[8-10] to study the vibrational levels in the outer well of the $E(0_g^+)$ component of this state. Due to the operation of the Franck–Condon principle, the outer well was accessed in this study since the pumped state was the lowest bound 0_u^+ component of $^3\Pi_u$ state which has a large equilibrium internuclear distance. In their experiment, the detected levels are well below the maximum of the double well. These workers also detected a second 0_g^+ state which they labeled as f.

We have identified a series of vibrational levels ascribed to the inner well of this state, beginning with the origin band, and extending well above the barrier. Although this state has three spin–orbit components, $\Omega = 0, 1$, and 2, we have apparently detected only one. We suggest that the observed component belongs to $\Omega = 1$ from the following considerations: (1) The $\Omega = 1$ component can "borrow oscillator strength" from the allowed $^1\Pi_g$, $\Omega = 1$ state of the same spin–orbit symmetry; (2) The observed band profiles of some of the best-resolved, most-cooled bands are essentially identical for both the singlet and triplet progression under the barrier and correspond to the shape expected for a single laser, two-photon transition with $\Omega = 0 \to \Omega = 1$ for which the Q branch line strength decreases rapidly with increasing J, whereas in other transitions, the line strength increases linearly with J.[14] It is clearly seen in Fig. 3 that the Q branch of the best resolved bands ascribed to both $^1\Pi_g$ and $^3\Pi_g$ are most prominent in the coldest spectra.

Previous information regarding the origin of the $^3\Pi_g$ inner well state is very poor. The data of Jureta *et al.*[11] indicates that the triplet vibrational levels lie roughly half way between those of the singlet system in disagreement with our data. The much higher resolution data of Comer *et al.*[13] show clearly that the triplet levels are unresolved from the singlet levels in agreement with our data. Although Comer *et al.* do not even discuss the triplet state, the spectra in their Fig. 2 taken at 5 eV scattered energy and 90° show fairly convincingly that the origin of the triplet system nearly coincides with, but is at slightly lower (by about 0.01 eV) energy than a hot band at about 7.881 eV, which is in excellent agreement with our value of 7.8696 eV. Careful comparison of their data taken at 5 eV and 90° with that taken at 100 eV and 2° reveals a broadening to the high energy side of all peaks except 0–0, indicating that all triplet bands except the origin are slightly above the singlet bands as is clearly observed in our spectra. Our identification of the origin is also supported by the isotope shift and the high temperature data which enabled us to make positive identification of possible misleading hot bands.

As in the case of $^1\Pi_g$ system, the vibrational level spacing in the region near the origin is fairly regular and very nearly that of the ion. This strongly suggests that a diabatic picture is more appropriate and that the observed red shift of heavier isotopes is not unexpected.

Due to the low intensity of the triplet bands and their frequent near coincidence with hot bands, their positions are not as reliably determined as in the case of the singlet system. This is particularly true in the region near the top of the barrier separating both wells where some erratic behavior can be expected as was observed by Moeller *et al.* (e.g., see their Fig. 5)[4] who studied the one-photon allowed 1 $^1\Sigma_u^+$ state which also has a double well potential. Due to these difficulties we cannot reliably determine the exact position of the top of the barrier of $^3\Pi_g$ state. However, we are able to identify levels above the barrier certainly down to the level at 70 074 cm^{-1}. Levels very near or below the barrier are probably identified up to $v' = 9$ at 69 220 cm^{-1}. Thus, the top of the barrier is probably located in the vicinity of 69 250 $\pm$ 100 cm^{-1} (8.586 eV), which is 5778 cm^{-1} (0.71 eV) above the $v' = 0$ level of the inner well.

The assignment of levels to either the inner well or above the barrier is readily done by making use of the striking difference in band profile and spacing. Levels of the inner well are shaded slightly to the blue while those above the barrier are shaded drastically to the red as can be seen from Figs. 2 and 3. This behavior is due to the change of rotational constant from a value somewhat larger to one much smaller than that of the ground state.[15]

We also have good evidence for variation of predissociation with vibrational quantum number of inner well levels of both $^1\Pi_g$ and $^3\Pi_g$ states. In Fig. 3 are shown vibrational band contours which were measured with the lowest possible laser powers in order to avoid broadening effects (saturation, ac Stark effects, etc.). The variation in linewidths is attributed to the variation of the overlap of the vibrational wave functions between the bound 4sσ Rydberg and the $\pi \to \sigma$ repulsive valence states ($^1\Pi_g$ and $^3\Pi_g$) as calculated

by Peyerimhoff and Buenker.[3]

C. Unidentified bands

Only two strong and a few very weak bands in our spectra remain unidentified. The strong band at 73 440 cm^{-1} (for two-photon energy) appears in all mass channels, has well resolved structure and very nearly zero isotope shift which suggests that it may be the origin band of a new system. Attempts at identification by comparison with the electron scattering data were inconclusive. An extension of this experiment to shorter wavelengths is necessary to complete the identification.

The other unidentified band at 66 230 cm^{-1} (and 66 165 cm^{-1}) of two-photon energy does not appear in the electron scattering spectrum at any energy and angle. This strongly suggests that it may be a three-photon resonance. The electron scattering spectrum shows a level at this energy (12.319 eV or 99 395 cm^{-1}). The level is assigned as the $v = 4$ level of an unidentified state which was thought to be spin forbidden from its energy and angle dependence. Our observed isotope shift is consistent with that vibrational quantum number but the band appearing in our spectrum was very strong and no other vibrational bands of this system were observed.

D. Photophysics

1. Effects of one-photon absorption by the C $^1\Pi_u$ repulsive state

Unlike most MPI experiments the first photon in our experiment is absorbed by the moderately strong dissociative continuum of the C $^1\Pi_u$ state. The decadic molar extinction coefficient varies from about 62 at 320 nm to 2.3 at 270 nm,[16] corresponding to absorption cross sections of 0.24 to 0.0009 mb (10^{-18} cm^2) over the range of our data and an oscillator strength f for the entire band of about 1.0×10^{-3}. The next nearest one-photon allowed transition of very much larger oscillator strength is the transition to the lowest optically allowed (with f probably of the order of 0.1) Rydberg state, the $4p\sigma_u$ $^1\Pi_u$ state at about 9.228 eV (from Comer et al.), with "virtual level lifetime" of about 10^{-16} s. This value is about two to three orders of magnitude shorter than the time required for the dissociating Cl_2 molecule on the $^1\Pi_u$ repulsive potential curve to extend beyond the range of significant transition probability to bound excited states. Thus, it is very plausible that the repulsive state serves as the main "transfer" level and we can expect some unusual effects, particularly on Franck–Condon factors.

In a multiphoton transition in which all significant transfer or virtual levels are very far off resonance compared to the widths of their respective Franck–Condon envelopes, an average energy denominator can be used, in the manner of the Bebb and Gold approximation,[17] in summing over all vibrational levels of a transfer level and the final result yields a Franck–Condon factor which to a good approximation, involves only initial and final states. In simplistic terms, the system remains in virtual levels for times very much shorter than a vibrational period and hence "does not move." The two-photon transition of NO is an example of such a case.

However, the present transition should provide a counter example and in fact the long progressions observed in Fig. 2 result from this circumstance. A detailed study of its ramifications in terms of ultrafast intramolecular dynamics will be discussed in a separate paper.[18] Although the relative intensities of Fig. 2 are only very crudely accurate, they are dramatically different from the electron scattering data of Comer et al.[13] taken at 100 eV and 2°. The relative vibrational band intensities of that data should represent the Franck–Condon factors between ground and excited states. While the electron impact data show a very strong decrease in relative intensity from the maximum at $v' = 2$ to $= 1\%$ of that at $v' = 6$ and undetectable peaks for $v' > 6$, our data extend to $v' = 15$ with no very great decrease in intensity. Actually the laser intensities at $v' = 0$ and $v' = 15$ are very close, but the $2 + 1$ MPI intensities are nearly the same for both peaks. This is as expected for transitions through a dissociating state to the attractive limb of the inner well. On the other hand, there seems to be no significant enhancement of the intensity of $v' = 0$ relative to $v' = 2$ as compared with the electron scattering data. This is readily explained since the wavelength region near $v' = 0$ (≈ 313 nm) is fairly close to the maximum of the absorption cross section at about 330 nm and therefore corresponds to a "vertical" transition to the repulsive curve with the resulting wave packet moving outward only. Since the potential curve of the $^1\Pi_g$ state is displaced slightly to a shorter internuclear distance than that of the ground state, significant enhancement of $v' = 0$ is not to be expected.

Another possible effect of the dissociative transfer state is significant excitation of outer well levels of approximate states. The electronic transition moments at the larger internuclear distances where these states have predominantly ionic character can be very large, corresponding to charge–transfer transitions. The Franck–Condon factors are not insignificantly small when the effects of kinetic energy on these factors are considered as pointed out first by R. S. Mulliken.[19] These outer well states are expected to be detected with very poor sensitivity in our experiment because of very low Franck–Condon factors in the ionization step. However, it is possible that some of our very weak unidentified bands may be due to these levels. Such outer well levels are probably much more readily detected by fluorescence as in the experiments of Tanaka et al.[8-10]

2. Production of atomic ions

The dominant mechanism for production of atomic ions is very probably due to photoionizatin of the resonant state to produce Cl_2^+ ions followed by photodissociation of the ions. A casual examination of the He I photoelectron spectrum[20] of Cl_2 would suggest that one-photon photodissociation of Cl_2^+ in the energy region of Fig. 2 (3.90–4.58 eV) would be extremely weak, since this energy region is well above the band envelope of the optically allowed $^2\Pi_u$ state in the PES. However, this inference is incorrect since the ionic ground $^2\Pi_g$ and the first excited $^2\Pi_u$ states have internuclear distances that are respectively smaller (1.89 Å) and larger (2.21 Å) than that of the neutral molecular (1.988 Å) which leads to a large shift of the Franck–Condon region for ab-

sorption by the ion. This transition has been studied in emission[21-23] and the optical and photoelectron spectra are in good agreement between themselves as well as with the calculated potential curves of Tuckett and Peyerimhoff.[21] The transition $^2\Pi_g \rightarrow {}^2\Pi_u$ is the type $\pi^* \leftarrow \pi$ and should be fairly strong. Tuckett and Peyerimhoff measured a radiative lifetime of $\simeq 410$ ns corresponding to an oscillator strength of the order of 0.02 which if distributed over an energy range of 0.5–1.0 eV yields a continuum cross section in the range $10^{-18}–10^{-17}$ cm², such a cross section would result in strong photodissociation at our laser power. The calculated potential curves indicate that the Franck–Condon region for $v'' = 0$ of the ion is centered about very high vibrational levels (extending weakly into the dissociative continuum) and that higher vibrational levels of the ion would be even more favorably photodissociated.

ACKNOWLEDGMENTS

1. C. Lee, M. Suto, and K. Y. Tang, J. Chem. Phys. 84, 5277 (1986).

F. Grein, S. D. Peyerimhoff, and R. J. Buenker, Can. J. Phys. 62, 1928 (1984).

3. S. D. Peyerimhoff and R. J. Buenker, Chem. Phys. 57, 279 (1981).

4. T. Moeller, B. Jordan, P. Gurtler, G. Zimmerer, D. Haaks, J. LeCalve, and M. C. Castex, Chem. Phys. 76, 295 (1983).

5. A. E. Douglas, Can. J. Phys. 59, 835 (1981).

6. R. P. Iczkowski, J. L. Margrave, and J. W. Green, J. Chem. Phys. 33, 1261 (1960).

7. J. Lee and A. D. Walsh, Trans. Faraday Soc. 55, 1281 (1959).

8. T. Ishiwata and I. Tanaka, Chem. Phys. Lett. 107, 434 (1984).

9. T. Ishiwata, T. Shinzawa, T. Kusayanagi, and I. Tanaka, J. Chem. Phys. 82, 1788 (1985).

10. T. Shinzawa, A. Tokunaga, T. Ishiwata, and I. Tanaka, J. Chem. Phys. 83, 5407 (1985).

11. J. Jureta, S. Cvejanovic, M. Kurepa, and D. Cvejanovic, Z. Phys. A 304, 143 (1982).

12. D. Spence, R. H. Huebner, H. Tanaka, M. A. Dillon, and R. G. Wang, J. Chem. Phys. 80, 2989 (1984).

13. R. J. Stubbs, T. A. York, and J. Comer, J. Phys. B 18, 3229 (1985).

14. R. G. Bray and R. M. Hochstrasser, Mol. Phys. 31, 1199 (1976).

15. Herzberg, Spectra of Diatomic Molecules (Van Nostrand Reinhold, New York, 1950).

16. D. J. Seery and D. Britton, J. Phys. Chem. 68, 2263 (1964).

17. H. B. Bebb and A. Gold, Phys. Rev. 149, 25 (1966).

18. L. Li, R. J. Lipert, H. Park, W. A. Chupka, and S. D. Colson, J. Chem. Phys. 88, 6767 1988.

19. R. S. Mulliken, J. Chem. Phys. 55, 309 (1971).

20. K. Kimura, S. Katsumata, Y. Achiba, T. Yamazaki, and S. Iwata, Handbook of HeI Photoelectron Spectra of Fundamental Organic Molecules (Japanese Scientific Societies, Tokyo, 1981).

21. R. P. Tuckett and S. D. Peyerimhoff, Chem. Phys. 83, 203 (1984).

22. F. P. Huberman, J. Mol. Spect. 20, 29 (1966).

23. A. B. Cornford, D. C. Frost, C. A. McDowell, J. L. Ragle, and I. A. Stenhouse, J. Chem. Phys. 54, 2651 (1971).

ADIABATIC DISSOCIATION OF PHOTOEXCITED CHLORINE MOLECULES

Leping LI, Robert J. LIPERT, Jim LOBUE, William A. CHUPKA and Steven D. COLSON

Sterling Chemistry Laboratory, Yale University, New Haven, CT 06511, USA

State-selected hot chlorine atoms are cleanly produced in the $^2P_{3/2}$ state by photodissociation of Cl_2 in the wavelength region between 323.6 and 331.0 nm. Ionization (by 3 + 1 MPI) with mass spectral analysis has been used to probe the atomic Cl state. The identification of the repulsive state is determined from a state correlation diagram based on Mulliken's work and from Franck–Condon considerations based upon potential energy curves calculated by Peyerimhoff and Buenker. The results are consistent with adiabatic dissociation of the photoexcited chlorine molecules.

1. Introduction

Continuous absorption by chlorine molecules near and in the UV region of the spectrum is due to electronic transitions from the ground $X\,^1\Sigma_g^+$ state to the repulsive limbs of the potential curves of various excited states [1–3]. Photoexcitation at these energies results in the generation of chlorine atoms which carry off excess energy in the form of translational as well as electronic excitation. The fragment energy will change with the photoexcitation energy, making the process very useful for hot atom reaction studies. Ideally, one can completely control the translational energy of the reactive atoms by tuning the excitation energy. Unfortunately, for systems like the halogens which have large spin–orbit splittings, one is often uncertain of the partitioning of the energy between translational and electronic (spin) excitation.

Chlorine atoms play a key role in numerous gas-phase chemical reactions, including stratospheric removal of ozone [4]. Their role in an electric discharge is central to the operation of the XeCl excimer laser. It is thus important to be able to prepare and detect chlorine atoms with high selectivity and sensitivity. Despite their important role in hot atom chemistry, photodissociation processes have not been easy to study in detail. Spectroscopically, dissociative transitions ordinarily appear as broad, almost structureless, continua, and in photochemical systems the dissociation fragments often lose their ini-

tial energy or react before being directly observed.

The development of the photofragment spectrometer by Wilson and co-workers [5] and its application to the study of the photodissociation of molecules have been highly successful [6]. In their experiment, the nature of the transitions between the ground state and repulsive state (i.e. parallel or perpendicular transitions) is determined from the angular distribution of the photofragment yield, while the product internal energy (electronic in diatomic but including rotational and vibrational in polyatomic molecules) is inferred from measurements of the translational energy distribution. As an alternative, we use resonance-enhanced multiphoton ionization (REMPI) to probe the chlorine atoms and measure directly the internal energies of the photofragments from which their translational energy is determined by energy conservation. This is especially convenient and accurate for diatomic molecules since their fragments are atoms which are much easier to analyze. From the exact knowledge of the electronic energies of the photofragments, the known dissociation energy of the ground state, and the photoexcitation energy used to dissociate the molecules, we are able to determine the translational energy of chlorine atoms with spectroscopic precision.

With this approach, we have carried out a study on chlorine in a molecular beam where both the photodissociation and the 3 + 1 MPI of the resulting chlorine atoms are accomplished with one laser op-

erating in the wavelength region from 323.6 to 331.0 nm. All the atomic peaks in the spectrum have been assigned exclusively to transitions from the lowest $^2P_{3/2}$ ground state of chlorine atom, even though transitions from the $^2P_{1/2}$ state are energetically accessible in our wavelength scan. Thus, all excess photon energy goes into translational energy of the photofragments and state-selected "hot" chlorine atoms are prepared with continuously adjustable translational energy in this wavelength region.

2. Experimental

A mixture of 1.0% Cl_2/He (CryoDyne Specialty Gases) was expanded continuously through a 25 μm nozzle at a backing pressure of 3 atm into a vacuum chamber maintained at 1×10^{-4} Torr. Approximately 1 mm away from the nozzle the molecular beam was crossed with a tunable UV laser beam focused by a 6″ focal length lens and obtained by doubling the output frequency of a Nd:YAG-pumped dye laser (Quanta-Ray LCR-2, PDL). The resulting photoions were accelerated into a time-of-flight mass spectrometer by a repelling field of 300 V/cm. Only $^{35}Cl^+$ and $^{37}Cl^+$ are observed between 3236 and 3110 Å, and both ions were monitored simultaneously as a function of wavelength. The resulting REMPI spectrum was not corrected for variations in laser power across the dye tuning curve.

In our experiment, the Cl atoms were produced by one-photon absorption and subsequent dissociation of Cl_2 in the UV region where the Cl atom has several three-photon-allowed transitions from both $^2P_{3/2}$ and $^2P_{1/2}$ states.

3. Results and discussions

The relevant energy levels for states involved in the photodissociation and the subsequent multiphoton ionization of chlorine atoms reported here are illustrated in fig. 1. The corresponding REMPI spectrum is shown in fig. 2 with assignment of each peak listed in table 1.

The assignment of the 3+1 MPI spectrum of the chlorine atom is based upon the data of Radziemski and Kaufman [7], guided by three-photon selection

rules [6,9], i.e. the absolute value of ΔJ must be less than or equal to 3, and the parity change must be odd.

A careful examination of our assignments reveals that no atomic $^2P_{1/2}$ state can be linked to any of the 14 observed peaks even though transitions from this state should occur in the same wavelength region. This fact immediately indicates that the repulsive Cl_2 state excited produces $^2P_{3/2}$ atoms exclusively. Thus the translational energy of the Cl atoms is precisely determined at a given wavelength, since the dissociation energy of the Cl_2 ground state is well known [1] (19997.28 cm^{-1}). In the wavelength range of this experiment the kinetic energy of the Cl atoms is varied over the range 0.63–0.68 eV.

It is interesting to note that, due to the large translational energy of the photofragments, we actually observe a double-peaked signal in each of the two atomic ion isotope mass channels. One peak is due to those ions produced with initial velocity in the forward direction and the other with initial velocity in the opposite direction. The difference in their arrival time is due to the time required to reverse the velocity of the second set of ions, i.e. the so-called "turn-around time". Ions with transverse velocity components have reduced collection efficiencies. Otherwise one would expect to see a peak broadening rather than a doubling. However, the precise shape of this double-peaked structure should depend on laser polarization, the direction of the transition moment (parallel or perpendicular) and instrumental parameters. Similar experiments have been successfully carried out (e.g. refs. [5,10]).

From the measured "turn-around time" and the value of the repelling field, we calculate the translational energy of photofragments to be in agreement with the exact value derived above. Conversely, we can use the known exact value to calibrate the effective field of the instrument for direct measurement of kinetic energies of photofragments from other molecules.

Although it is easy to determine the product state, it is not trivial to determine the repulsive state of Cl_2 involved in the photodissociation. The reassignment of the state symmetry near this wavelength region to $C^1\Pi_u$ by Wilson and co-workers [10] illustrates the difficulty met by previous workers.

However, the high quality, ab initio calculation of Peyerimhoff and Buenker [11] enables us to predict
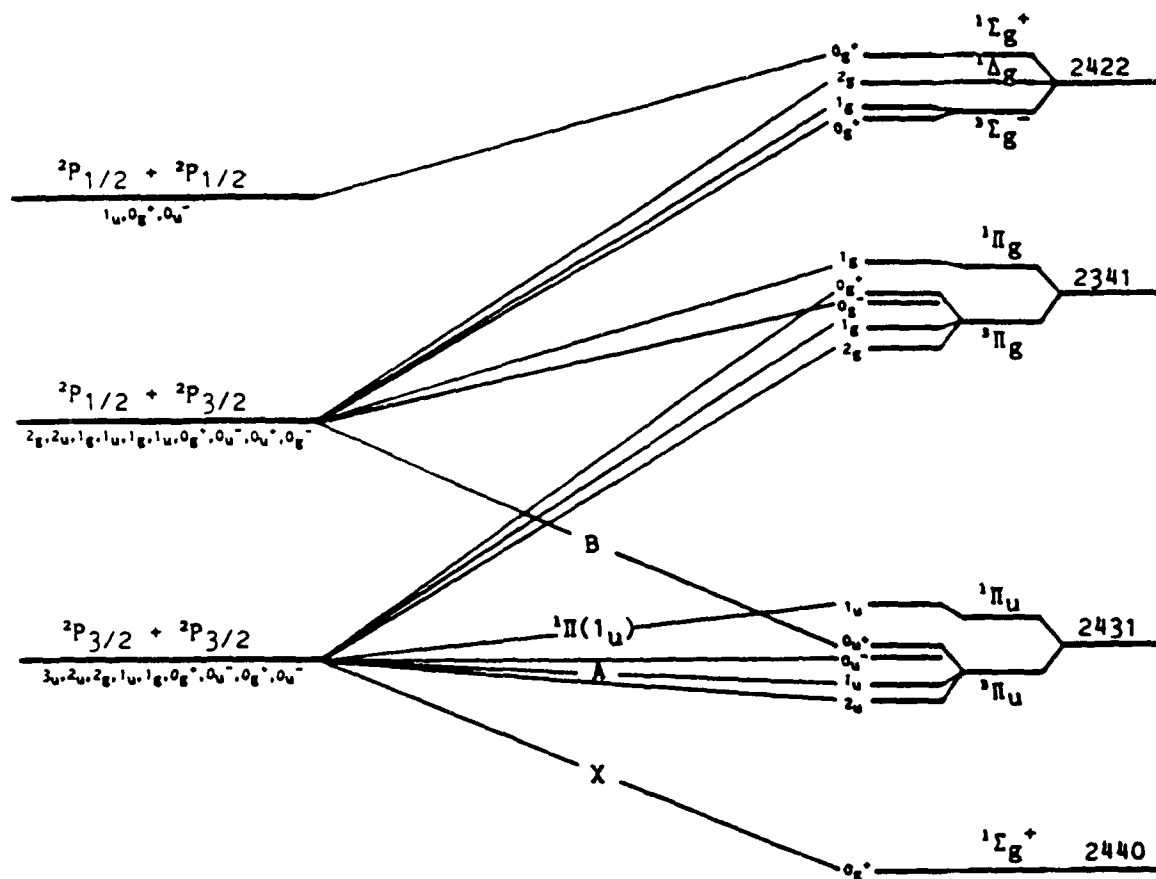
336

Fig. 1. State correlation diagram of chlorine. The configuration designation (e.g. 2440) corresponds to the occupation number of the $(5\sigma_g)$, $(2\pi_u)$, $(2\pi_g)$ and $(5\sigma_u)$ orbitals respectively.

which repulsive state of Cl_2 is most likely to be excited. It is quite clear from their calculated potential curves that the best candidate is the $^1\Pi_u$ state, since it falls into the region where the one-photon excitation from the ground $X\,^1\Sigma_g^+$ state has the most favorable Franck–Condon factor for transitions to those states originating from $^2P_u + ^2P_u$ atoms.

Following Mulliken [12] and using the non-crossing rule (states of the same Ω and same u or g symmetry cannot cross) a correlation diagram can be constructed for all 23 Ω components derived from two Cl atoms in their ground configuration (see fig. 2). It can be seen from the figure that the $^1\Pi_u$ state correlates with two $^2P_{1/2}$ atoms. However the products predicted by the correlation diagram will be produced only to the extent that the dissociation

process proceeds *adiabatically*. Our observation that only $^2P_{3/2}$ atoms are detected shows that the process is indeed highly adiabatic in this wavelength region.

Finally, we wish to point out that for $\lambda < 320.0$ nm Cl^+ were produced predominantly by photodissociation of the molecular ion [13], i.e.

$$Cl_2^+(X\,^2\Pi_g \xrightarrow{h\nu} Cl_2^+(A\,^2\Pi_u)$$

$$\rightarrow\rightarrow Cl^+(^3P_g) + Cl(^2P_u)\,.$$
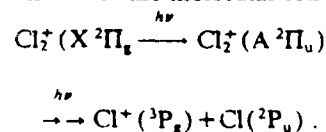
When λ is greater than 323.6 nm, no Cl_2^+ is detected up to 331.0 nm. We also note that in an MPI cell experiment on Cl_2 near 400.0 nm, multiphoton transitions originating from both $^2P_{1/2}$ and $^2P_{3/2}$ states have been identified in a recent paper [14]. Both

337
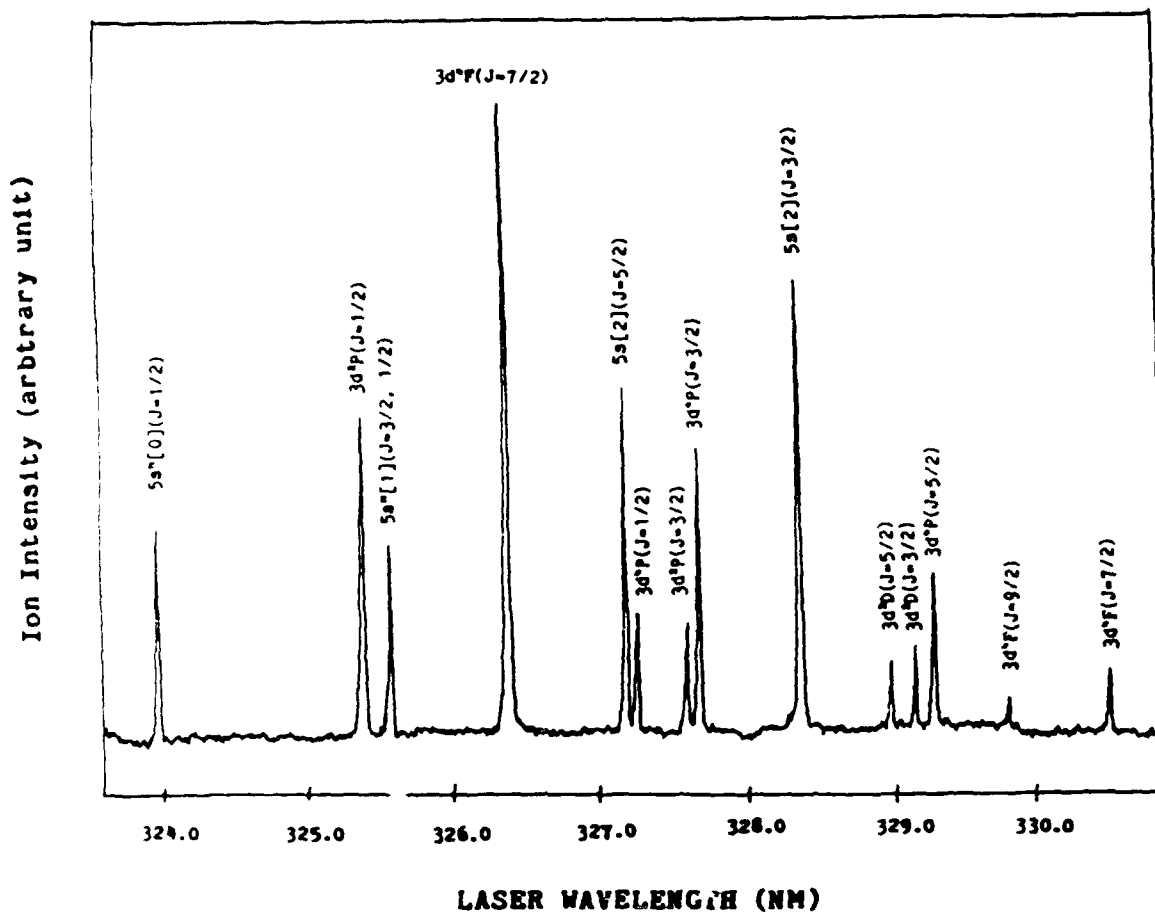
Fig. 2. 3 + 1 multiphoton ionization spectrum of atomic chlorine.

Table 1
Assignment of three-photon resonance-enhanced multiphoton ionization spectrum of chlorine atoms

Symbol	J	Term value (cm^{-1})	Symbol	J	Term value (cm^{-1})
3d ^{4}P	1/2	91660.58	3d ^{2}F	7/2	91906.79
	3/2	91538.50		5/2	91089.45
	5/2	91069.02			
3d ^{4}F	9/2	90948.53	5s[2]	5/2	91680.99
	7/2	90749.36		3/2	91343.50
3d ^{2}P	1/2	92194.19	5s'[1]	3/2	92151.38
	3/2	91564.30		1/2	92140.13
			5s"[0]	1/2	92602.70

338

53

results demonstrate the wavelength selectivity of dissociative state excitation as well as the high sensitivity of the MPI technique in detecting and identifying small amounts of chlorine atoms.

Acknowledgement

References

[1] K.P. Huber and G. Herzberg, Constants of diatomic molecules (Van Nostrand Reinhold, New York, 1978).

[2] J.A. Coxon, Molecular spectroscopy, Vol. 1 (Chem. Soc., London, 1973) p. 177, and references therein.

[3] J.T. Turner, in: MTP international review of science, Inorganic chemistry, Series 1, Vol. 3, ed. V. Gutmann (Butterworths, London, 1972) p. 253.

[4] E. Tschuikow-Roux, T. Yano and J. Niedzielski, J. Chem. Phys. 82 (1985) 65, and references therein.

[5] G.E. Busch, J.F. Cornelius, R.T. Mahoney, R.I. Morse, D.W. Schlosser and K.R. Wilson, Rev. Sci. Instr. 41 (1970) 1066.

[6] G. Hancock and K.R. Wilson, in: Proceedings of the Esfahan Symposium, August 20–September 5, 1971, eds. M.S. Feld, A. Javan and N. Kurnit (Wiley, New York, 1973).

[7] L.J. Radziemski Jr. and V. Kaufman, J. Opt. Soc. Am. 59 (1969) 424.

[8] G. Grynberg, F. Biraben, E. Giacobino and B. Cagnac, J. Phys. (Paris) 38 (1977) 629.

[9] G. Grynberg, J. Phys. (Paris) 40 (1979) 965.

[10] G.E. Busch, R.T. Mahoney, R.I. Morse and K.R. Wilson, J. Chem. Phys. 51 (1960) 449.

[11] S.D. Peyerimhoff and R.J. Buenker, Chem. Phys. 57 (1981) 279.

[12] R.S. Mulliken, Phys. Rev. 36 (1930).

[13] L.P. Li, R.J. Lipert, H. Park, W.A. Chupka and S.D. Colson, J. Chem. Phys. 88 (1988) 4608.

[14] L.P. Li, M. Wu and P.M. Johnson, J. Chem. Phys. 86 (1987) 1131.

339

54

Production of vibrationally state-selected O_2^+ via newly discovered 4s–3d and 5s–4d Rydberg states of O_2[a)]

Haiyoon Park, Paul J. Miller, William A. Chupka, and Steven D. Colson

Sterling Chemistry Laboratory, Yale University, New Haven, Connecticut 06511-8118

While resonant multiphoton ionization via Rydberg states has proved to be an effective method for preparation of vibronically state-selected ions in some cases,[1,2] this method has not previously been successful in the important case of O_2. For example, (2 + 1) multiphoton ionization-photoelectron spectroscopy (MPI-PES) of the $3s\sigma_g$ O_2 $C\,^3\Pi_g$ ($v' = 0$–3) Rydberg state has shown strong non-Franck–Condon behavior in one-photon ionization of the $v' = 1$–3 levels.[3,4] [Ionization via the $v' = 0$ level occurs exclusively with $\Delta v = 0$ ($\Delta v = v^+ - v'$) solely because the ground state O_2^+, $v^+ = 0$ level is the only one accessible at the three-photon total energy.] The presence of significant intensity in the $\Delta v \neq 0$ photoelectron peaks has been attributed in large part to the presence of a shape resonance in the σ_u ionization channel at threshold (and probably a Fano-type resonance in the π_u channel as well).[4,5] Due to the shape resonance, the transition dipole moment of the one-photon ionization step is strongly R dependent. As a result, the Franck–Condon approximation is no longer applicable and significant off-diagonal ($\Delta v \neq 0$) photoelectron peaks are observed.

The presence of the σ_u shape resonance makes production of state-selected O_2^+, $v^+ > 0$ unfeasible via one-color (2 + 1) MPI of the O_2 $3s\sigma_g$ Rydberg state. O_2^+ is obviously an important molecule in atmospheric chemistry and the facile production of state-selected ions with $v^+ > 0$ would be invaluable for studies of ion–molecule reactions and other chemical and physical processes. Since the width of a shape resonance typically increases with decreasing internuclear distance (hence increasing energy),[6] its influence on the photoionization cross section would be expected to decrease at higher energies above threshold. Therefore, the use of one-color (2 + 1) MPI of O_2 via Rydberg levels energetically above the $3s\sigma_g$ state holds better promise for preparing vibrationally excited state-selected O_2^+ ions. However, spectroscopic observation of higher gerade Rydberg levels has not, to our knowledge, been achieved to date. With this goal in mind, we have investigated by (2 + 1) MPI spectroscopy the energy region corresponding to the O_2 4s–3d and 5s–4d Rydberg states. Wavelength scans were performed in a time-of-flight mass spectrometer while monitoring the $m/e = 32$ mass channel and photoelectron spectra were obtained using

a time-of-flight photoelectron spectrometer with 2π sr collection efficiency.[7]

The triplet 4s–3d Rydberg state origins were calculated by Cartwright *et al.*[8] to lie in the 10.39–10.61 eV energy region. (We note that the $3d\delta_g$ states were not considered in Ref. 8.) The lowest 5s–4d Rydberg state is calculated to be at 11.17 eV. In addition, although Rydberg states in the singlet manifold are formally spin forbidden, they cannot be completely ruled out as evidenced by the appearance of $3s\sigma_g$ $^1\Pi_g$ levels in (2 + 1) MPI from the O_2 $X\,^3\Sigma_g^-$ ground state.[9,10]

A search for the 4s–3d levels by (2 + 1) MPI has revealed at least five vibrational progressions (labeled A, B, C, D, and E in Fig. 1) corresponding to the $v' = 0$–3 levels of these states. Also observed, as verified by photoelectron spectroscopy, are $v' = 0$ levels attributable to 5s–4d resonances [Fig. 1(d)]. Additional 5s–4d, $v' > 0$ levels have also been seen and will be presented in a later publication.

A significant feature of the progressions in Fig. 1 is the sharpness of the rotational structure. The rotational linewidths (FWHM) are on the order of ≈ 1.0 cm^{-1}, which is the bandwidth limit of the frequency-doubled laser radiation. In contrast, the lower $3s\sigma_g$ $^3\Pi_g$ Rydberg levels are much more strongly predissociated and only the $v' = 2$ level has resolvable rotational structure (FWHM ≈ 6 cm^{-1}).[11] In addition, the vibrational spacings of the 4s–3d bands are nearly identical to those of the ion. The sharpness of the rotational structure and the spacings of the vibrational levels suggest that the 4s–3d states are relatively unperturbed and their potential energy curves should be nearly identical with that of ground state O_2^+. Nevertheless, some off-diagonal ($\Delta v \neq 0$) photoelectron peaks are observed[12] (especially in progressions B, C, and D) which would indicate an R-dependent transition moment that can be attributed to strongly R-varying features (e.g., a shape resonance) in the ionization continuum at the three-photon energy. The $\Delta v \neq 0$ PES peaks are reduced in intensity relative to the $\Delta v = 0$ peak as compared to those in the PES spectra of the $3s\sigma_g$ levels,[4] which is to be expected for a shape resonance increasing in width at higher energies.

Possible overlap between two Rydberg states differing by one vibrational quantum number may also be affecting the observed photoelectron spectra obtained for the levels of
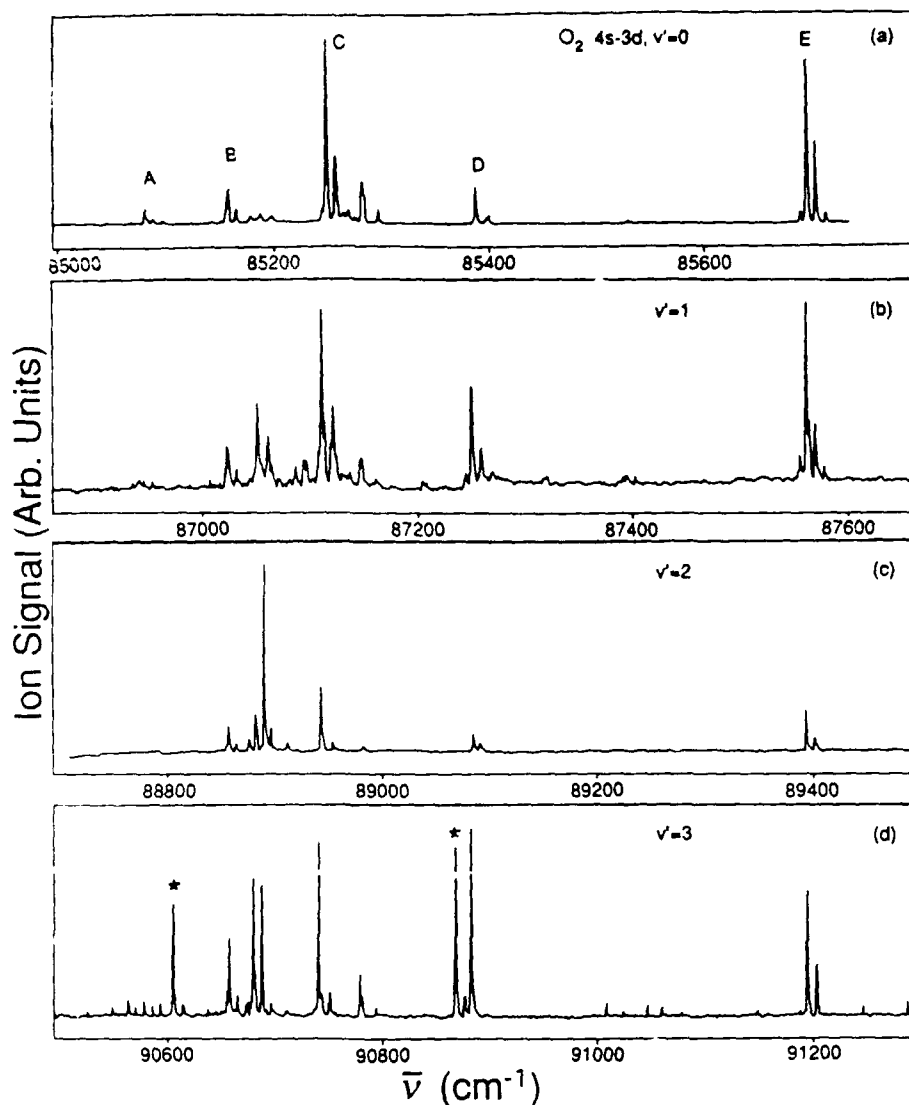
FIG. 1. The (2 + 1) MPI spectra of the $4s-3d$, $v' = 0-3$ and $5s-4d$, $v' = 0$ (starred peaks) Rydberg states of O_2. Frequency units (in wave numbers) of the abscissa scale correspond to the two-photon total energy.

progression C. The PES show two predominant peaks corresponding to v' and $v' + 1$. The two peaks have different wavelength dependences indicating they arise from different states. However, a search for the origin of the band with $v' + 1$ excitation failed to find a state with any appreciable intensity at the appropriate energy. If there is indeed an overlapping $v' + 1$ state, it may only be observable by intensity borrowing from the nearly coincident C, v' level. Therefore, this state would not be readily observable below the C, $v' = 0$ level.

The vibrationally cleanest photoelectron spectra are obtained for progression E and show over 80% production of O_2^+ X $^2\Pi_g$ $(v^+ = v')$.[12] The electronic assignment of this progression has not been determined, although a plausible argument can be made for a $3d\delta_g$ state. Observation of the E, v' bands at higher energies than the other v' bands would be consistent with the usual energy level splittings of $nd\lambda$ Rydberg states, i.e., increasing energy from $nd\sigma$ to $nd\pi$ to $nd\delta$. Ejection of an $nd\delta_g$ electron would not occur through the σ_u continuum, thus avoiding the influence of the shape resonance. Unfortunately, the angular momentum coupling case is an intermediate one for the $4s-3d$ states[8] which makes

electronic and rotational state assignments difficult. Detailed analysis and theoretical calculations will be necessary to interpret our spectra more fully.

[1] S. T. Pratt, P. M. Dehmer, and J. L. Dehmer, J. Chem. Phys. 80, 1706 (1984).
[2] W. E. Conaway, R. J. S. Morrison, and R. N. Zare, Chem. Phys. Lett. 113, 429 (1985).
[3] S. Katsumata, K. Sato, Y. Achiba, and K. Kimura, J. Electron Spectrosc. Relat. Phenom. 41, 325 (1986).
[4] P. J. Miller, L. Li, W. A. Chupka, and S. D. Colson, J. Chem. Phys. 89, 3921 (1988).
[5] J. A. Stephens, M. Braunstein, and V. McKoy, J. Chem. Phys. 89, 3923 (1988).
[6] J. L. Dehmer, A. C. Parr, and S. H. Southworth, in Handbook on Synchrotron Radiation, edited by G.V. Marr (North-Holland, Amsterdam, 1986), Vol. II.
[7] P. Kruit and F. H Read, J. Phys. E 16, 313 (1983).
[8] D. C. Cartwright, W. J. Hunt, W. Williams, S. Trajmar, and W. A. God-

J. Chem. Phys., Vol 89, No. 6, 15 September 1988

56

dard, III, Phys. Rev. A **8**, 2436 (1973).

[9]A. Sur, C. V. Ramana, and S. D. Colson, J. Chem. Phys. **83**, 904 (1985).

[10]R. D. Johnson III, G. R. Long, and J. W. Hudgens, J. Chem. Phys. **87**, 1977 (1987).

[11]A. Sur, C. V. Ramana, W. A. Chupka, and S. D. Colson, J. Chem. Phys. **84**, 69 (1986).

[12]P. J. Miller, H. Park, W. A. Chupka, and S. D. Colson, J. Chem. Phys. (submitted).

Shape resonance and non-Franck–Condon behavior in the photoelectron spectra of O$_2$ produced by (2+1) multiphoton ionization via 3sσ Rydberg states[a]

Paul J. Miller, Leping Li, William A. Chupka, and Steven D. Colson

Sterling Chemistry Laboratory, Yale University, New Haven, Connecticut 06511-8118

Recently, Sur *et al.*[1] and Katsumata *et al.*[2] have reported photoelectron spectra resulting from $(2 + 1)$ multiphoton ionization (MPI) through the $3s\sigma_g$ $^3\Pi_g$ ($v' = 2$) state of O$_2$. In addition to the strong $\Delta v = 0$ peak, the latter also observed significant intensities due to $\Delta v \neq 0$ transitions. For the $\Delta v = 0$ peak, their spectra showed the strong angular dependence expected for direct photoionization of a $3s\sigma_g$ Rydberg electron, while the $\Delta v \neq 0$ peaks showed no significant angular dependence, indicating non-Franck–Condon behavior associated with shape and/or autoionizing resonances.

We have measured the $(2 + 1)$ MPI photoelectron spectra of the $v' = 0$–3 vibrational levels of both $^1\Pi_g$ and $^3\Pi_g$ states of the $1\pi_g 3s\sigma_g$ Rydberg configuration. The spectra of the $^3\Pi_g$ states, obtained by a 2π steradian photoelectron spectrometer,[3] are shown in Fig. 1. Strong deviation from v conservation is apparent for $v' > 0$. The spectra resemble those of H$_2$ via the C $^1\Pi_u$ Rydberg state[4-7] in which the anomalies are due to autoionization of a repulsive state having an autoionization lifetime comparable to or greater than the dissociation time.[6,7]

Since the vibrational spacings of the O$_2$ Rydberg levels and the rotational constant for $v' = 2$ are nearly the same as those of the ground state of the ion, we conclude that the Rydberg–valence interaction is too weak (especially for $v' = 2$) to produce the observed $\Delta v \neq 0$ photoelectron intensity. In addition, preliminary photoelectron spectra of many levels of the $4s$–$3d$ complex exhibit similar anomalies even though these levels are much less predissociated (perturbed) than the $3s\sigma_g$ levels. Another potential mechanism for $\Delta v \neq 0$ processes is autoionization following Rydberg core excitation. However, consideration of the excited core $3s\sigma_u$ Rydberg states seen in the one-photon spectrum[8,9] shows that core excitation transitions are not resonant except for $v' = 1$ and would have very small Franck–Condon factors and low transition probabilities. Photoelectron spectra in this region[10-12] do not support attribution of our anomalies to this process.

According to calculations,[13-16] the Franck–Condon region at our three-photon energies is crossed by the repulsive parts of a number of valence state potential curves. Only one of these states, the lowest $^1\Pi_u$ state of configuration $\pi_g\sigma_u$, is strongly allowed ($3s\sigma_g \rightarrow \sigma_u$) and should have fairly large

oscillator strength. However, the configuration of this valence state differs from that of the continuum with the same symmetry by only one molecular orbital. Hence above the ionization limit it adds to the oscillator strength density of the σ_u channel and the state exists only as a shape resonance in this channel. Such a shape resonance has been calculated to occur in the threshold region for $(1\pi_g)^{-1}$ photoionization of O$_2$.[17] If we estimate[6] its width from the calculated minimal splitting between this valence state and the $(3p\sigma_u)$ $^1\Pi_u$ Rydberg state,[14] we obtain ≈ 3.1 eV. This value is a lower limit, since shape resonances typically increase in width with decreasing internuclear distance.[18] Since this width is much larger than the vibrational spacing (i.e., autoionization is fast compared to nuclear motion), the adiabatic approximation of Dehmer *et al.*[19] is appropriate and the departure from the Franck–Condon approximation is attributed to an R-dependent transition moment due to the shape resonance. This mechanism for inducing non-Franck–Condon vibrational distributions was predicted[19] and observed[20]
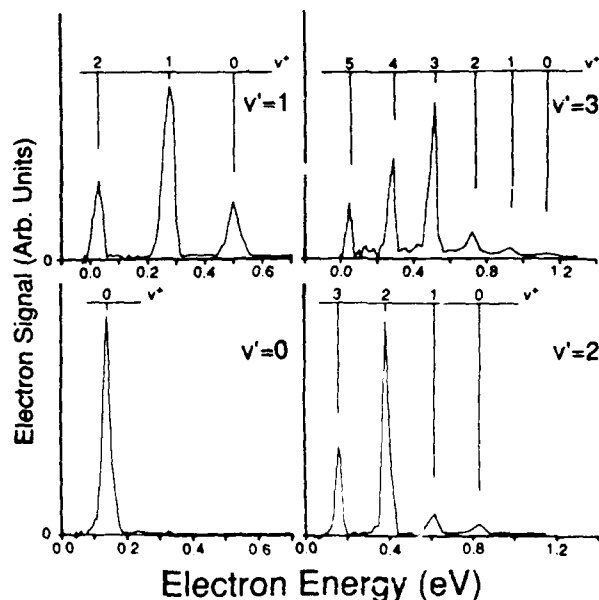

FIG. 1. Photoelectron spectra from $(2 + 1)$ multiphoton ionization via the $(3s\sigma_g)$ $^3\Pi_g$ levels $v' = 0$–3. All energetically accessible peaks are detectable for each value of v', for example, only $v^+ = 0$ is energetically possible from $v' = 0$.

Shape resonance influence on the photoelectron angular distributions from O_2 $C\,{}^3\Pi_g$, $V=0$–3

P. J. Miller and W. A. Chupka

Sterling Chemistry Laboratory, Yale University, New Haven, Connecticut 06511-8118

J. Winniczek and M. G. White

Chemistry Department, Brookhaven National Laboratory, Upton, New York 11973

Vibrationally resolved, photoelectron angular distributions are reported for the $(2 + 1)$ REMPI of the $C\,{}^3\Pi_g$ $(3s\sigma_g)$, $v' = 0$–3 Rydberg levels of O_2. Ionization transitions leading to different vibrational final states (v^+) of O_2^+ exhibit markedly different angular distributions, suggesting different ionization mechanisms. The experimental data are qualitatively reproduced by very recent *ab initio* calculations which attribute the non-Franck–Condon behavior to the presence of a $k\sigma_u$ shape resonance imbedded in the ionization continuum. Much of the remaining anomalous behavior is attributed to a Fano-type resonance in the Π_u channel.

I. INTRODUCTION

Recent $(2 + 1)$ resonantly enhanced multiphoton ionization-photoelectron spectroscopy (REMPI-PES) studies of the O_2, $C\,{}^3\Pi_g$ $(3s\sigma_g)$, $v' = 0$–3 Rydberg levels have revealed strong non-Franck–Condon behavior in the one-photon ionization step of the intermediate resonant level.[1,2] Such an effect was surprising since the potential energy curve of the $3s\sigma_g$ Rydberg state is expected to be quite similar to that of the ground state ion. This is based on the fact that the rotational analysis of the $3s\sigma_g$, $v' = 2$ level (the only level with resolvable rotational structure) gives a rotational constant virtually identical to that of the ion.[3] In addition, the vibrational spacings of the Rydberg and ion levels are also nearly identical. In one-photon transitions between states of similar geometry, the Franck–Condon principle strongly favors $\Delta v = 0$ transitions over all others. The presence of significant intensity in $\Delta v \neq 0$ transitions has important implications in techniques that rely on v-conserving ionizing transitions, e.g., the preparation of state-selected molecular ions for subsequent ion–molecule reaction studies.[4,5]

Previously, strong non-Franck–Condon behavior in the REMPI-PES of H_2, $C\,{}^1\Pi_u$ $(v' = 0$–4) has been observed by Pratt *et al.*[6,7] Photoelectron angular distribution measurements have shown significantly different behavior for the $\Delta v = 0$ and $\Delta v \neq 0$ photoelectron peaks.[7] The anomalous photoelectron spectra were subsequently attributed to excitation of the Rydberg ion core followed by electronic autoionization of the doubly excited state.[8,9] This indirect ionization process was shown to account for the intensities of the $\Delta v \neq 0$ photoelectron peaks observed in REMPI-PES. Such a situation, however, is not expected in the case of O_2 since the only energetically accessible core-excited levels all have very small Franck–Condon factors, three are formally spin forbidden $({}^2\Pi \rightarrow {}^4\Pi)$, and only one is accidentally resonant. A second mechanism involving a shape resonance at the ionization threshold has been proposed to account for the non-Franck–Condon behavior of $(2 + 1)$ REMPI-PES of the O_2, $C\,{}^3\Pi_g$ Rydberg state.[2,10] To further investigate the role of a shape resonance at the three-photon energy, we have obtained the photoelectron angular distributions for the $C\,{}^3\Pi_g$, $v' = 0$–3 levels. Our results strongly support a resonant ionization mechanism (i.e., a shape resonance and possibly autoionizing valence states as well) as being responsible for the $\Delta v \neq 0$ photoelectron peaks.

Photoelectron angular distributions measured by $(n + 1)$ REMPI using a single, linearly polarized light source are expressed by[11-15]

$$W_e(\theta) \propto \sum_{k=0} a_{2k} P_{2k}(\cos\theta). \tag{1}$$

Here $P_{2k}(\cos\theta)$ terms are Legendre polynomials (order $2k$), θ is the angle between the light polarization and the photoelectron propagation vectors, and the a_{2k} coefficients contain information on the partial wave character of the outgoing photoelectron in addition to alignment information of the resonant intermediate state. For spherically symmetric states $(J \leqslant 1/2)$ or states depolarized by collisions, the highest-order, nonzero Legendre polynomial in Eq. (1) is $P_2(\cos\theta)$. Higher-order terms may become important in one-photon ionization of highly aligned states. The maximum order is limited by $k_{max} = n + 1$ but angular momentum constraints can reduce k_{max} further. In an $(n + 1)$ REMPI process in which only one intermediate J' level is populated and the rotational state of the ion is unresolved, k_{max} is given by the smaller of $n + 1$, $J' + 1$, or l_{max} (where l_{max} is the maximum orbital angular momentum of the ejected photoelectron).[14,15] For our purposes, information on l_{max} would be very useful in determining the extent of the contribution of high l partial wave components to the outgoing electron. Indeed, a shape resonance can be ascribed to a high centrifugal barrier (hence high l contribution) which leads to temporary trapping of the electron. Any fit of the photoelectron angular distributions that involves higher order terms $(k = 2,3)$ terms may be the signature of higher l contributions to the outgoing photoelectron angular momentum due to scattering by the ion core and would be in accord with the presence of a shape resonance. The angular distributions presented in the following sections are intended to investigate this possibility.

in ground state photoionization of N_2, and later treated quantitatively by employing accurate (Hartree–Fock) photoelectron wave functions.[21] Such calculations have now been carried out on O_2 (see the following paper) and show that the σ_u shape resonance is responsible for a significant part of the non-Franck–Condon effects observed in our data. While these calculations yield significant intensities for $\Delta v \neq 0$ transitions and agree reasonably well for the $\Delta v < 0$ transitions (except for $v' = 1$ which is the most perturbed level and for which an accidental resonance occurs at the three-photon level), they suggest that still other mechanisms which preferentially enhance $\Delta v > 0$ processes play a significant part.

These remaining discrepancies could be due to several factors, the most likely of which are the following. First, initial states may be more perturbed than supposed. Second, a number of autoionizing valence states have been calculated[13,16] to cross the ion potential energy curve in the same region as the shape resonance and could lead to enhancement of $\Delta v > 0$ transitions, although such excitations from the Rydberg state require configuration mixing. Of particular importance is the $^3\Sigma_u$ (Schumann–Runge) state which interacts strongly with $np\pi_u$ Rydberg states[14] and thus interacts with the π_u ionization continuum with a width we calculate to be ≈ 0.6 eV. This can result in a Fano-profile structure (probably with $q \approx 0$) in the $^3\Sigma_u$ part of the π_u ionization channel at fixed R. The position of the feature will vary rapidly with R, yielding off-diagonal Franck–Condon factors even in the adiabatic approximation, which will be only weakly valid. A similar interaction in the $^3\Delta_u$ part of the π_u channel is very narrow ($q \approx 0.004$ eV) and probably too low in energy. These mechanisms are discussed further in the following paper. Finally, since the very broad $\pi_g \sigma_u$ repulsive valence state (shape resonance) overlaps the threshold region, this implies strong excitation of vibrationally excited high-n Rydberg states which can autoionize with preference for highest values of v.[22]

While a complete explanation of our data requires more theoretical effort, this work shows the importance of shape resonances in photoionization of Rydberg states and suggests that the study of shape resonances by photoionization of Rydberg states can valuably complement standard techniques. Choice of Rydberg orbital allows some variation of the outgoing partial waves.

Several vibrational levels can be used, making accessible a wide range of internuclear distances as compared with the narrow range afforded by the $v = 0$ ground state now used exclusively. In the present case, the very extensive autoionization features which hinder the study of excitation from the ground state are suppressed. Two-color experiments should greatly extend these studies.

[1] A. Sur, C. V. Ramana, W. A. Chupka, and S. D. Colson, J. Chem. Phys. **84**, 69 (1986).
[2] S. Katsumata, K. Sato, Y. Achiba, and K. Kimura, J. Electron Spectrosc. Relat. Phenom. **41**, 325 (1986).
[3] P. Kruit and F. H. Read, J. Phys. E **16**, 313 (1983)
[4] S. T. Pratt, P. M. Dehmer, and J. L. Dehmer, Chem. Phys. Lett. **105**, 28 (1984).
[5] S. T. Pratt, P. M. Dehmer, and J. L. Dehmer, J. Chem. Phys. **85**, 3379 (1986).
[6] W. A. Chupka, J. Chem. Phys. **87**, 1488 (1987).
[7] A. P. Hickman, Phys. Rev. Lett. **59**, 1553 (1987).
[8] P. M. Dehmer and W. A. Chupka, J. Chem. Phys. **62**, 4525 (1975)
[9] E. Nishitani, I. Tanaka, K. Tanaka, T. Kato, and I. Koyano, J. Chem. Phys. **81**, 3429 (1984).
[10] J. L. Bahr, A. J. Blake, J. H. Carver, J. L. Gardner, and V. Kumar, J. Quant. Spectrosc. Radiat. Transfer **11**, 1853 (1971).
[11] K. Tanaka and I. Tanaka, J. Chem. Phys. **59**, 5042 (1973).
[12] D. M. P. Holland and J. B. West, Z. Phys. D **4**, 367 (1987).
[13] H. H. Michels, in *Advances in Chemical Physics*, edited by J. Wm. McGowan (Wiley, New York, 1981), Vol. XLV.
[14] R. J. Buenker and S. D. Peyerimhoff, Chem. Phys. Lett. **34**, 225 (1975).
[15] R. P. Saxon and B. Liu, J. Chem. Phys. **67**, 5432 (1977).
[16] S. L. Guberman, in *Physics of Ion–Ion and Electron–Ion Collisions*, edited by F. Brouillard (Plenum, New York, 1983), pp. 167–200.
[17] A. Gerwer, C. Asaro, B. V. McKoy, and P. W. Langhoff, J. Chem. Phys. **72**, 713 (1980).
[18] J. L. Dehmer, A. C. Parr, and S. H. Southworth, in *Handbook on Synchrotron Radiation*, edited by G. V. Marr (North-Holland, Amsterdam, 1986), Vol. II.
[19] J. L. Dehmer, D. Dill, and S. Wallace, Phys. Rev. Lett. **43**, 1005 (1979).
[20] J. B. West, A. C. Parr, B. E. Cole, D. L. Ederer, R. Stockbauer, and J. L. Dehmer, J. Phys. B **13**, 1105 (1980).
[21] R. R. Lucchese and V. McKoy, J. Phys. B **14**, L629 (1981).
[22] W. A. Chupka, P. J. Miller, and E. E. Eyler, J. Chem. Phys. **88**, 3032 (1988).

J. Chem. Phys., Vol. 89, No. 6, 15 September 1988

59

II. EXPERIMENTAL

Angle-averaged photoelectron spectra of the O_2, $C^3\Pi_g$, levels were obtained at Yale University using a time-of-flight (TOF) "magnetic bottle" photoelectron spectrometer, the details of which are published elsewhere. In order to perform angle-resolved photoelectron studies, a TOF spectrometer with $\approx 1 \times 10^{-3}$ sr collection angle was employed at Brookhaven National Laboratory. Details of the Brookhaven TOF spectrometer have been described previously. The laser instrumentation used consisted of a Nd:YAG-pumped dye-laser (Quanta Ray DCR-2A and PDL) using the dyes R590, R610, and SR640 (Exciton). The frequency-doubled output (Quanta Ray WEX) of the dye laser was focused by a 100 mm fused-silica lens into the spectrometer where it intersected a cw beam of O_2 at right angles to the flight tube axis. The effusive beam was produced by expansion of 5–10 Torr of neat O_2 through a 0.070 mm nozzle and resulted in no observable rotational cooling. Laser powers were kept sufficiently low in order to minimize Coulomb broadening effects in the photoelectron spectra.

For angle-resolved studies, the laser polarization was defined by a Glan polarizing prism and rotated by a Soleil–Babinet compensator (Karl Lambrecht). Electron signal was collected as a function of the angle (θ) between the laser polarization vector and the flight tube axis of the spectrometer. Signal averaging was accomplished by using a transient digitizer (Le Croy, 8828) in a "boxcar" mode in which the appropriate vibrational peak was integrated after averaging the TOF spectrum for a given number of laser shots. For the stronger $\Delta v = 0$ photoelectron peaks, angular distributions were obtained in 10° increments at 100 laser shots per increment over twenty 360° scans. Angular distributions of the weaker $\Delta v \neq 0$ peaks were obtained in 20° increments at 100 laser shots per increment over 40 scans of 360°. Data collection and polarization rotations were controlled through the appropriate CAMAC modules interfaced to a PDP 11/73 minicomputer.

III. RESULTS

The $(2+1)$ REMPI photoelectron spectra of the $C^3\Pi_g$, $v' = 0$–3 levels have been presented previously[1,2] and the $v' = 2$ spectrum is reproduced in Fig. 1. Also shown are the photoelectron angular distributions for the v^+ vibrational final states of O_2^+. The experimental angular data are
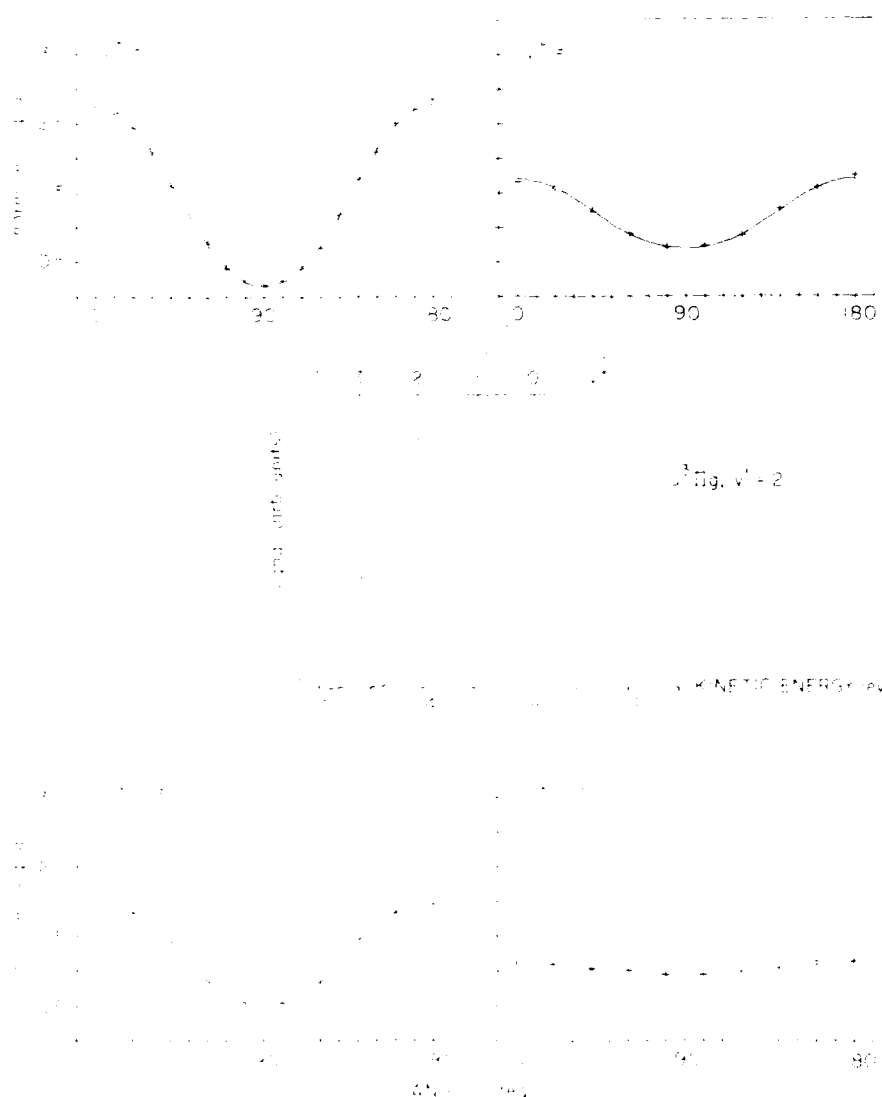

Fig. $v' = 2$

FIG. 1. $(2+1)$ REMPI photoelectron spectrum and angular distributions for the $C^3\Pi_g$, $v' = 2$ intermediate state of O_2. The laser wavelength was 287.955 nm. The solid curves in the angular distributions are least-squares fits to the data points ($+$) and ($\cdot$) (see the text).

TABLE I. Angular distribution coefficients for $(2 + 1)$ REMPI of O_2 $C^3\Pi_g, v' = 0-3$

	v'	a_2 (Expt)[a]	a_2 (Theory)[b]	a_4 (Expt)[a]	a_6 (Expt)[a]
0	0	1.38	1.46	−0.02	−0.05
1	0	0.27	0.17	0.09	0.07
1	1	1.66	1.53	−0.08	−0.15
1	2	0.94	0.55	0.00	0.09
2	0	0.12	0.43	0.00	0.02
2	1	0.67	0.27	0.05	−0.02
2	2	1.75	1.63	0.06	−0.03
2	3	1.04	0.51	0.02	−0.08
3	0	0.36	0.23	0.15	0.06
3	1	0.15	0.26	0.17	0.08
3	2	0.98	0.35	0.65	−0.01
3	3	1.64	1.66	−0.14	−0.06
3	4	0.89	0.79	0.10	−0.02

[a] Error estimated to be ±0.05.
[b] Reference 16, velocity form only.

shown as points and the smooth curves are least-squares fits of the data to Eq. (1) with $k_{max} = 3$. Fitted coefficients, a_{2k}, are given in Table I for all the C, $v' = 0-3$ intermediate states investigated in this work. Excitation wavelengths were chosen to match those used in the previous angle-integrated studies[2] and no attempt was made to excite specific rotational lines within a v' vibrational band. As can be seen from Fig. 1 and Table I, the $\Delta v = 0$ photoelectron angular distributions are strongly peaked at $\theta = 0°$ (and 180°) and are very well described by a simple $1 + a_2 P_2(\cos \theta)$ distribution with $a_2 \sim 1.6$. In this case, we can roughly identify a_2 with the usual β asymmetry parameter used to describe angular distributions in conventional PES from unaligned ground states. This approximation ignores small contributions to a_2 which depend on higher moments of the alignment distribution (A_2 and A_4). The asymmetry parameter can take on values in the range $-1 \leqslant \beta \leqslant 2$ with the maximum ($\beta = 2$) corresponding to ionization into a single $l = 1$ continuum. The relatively high value of a_2 (or β) for the $\Delta v = 0$ transitions is consistent with ionization from a $3s\sigma_g$ Rydberg state for which "p" ($l = 1$) continua are expected to be strong. By contrast, the $\Delta v \neq 0$ angular distributions exhibit much less asymmetry with an overall trend of decreasing a_2 coefficient for decreasing v' ($v' = v'_{max}$ to $v' = 0$). Furthermore, several $\Delta v \neq 0$ distributions have substantial $P_4(\cos \theta)$ character (e.g., $v' = 3/v' = 2$) indicative of high l continua and excitation-induced alignment. The large variations in the angular distributions for the different Δv ionization channels clearly indicates a strongly R-dependent ionization mechanism.

Table I also includes theoretically calculated a_2 values which include the effects of a $k\sigma_u$ shape resonance predicted to lie near the three-photon energy.[16] These calculations treat the R dependence of the transition dipole moment explicitly and have been successful in accounting for much of the $\Delta v \neq 0$ peak intensities.[2,10] Excitation-induced alignment of the intermediate state was not included in the calculations, so that only a_2 coefficients could be derived. For the $\Delta v = 0$ transitions, the calculated a_2 coefficients are in excellent quantitative agreement with experiment. Agreement is less satisfactory for the $\Delta v \neq 0$ values, although it should be noted that the experimental uncertainties are larger due to the weaker signal of the "off-diagonal" peaks (see Fig. 1). On a qualitative basis, the inclusion of the shape resonance reproduces the overall decreasing trend in the off-diagonal a_2 values and their small value relative to the $\Delta v = 0$ transition.

Since the calculated shape resonance is associated with strong enhancement of $l = 3$ continua, it is somewhat surprising that angular terms with $k = 2$ and 3 [see Eq. (1)] are not more prominent in the observed angular distributions. As noted earlier, the a_{2k} ($k > 1$) coefficients depend on both the ionization dynamics associated with higher l continua and higher order moments of the alignment distribution. Either factor could result in small contributions from higher order terms. In the present experiments, rotationally non-specific excitation could lead to a nearly spatially isotropic distribution of intermediate C state levels by exciting through overlapping branches which result in opposite alignments, e.g., R and Q branches. Alternatively, the contribution to the dynamical factors from the various l continua may cancel and substantially reduce the a_{2k} coefficients. Cancellation of this kind was found in a theoretical study of $(3 + 1)$ REMPI of H_2[17] in which ionizing transitions with $\Delta J = \pm 3$ are suppressed as a result of algebraic cancellation of $d\sigma$ and $d\pi$ transition strengths. The overall d-wave contribution to the ionization step, however, was strong. Given the success of the present calculations in predicting the a_2 coefficients (which also depend heavily on the inclusion of f-wave ($l = 3$) continua), the observation of small a_4 and a_6 coefficients most likely results from a combination of the factors discussed above and *not* to the absence of high l components in the continua.

IV. DISCUSSION

The decreasing a_2 values for the $\Delta v \neq 0$ peaks is qualitatively similar to that previously observed in $(3 + 1)$ MPI of H_2 $C^1\Pi_u$ ($v' = 0-4$).[7] In the case of H_2, non-Franck–Condon behavior has been attributed to excitation of the Rydberg ion core ($1s\sigma_g \rightarrow 2p\sigma_u$) followed by electronic autoionization.[8,9] In the present case of $(2 + 1)$ REMPI of the O_2, $C^3\Pi_g$ state, the angular distributions and vibrational branching ratios are qualitatively, and in some instances quantitatively, reproduced by the shape resonance calculations of Stephens *et al.*[10,16] As a result, the observed non-Franck–Condon behavior can be ascribed in large part to the existence of a $k\sigma_u$ shape resonance in the $3\sigma_u \rightarrow k\sigma_u$ ionization continua. Discrepencies between the calculated and observed $\Delta v \neq 0$ peak intensities and angular distributions still remain and cannot be solely attributed to the effect of the shape resonance. Including the effects of intermediate state alignment could improve the angular distribution calculations, however, lack of rotational selection in the present experiment precludes an accurate assessment of this effect. The additional intensity in the off-diagonal photoelectron peaks may possibly be accounted for by a repulsive state which is autoionizing on a time scale comparable to or faster than its dissociation time as in the case of H_2. The prime candidate for this second mechanism is the $\pi_u^3 \pi_g^3 {}^1\Sigma_u$ va-

lence state responsible for the broad Schumann–Runge absorption bands seen below threshold. In the single-configuration approximation, this valence state would not be accessible via one-photon absorption from a $3s\sigma_g$ Rydberg level ($\pi_u^3 \pi_g 3s\sigma_g$) since it requires a two-electron change. However, strong configuration interaction occurs, at least in the final state, since calculations[8] and experiment[19] have shown strong Rydberg-valence mixing between this valence state and the $3p\pi_u$ Rydberg state ($\pi_u^3 \pi_g 3p\pi_u$). This interaction will also extend to higher $np\pi_u$ Rydberg states and to the adjoining π_u continuum yielding a calculated (see Fig. 1 of Ref. 7) autoionization width of ≈ 0.6 eV (about twice a vibrational spacing). This interaction should result in a Fano-profile feature in the π_u ionization channel with $q \approx 0$, i.e., a "window resonance," at an energy which is a strong function of internuclear distance and therefore produces an R-dependent photoionization cross section. Thus, even in the adiabatic approximation, off-diagonal Franck–Condon factors are expected. However, since the autoionization and dissociation lifetimes are comparable, neither the adiabatic approximation nor the method applied to the H_2 case are very appropriate and a more complicated theoretical treatment is indicated. Nevertheless it is very likely that this state, embedded in the π_u continuum, can lead to non-Franck–Condon effects as well as anomalous angular distributions.

Also, it may be important to consider the interaction of the $k\sigma_u$ shape resonance with high lying $np\sigma_u$ Rydberg states in addition to the ionization continuum. As noted previously, the $k\sigma_u$ shape resonance arises from the $^3\Pi_u$ ($\pi_g\sigma_u$) valence configuration extended above threshold. Below threshold, this valence state has been calculated to mix strongly with the $3p\sigma_u$ Rydberg state.[3] It will therefore also mix strongly with higher $np\sigma_u$ Rydberg levels as it continues up into the ionization continuum. The populating of vibrationally excited high-n Rydberg levels that can autoionize will favor production of O_2^+ in the highest v^+ levels[20] and consequently affect the angular distributions.

Very recently, several vibrational levels of the $4s$–$3d$ and $5s$–$4d$ complexes of O have been observed and their $(2 + 1)$ REMPI-PES measured.[21] The photoelectron spectra of many of these levels continue to show very significant $\Delta v \neq 0$ processes and offer the opportunity of extending the investigation of the continuum resonances to still higher energies. Angular distribution studies of these photoelectron spectra are underway and will be even more valuable if carried out

with rotational resolution as has been demonstrated for NO.[22]

[1] S. Katsumata, K. Sato, Y. Achiba, and K. Kimura, J. Electron. Spectrosc. Relat. Phenom. 41, 325 (1986).

[2] P. J. Miller, L. Li, W. A. Chupka, and S. D. Colson, J. Chem. Phys. (in press).

[3] A. Sur, C. V. Ramana, W. A. Chupka, and S. D. Colson, J. Chem. Phys. 84, 69 (1986).

[4] R. J. S. Morrison, W. E. Conaway, T. Ebata, and R. N. Zare, J. Chem. Phys. 84, 5527 (1986).

[5] T. M. Orlando, S. L. Anderson, J. R. Appling, and M. G. White, J. Chem. Phys. 87, 852 (1987).

[6] S. T. Pratt, P. M. Dehmer, and J. L. Dehmer, Chem. Phys. Lett. 105, 28 (1984).

[7] S. T. Pratt, P. M. Dehmer, and J. L. Dehmer, J. Chem. Phys. 85, 3379 (1986).

[8] W. A. Chupka, J. Chem. Phys. 87, 1488 (1987).

[9] A. P. Hickman, Phys. Rev. Lett. 59, 1553 (1987).

[10] J. A. Stephens, M. Braunstein, and V. McKoy, J. Chem. Phys. (in press).

[11] P. Lambropoulos, Adv. At. Mol. Phys. 12, 87 (1976).

[12] M. E. Strand, J. Hansen, R.-L. Chien, and R. S. Berry, Chem. Phys. Lett. 59, 205 (1978).

[13] S. N. Dixit and P. L. Lambropoulos, Phys. Rev. Lett. 46, 1278 (1978); Phys. Rev. A 27, 168 (1983).

[14] S. N. Dixit and V. McKoy, J. Chem. Phys. 82, 3546 (1985).

[15] J. R. Appling, M. G. White, W. J. Kessler, R. Fernandez, and E. D. Poliakoff, J. Chem. Phys. 88, 2300 (1988).

[16] M. Braunstein, J. A. Stephens, and V. McKoy (private communication).

[17] D. L. Lynch, S. N. Dixit and V. McKoy. Chem. Phys. Lett. 123, 315 (1986).

[18] R. J. Buenker and S. D. Peyerimhoff, Chem. Phys. Lett. 34, 225 (1975).

[19] P. J. Miller, L. Li, W. A. Chupka, and S. D. Colson, J. Chem. Phys. 88, 2972 (1988).

[20] W. A. Chupka, P. J. Miller, and E. E. Eyler, J. Chem. Phys. 88, 3032 (1988).

[21] H. Park, P. J. Miller, W. A. Chupka, and S. D. Colson (unpublished results).

[22] K. S. Viswanathan, E. Sekreta, E. R. Davidson, and J. P. Reilly, J. Phys. Chem. 90, 5078 (1986).

J. Chem. Phys. Vol. 89, No. 7, 1 October 1988

63

Multiphoton optical and photoelectron spectroscopy of 4s–3d and 5s–4d Rydberg complexes of O_2

Haiyoon Park, Paul J. Miller, William A. Chupka, and Steven D. Colson

Sterling Chemistry Laboratory, Yale University, New Haven, Connecticut 06511-8118

The 4s–3d and 5s–4d Rydberg complexes of O_2 have been observed by (2 + 1) resonance-enhanced multiphoton ionization spectroscopy. All states show sharp rotational structure. Vibrational analysis (and rotational analyses of two bands) shows that all observed states are purely Rydberg in character with no detectable perturbations. Photoelectron spectra of the more intense peaks show the $\Delta v = 0$ transition to be dominant, but large contributions from $\Delta v \neq 0$ transitions are observed and attributed to features in the ionization continuum. The $\Delta v \neq 0$ transitions are relatively weak for bands ascribed to excitation of a $3d\delta$ Π_g state and provide a method for producing nearly pure vibrational preparations ($v^+ = 0$–3) of O_2^+ ions in the ground electronic state. Large amounts of O^+ ions are observed and possible mechanisms of formation are discussed.

INTRODUCTION

A large number of Rydberg series extending to high principal quantum numbers and converging to excited states of the O_2^+ ion have been identified.[1–3] In contrast, only the very lowest members of Rydberg series converging to the ground state have previously been identified. This situation is due in large part to the fact that the $np\pi$ $^3\Sigma_u^-$ and $np\sigma$ $^3\Pi_u$ Rydberg series, which are single-photon optically allowed from the X $^3\Sigma_g^-$ ground state, interact very strongly with valence states of the same symmetry, yielding adiabatic potential curves which differ greatly from that of the ground state O_2^+ ion. This results in very complex spectra and identification of the higher members of the series has not been made.[4,5] With the assistance of high quality theoretical calculations, the lowest member of these series have only recently been reliably identified and well characterized.

Among the optically forbidden Rydberg states converging to the ground state of the O_2^+ ion, only the $3s\sigma$ $^3\Pi_g$ and $^1\Pi_g$ states had been identified in inelastic electron scattering experiments.[6,7] Recently, these states were studied by a (2 + 1) resonance-enhanced multiphoton ionization (REMPI) process.[8–11] In these studies, rotational analysis of the $v' = 2$ band of the $3s\sigma$ $^3\Pi_g \leftarrow\leftarrow X$ $^3\Sigma_g^-$ transition, the $v' = 0$ band of the $3s\sigma$ $^1\Pi_g \leftarrow\leftarrow X$ $^3\Sigma_g^-$ transition and the $v' = 3$ band of the $3s\sigma$ $^1\Pi_g \leftarrow\leftarrow a$ $^1\Delta_g$ transition were reported. Most of the other bands of these systems were strongly predissociated and showed no rotational structure.

In a continuation of the above studies, it was recognized that the photoelectron spectrum produced in these experiments exhibited strong non-Franck–Condon behavior due to a shape resonance and an autoionizing resonance in the associated ionization continua.[12] The O_2 molecule serves as a convenient molecule for investigating these effects since good theoretical calculations of the position of the shape resonance and its effect on the R (internuclear distance) dependence of the photoionization cross section exist.

The purpose of this investigation was (i) to extend the ns Rydberg series to higher principal quantum numbers, (ii)

to detect and identify members of nd series, (iii) to take photoelectron spectra via these series in order to explore the possibility of production of vibronically state selected O_2^+ ions, and (iv) to extend the study of resonances in the ionization continua. The studies of the ionization continua should form a valuable complement to the similar studies[12] on the $3s$ state for several reasons. The higher members of both ns and nd series are expected to be significantly less perturbed or predissociated by valence states than is the $3s$ member. The higher photon energies of this single-color experiment permit the exploration of higher energy regions of the ionization continuum. The photoionization via nd levels (especially $nd\delta$) permit some variation in the photoionization continuum channels.

EXPERIMENTAL

The (2 + 1) resonance-enhanced multiphoton ionization spectra of O_2 were obtained by detecting the O_2^+ and O^+ ions with a time-of-flight mass spectrometer. The output of a XeCl excimer pumped dye laser (Questek 2240, Lambda Physik FL2002) was frequency doubled by focusing into a β–BaB_2O_4 (BBO) crystal. The frequency-doubled laser beam was refocused into a molecular beam formed by supersonic expansion of gas from either a pulsed or cw nozzle. The gas used was either pure oxygen or a 25% mixture of O_2 in argon. In this experiment, the fundamental laser beam was not separated from the frequency-doubled beam since there was no evidence that it had any effect on the REMPI spectra or photoelectron spectra.

The ionization signal was detected and amplified by an electron multiplier tube and/or microchannel plate, and fed into a Tektronix 7912D programmable digitizer interfaced to an LSI 11/23 computer for mass analysis and signal averaging. Wavelength scans in the 240–210 nm region were obtained by recording the ionization signal in the $m/z = 32$ (O_2^+) and $m/z = 16$ (O^+) mass channels.

Photoelectron spectra were obtained at different excitation energies by focusing the frequency-doubled laser beam to a point about 5 mm from an effusive nozzle in a time-of-

light, otoelectron spectrometer with 2π sr collection efficiency.[13] The photoelectron signal was detected and amplified by microchannel plates.

RESULTS AND DISCUSSION

The $(2 + 1)$ REMPI spectra are shown in Figs. 1 and 2. Figure 1 shows predominantly the bands associated with the $v' = 0-4$ levels of 4s–3d complex, while Fig. 2 shows predominantly those bands associated with excitation of the $v' = 0-2$ levels of 5s–4d complex. Since the $v' = 3$ and $v' = 4$ levels of the 4s–3d complex overlap the $v' = 0$ and $v' = 1$ levels of the 5s–4d complex, these sections of the spectrum are reproduced in both figures, aligned in frequency so as to exhibit the vibrational progressions within the two Rydberg complexes. With a few possible exceptions, all the rotational peaks are laser resolution limited in width (≈ 1 cm^{-1}). The few possible exceptions may be composite or slightly ac Stark broadened features. In no case is the rotational linewidth (FWHM) greater than 3 cm^{-1}. The extent and complexity of the cold spectra of Figs. 1 and 2 immediately indicate that it is not due to the $4s\sigma$ and $5s\sigma$ Rydberg states alone but must be due to the 4s–3d and 5s–4d complexes, as expected from theoretical calculations. Nevertheless, the spectra must contain bands due to the $4s\sigma$ and $5s\sigma\,^3\Pi_g$ Rydberg states and possibly the $4s\sigma$ and $5s\sigma\,^1\Pi_g$ states as well
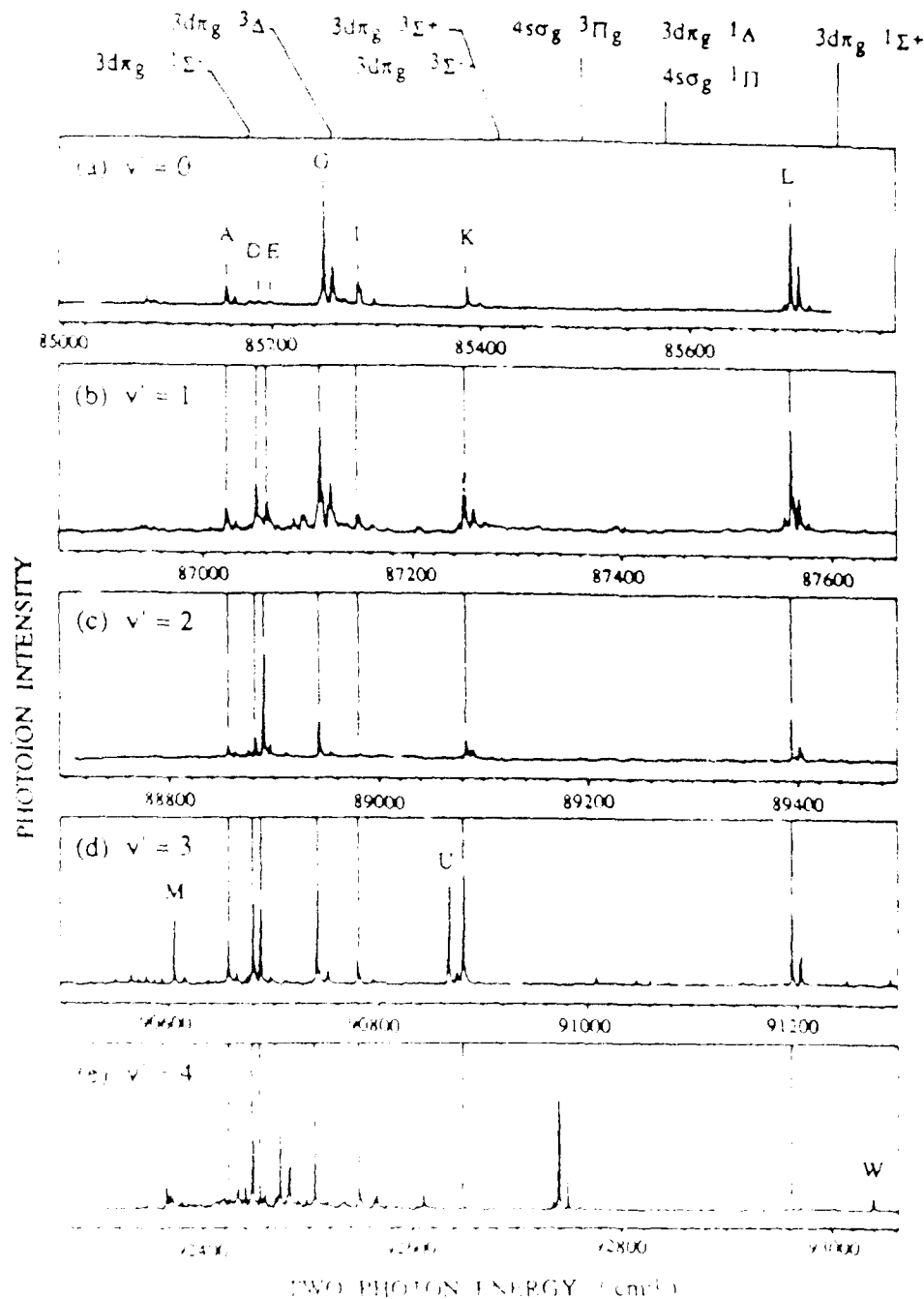

FIG. 1. The $(2 + 1)$ REMPI spectra of the 4s–3d, $v' = 0-4$ Rydberg states of O$_3$. Frequency units (in wave numbers) of the abscissa scale correspond to the two photon total energies. The top panel shows the energies calculated by Cartwright *et al.* (Ref. 6).

Chem. Phys., Vol. 89, No. 11, 1 December 1988

65

FIG. 2. The $(2 + 1)$ REMPI spectra of the $5s-4d$, $v' = 0-2$ Rydberg states of O_2. Bands (W) and (X) correspond to the higher members of this series. Frequency units (in wave numbers) of the abscissa scale correspond to the two photon total energies. The top panel shows the energies calculated by Cartwright et al. (Ref. 6).
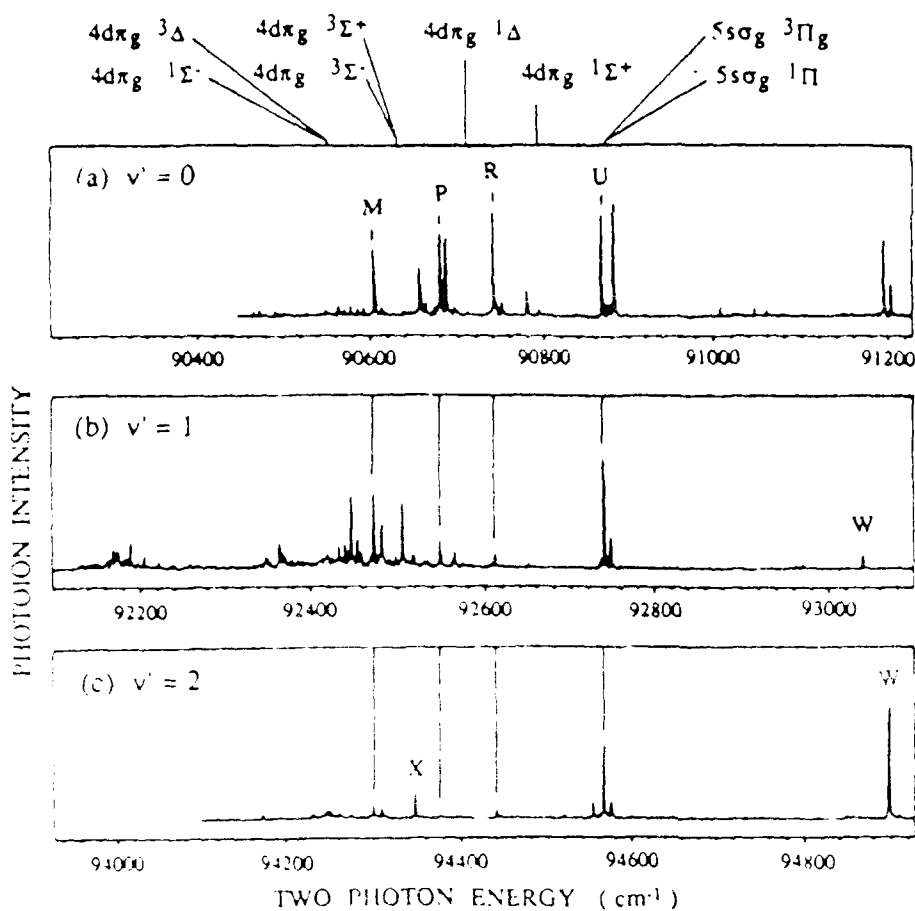
We note that although the $3s\sigma$ members of these two series are fairly strongly predissociated, the $4s\sigma$ members (mixed at least to some extent with $3d\sigma$) are much less predissociated. This is expected since the square of the perturbation matrix element for a Rydberg-valence interaction is expected to scale approximately as $(n^*)^{-3}$, where n^* is the effective principal quantum number. Therefore, predissociation should be lower for the $4s\sigma$ state by approximately the factor $(1.88/3.00)^3 \approx 0.25$ if the Franck-Condon factor is neglected. A visual comparison of the two spectra suggests that the degree of narrowing for the $4s\sigma$ state may be several times more than that, indicating that the Franck-Condon factors for the Rydberg-valence mixing are smaller as well. This is expected for the strongly repulsive state assumed to be responsible for the predissociation. This lack of predissociation together with the unperturbed nature of the vibrational levels give assurance that any significant non-Franck-Condon peaks in the photoelectron spectrum must be due to either the invalidity of the Born-Oppenheimer separation or to unusual features in the ionization continua.

Electronic state assignment

The ground state of the O_2 molecule has the configuration $(1\sigma_g)^2(1\sigma_u)^2(2\sigma_g)^2(2\sigma_u)^2(3\sigma_g)^2(1\pi_u)^4(1\pi_g)^2$. The Rydberg series which converge to the ground state of the O_2^+ ion and which are the strongest two-photon allowed series from the ground state of O_2 involve excitation from the $1\pi_g$ valence orbital to $ns\sigma$ and $nd(\sigma,\pi,\delta)$ orbitals giving $^3\Sigma_g^-$,

$^3\Pi_g$ and $^3\Delta_g$ states formed on the O_2^+ X $^2\Pi_g$ ion core. The lowest member of the series, the $3s\sigma$ $^3\Pi_g$ state has been previously identified by $(2 + 1)$ REMPI.[8] The next member of the ns series, $4s\sigma$ $^3\Pi_g$, is expected to form part of a $4s-3d$ complex since s and d electrons have comparable quantum defects, modulo one, and indeed the spectra shown in Figs. 1 and 2 can be explained by such a complex. Such complexes have been very well investigated in the case of NO.[14] In that case, it was shown that this interaction results in a strong mixing between the $nd\sigma$ and $(n + 1)s\sigma$ series with a value of 910 cm^{-1} for the interaction matrix element for the $4s\sigma-3d\sigma$ pair. A comparable interaction strength in oxygen is suggested by the calculations of Cartwright et al.[6] who calculate the $4s\sigma-3d\sigma$ energy difference to be 0.22 eV compared to 0.23 eV for NO, although the energy order is reversed. It is plausible to attribute much of this energy difference to $s-d$ interaction since otherwise the calculated energy difference seems too large.

Table I shows the theoretical T_{00} values for the gerade Rydberg states of O_2 obtained by the ab initio calculations of Cartwright et al.[6] Also shown are the measured energies of peaks (A)–(X) (see Figs. 1 and 2) as well as those of the previously observed $3s\sigma$ Rydberg states. The calculated energies, after a slight downward adjustment, are also shown at the top of Figs. 1 and 2. This adjustment, 75 cm^{-1} for $4s-3d$ and 30 cm^{-1} for $5s-4d$, was estimated by comparing the calculated values for the $3s\sigma$ states with the experimental

J. Chem. Phys., Vol. 89, No. 11, 1 December 1988

66

TABLE I. Theoretical T_ω values and observed peak positions (in eV) for Rydberg states of O_2.

Theoretical T_ω values (eV)[a]				Major observed peaks (eV)	
Rydberg orbital		Triplet states	Singlet states		
$1\omega_g$	Π	8.23	8.34	$3s\sigma_g$ $^3\Pi_g$	8.143[b]
$3d\sigma_g$	Π	10.39	10.41	$3s\sigma_g$ $^3\Pi_g$	8.228[c]
$3d\pi_g$	Σ^+	10.60	10.64		
	Δ	10.58	10.62	Peak A	10.558
	Σ^-	10.60	10.57	D	10.562
$3d\delta_g$	Π	...	...	E	10.563
	Φ	...	...	G	10.570
$4\omega_g$	Π	10.61	10.62	H	10.571
$4d\sigma_g$	Π	11.17	11.18	I	10.574
$4d\pi_g$	Σ^+	11.24	11.26	K	10.587
	Δ	11.23	11.25	L	10.625
	Σ^-	11.24	11.23	M	11.234
$4d\delta_g$	Π	...	...	R	11.251
	Φ	...	...	U	11.266
$5\omega_g$	Π	11.27	11.27	W	11.536
				X	11.698

[a] Reference 6
[b] Reference 7
[c] Reference 8

ones and scaling the error in the ionization potentials by $(n^*)^{-3}$. Two states, the $3d\sigma$ $^3\Pi_g$ and $^1\Pi_g$ ($v' = 0$) states, are not shown in Fig. 1 since they are off scale to lower energies. However, their calculated energies are coincidentally about one vibrational spacing (≈ 1870 cm^{-1}) below peak (G). The photoelectron spectrum of peak (G) is shown in Fig. 3. The spectrum shows an unusually large intensity of the $v^+ = 1$ peak, namely about one third of that of the expected $v^+ = 0$ peak, while all other peaks are much lower. These two photoelectron peaks also show very different wavelength dependence, as shown in Fig. 5, indicating that the region about peak (G) probably contains two overlapping bands corresponding to the $v' = 0$ and $v' = 1$ levels of two different electronic states. The same situation holds for all higher vibrational bands of that region. Therefore, we tentatively assign the $v' = 1$ band of Fig. 5 to the $3d\sigma$ $^3\Pi_g$ (or possibly $^1\Pi_g$) state. An REMPI-MS wavelength scan of the region where the corresponding $v' = 0$ level should be located yielded a very weak structure (see Fig. 6) about 30 times less intense than the $v' = 1$ peak of Fig. 5. From Franck–Condon factors alone one would expect it to be lower only by a factor of 2 or so. The reason for this discrepancy is not known. It is possible that the $v' = 0$ peaks are abnormally
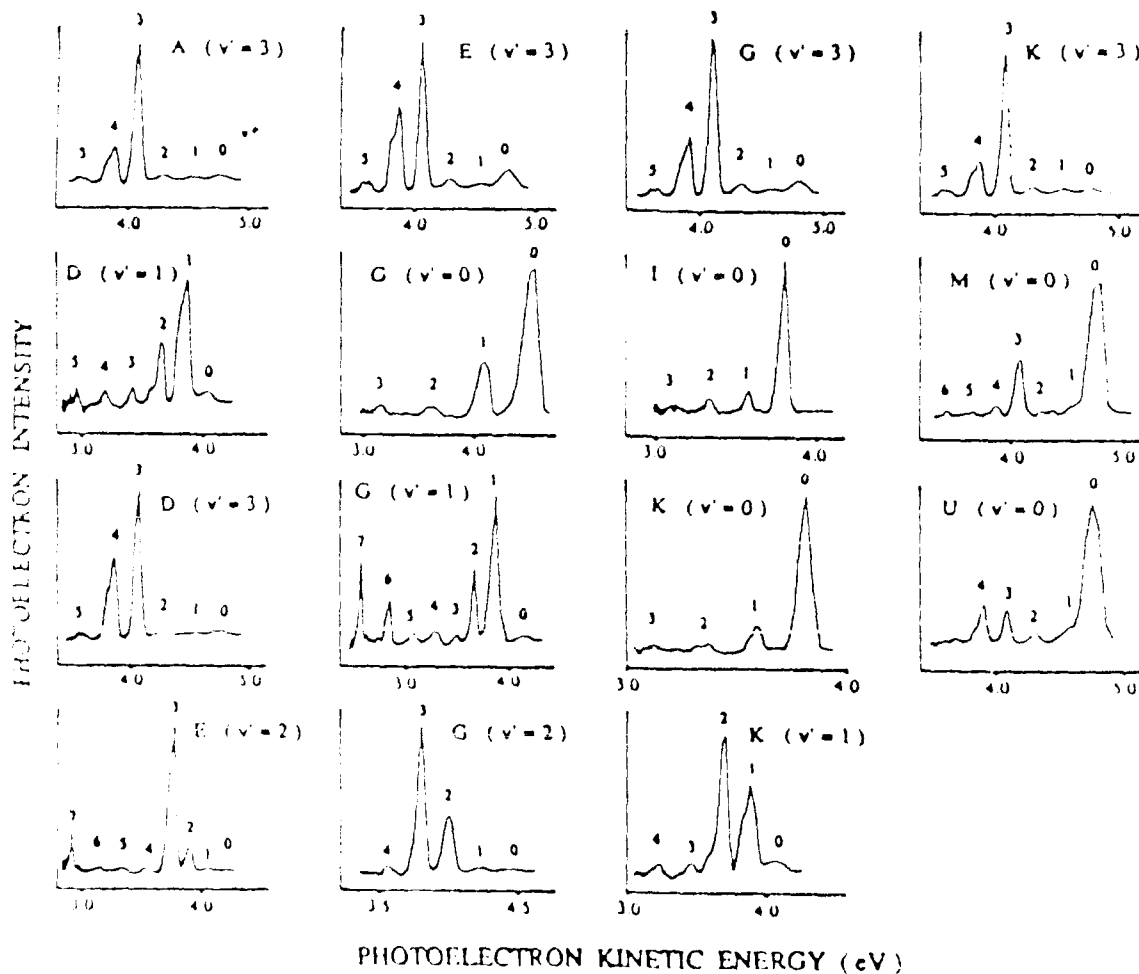

FIG. 3. Photoelectron spectra of various bands indicated in Figs. 1 and 2. Note that the region about the band (G) appears to consist of overlapped bands differing by one unit of the vibrational quantum number (see the text and Fig. 4).
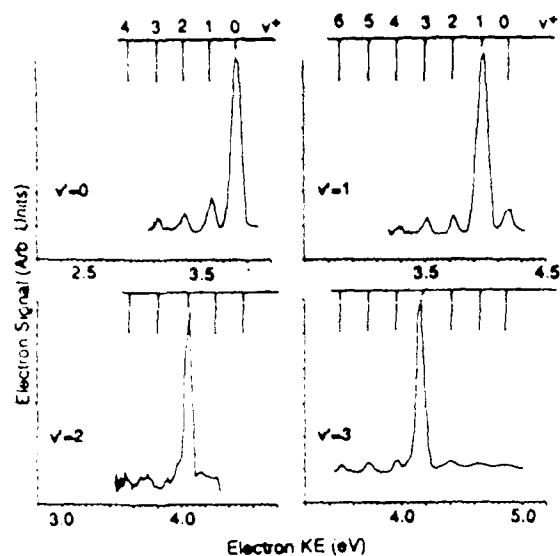
PHOTOELECTRON KINETIC ENERGY (eV)

J. Chem. Phys., Vol. 89, No. 11, 1 December 1988

67

FIG 4 Photoelectron spectra of $v' = 0-3$ levels of the band (L) in Fig. 1 and tentatively assigned to the $3d\delta$ Rydberg state (see the text) This band yields the purest preparations of vibrationally excited O_2^+ ion.

high due to intensity borrowing from near resonant $v' \pm 1$ levels.

Unfortunately, Cartwright *et al.*[6] have not calculated the position of the $3d\delta$ $^3\Pi_g$ or $^1\Pi_g$ state. We tentatively assign peak (L) (also its progression) to that state for the following reasons. The calculated average energy of the $3d\pi$ triplet complex is 10.59 eV. Both the $3d\pi$ and $3d\delta$ are unperturbed by the $4s\sigma$. The normal splitting pattern of a d orbital has the energy increasing with λ, i.e., δ above π above σ. Thus, we expect $3d\delta$ to be above the average of $3d\pi$, probably at 10.60 eV or slightly higher. The $3d\delta$ Rydberg orbital will be split by interaction with the $^2\Pi_g$ ion core into Π and Φ state at higher and lower energies, respectively. This splitting will be about twice that of the $3d\pi$ orbital into Σ and Δ states (0.02 eV total splitting) yielding the Φ states (optically forbidden in two-photon absorption) at ≈ 10.58 eV and
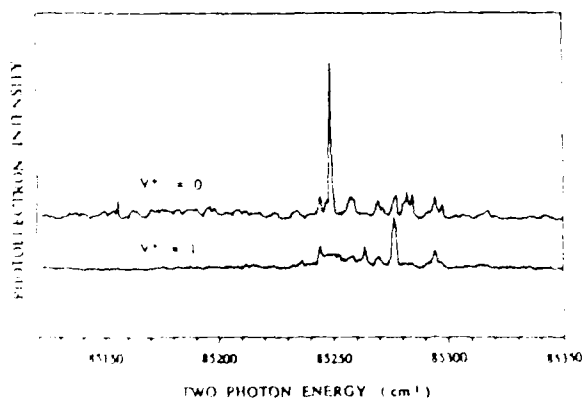

FIG 5 Wavelength scan of the photoelectron intensity in the region of band (G), monitoring both $v^+ = 0$ and $v^+ = 1$ photoelectron peaks. Relative rotational peak intensities differ to a small extent between this scan and that of the total ion scan shown in Fig. 1 due to the different rotational temperature and laser intensity employed in the photoelectron scan.
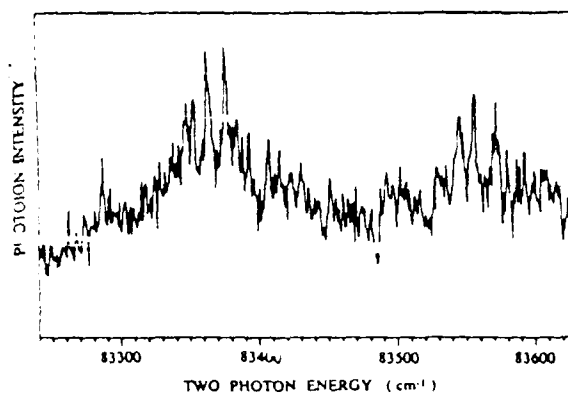

FIG. 6. Wavelength scan of the O_2^+ intensity in the region expected for two photon excitation of the $v' = 0$ $3d\sigma$ Rydberg state (see the text).

the Π states at about 10.62 eV (or ≈ 85660 cm^{-1}) or somewhat higher which is in fair agreement with the position of the (L) band.

While it is clear that the calculated general placement of the $4s$-$3d$ complex is very good and some correlations are suggestive, no reliable assignments can be made. In fact the assignment of states is more complex than the table of calculated energies and a thoughtless application of selection rules suggests.

The complexity of any analysis is due in large part to the fact that the angular momentum coupling case is intermediate between LS and JJ. The singlet–triplet splittings calculated for various states of the complex range from 0.01 to 0.04 eV and are thus comparable to the spin–orbit splitting in the $^2\Pi_g$ ground state of the O_2^+ ion. This is in contrast to the case of the $3s\sigma$ states where the singlet–triplet splitting is found to be about 700 cm^{-1} for $v' = 0$, and LS coupling is appropriate resulting in a fairly normal triplet structure for the $^3\Pi_g$ state with a spin–orbit coupling constant of ≈ 100 cm^{-1}. Even in that case, the significant intensities of the $^1\Pi_g$ transitions are at least partly due to LS uncoupling with resultant singlet–triplet mixing. In the case of the $4s$-$3d$ complex this mixing will be very strong, reducing the distinction between singlets and triplets, and therefore we cannot assume that transitions to singlet levels will be weak.

Since the singlet–triplet splitting of these Rydberg states will scale roughly as $(n^*)^{-3}$, we can expect that at sufficiently high values of n^*, a JJ coupling scheme will become appropriate and will be characterized by pairs of bands separated by ≈ 197 cm^{-1}, the value of the spin–orbit splitting of the O_2^+ ion. This situation is apparently still not reached for the $5s$-$4d$ complex since no such separations are clearly evident. The spectrum is further complicated by the fact that term splittings, which also scale with $(n^*)^{-3}$, are now comparable to, and in some cases less than the spin–orbit coupling. In principle, rotational analysis of the more extensive spectrum of a warmer gas should be a great help in the assignment. However, for much of the spectrum this will probably require both higher resolution and greater intensities than used in this experiment, although ac Stark effects will be a limiting factor. Experimentally, some help in state assignment may possibly result from a study of photoelectron angular distributions.

J Chem. Phys., Vol. 89, No. 11, 1 December 1988

68

Vibrational analysis

While a detailed electronic assignment is not done in this work, assignment of vibrational levels can be made with confidence, primarily from the result of the photoelectron spectra (see Figs. 3 and 4), and the great similarity of the bands corresponding to different vibrational levels. The spectra in Fig. 1 have been vertically aligned using the peak (L) and its counterparts in the higher vibrational quantum number band systems. Those of Fig. 2 used the peak (U). The excellent correspondence of most of the other strong peaks is evident. Table II lists the observed energies of the most intense peaks, the values of ω_e and $\omega_e x_e$ calculated from each progression and the values for the O_2^+ ion in its ground state. The close agreement between the vibrational constants for all the Rydberg states and those of the O_2^+ ion is convincing evidence that none of the states are detectably perturbed. This is an important consideration in the interpretation of the photoelectron spectra to be discussed later.

Table II also contains some evidence relevant to electronic state assignment. We note that peak (L) and its progression yield the largest values of ω_e and $\omega_e x_e$. This implies that the Rydberg electron in this orbital is slightly less antibonding (or slightly more bonding) than the electron in the other Rydberg orbitals. A consideration of the molecular orbital correlation diagram[15] shows that the $3d\delta$ orbital has just that characteristic.

The origins ($v' = 0$ bands) of the 5s–4d complex were found to overlap the $v' = 3$ region of the 4s–3d complex. This was readily established by inspection of this region [see Fig. 2(d)], noting the presence of additional structure absent for the lower energy regions and by noting that this additional structure appears at energies corresponding to effective principal quantum numbers increased by approximately one above those for the 4s–3d origin. This assignment was confirmed by the photoelectron spectra of two of the most prominent bands attributed to the 5s–4d complex. Figure 2 shows the spectra attributed to the $v' = 0$–2 bands of the 5s–4d complex, aligned using the peak (U) so as to exhibit the nearly identical line positions for these vibrational levels. Since the vibrational progressions could be observed only for the first three members, vibrational constants could not be accurately measured. As expected, the energy difference between $v' = 0$ and $v' = 1$ bands is nearer to that of the O_2^+ ion than for the 4s–3d complex but the second difference is too large for undetermined reasons.

TABLE II. Observed position of band origins and derived vibrational constants (in cm^{-1}) for the 4s–3d complex.

Peak	v	obs.	Δv	ω_e	$\omega_e x_e$	n^*
A	0	85 156.8	0.0	1898.1	16.2	2.998
	1	87 022.4	0.1			
	2	88 856.4	−0.6			
	3	90 656.8	−0.1			
	4	92 425.3	−0.1			
D	0	85 187.3	0.0	1895.1	16.05	3.002
	1	87 050.3	0.0			
	2	88 881.2	0.1			
	3	90 680.1	−0.1			
	4	92 446.8	−0.1			
E	0	85 198.0	0.0	1893.8	15.95	3.003
	1	87 060.6	−0.7			
	2	88 889.5	0.4			
	3	90 687.0	1.0			
	4	92 454.0	0.2			
G	0	85 248.4	0.0	1895.2	16.15	3.009
	1	87 110.8	0.5			
	2	88 942.6	−0.7			
	3	90 740.6	−0.4			
	4	92 506.1	0.1			
H	0	85 256.8	0.0	1896.0	16.1	3.010
	1	87 121.1	−0.5			
	2	88 953.4	−1.2			
	3	90 751.0	0.6			
	4	92 518.7	0.1			
I	0	85 282.0	0.0	1897.1	16.1	3.014
	1	87 147.4	−0.5			
	2	88 980.6	−1.0			
	3	90 779.5	0.6			
	4	92 548.3	0.1			
K	0	85 386.9	0.0	1893.8	15.6	3.026
	1	87 248.8	0.7			
	2	89 083.9	−3.0			
	3	90 881.1	−0.7			
	4	92 650.0	0.1			
L	0	85 694.5	0.0	1899.3	16.45	3.066
	1	87 560.9	0.0			
	2	89 393.8	0.6			
	3	91 195.0	0.0			
	4	92 962.8	−0.1			
$3s\sigma$	$^2\Pi_g$					1.882
$3p\sigma$	$^2\Pi_g$					1.861
O_2^+	X	$^2\Pi_g$		1904.7	16.25	

$^a\Delta v = v_{obs} - v_{cal}$

$^b n^*$ effective principal quantum number

TABLE III. Observed position of band origins for the 5s–4d complex and higher members.

Peak	v'	Obs. (cm^{-1})	Δ	Δ^2	n^*
M	0	90 604.2			4.028
	1	92 472.9	1868.7		
	2	94 300.8	1827.9	40.8	
N	0	90 613.7			4.031
	1	92 428.7	1869.0		
	2	94 311.0	1828.3	40.7	
P	0	90 680.1^a			4.051
	1	92 548.3	1868.2		
	2	94 377.1	1828.8	39.4	
R	0	90 740.6^b			4.069
	1	92 610.4	1869.8		
	2	94 440.5	1830.1	39.7	
U	0	90 867.9			4.109
	1	92 738.3	1870.4		
	2	94 567.9	1829.6	40.8	
W	0	93 035.5			5.036
	1	94 899.7	1864.2		
X	0	94 349.1			6.031

^{a} Overlapped with peak (D) ($v' = 3$).

^{b} Overlapped with peak (G) ($v' = 3$).

J. Chem. Phys., Vol. 89, No. 11, 1 December 1988

69

The two fairly large peaks, peak (W) and peak (X) in Fig. 2 do not fit into the 5s–4d complex. They may correspond to the $v' = 0$ bands of the strongest members of the 6s–5d and 7s–6d complexes as suggested by the values of their apparent effective principal quantum numbers.

Rotational analysis

If we assume that band progression (L) corresponds to $3d\delta\ ^1\Pi_g$ or $^3\Pi_g \leftarrow -X\ ^3\Sigma_g^-$ transition and that the upper state behaves like Hund's case (a), we expect 15 rotational branches corresponding to $\Delta J = 0,\ \pm 1,\ \pm 2$ for each of the spin components in the ground state. But, since the three spin components of each N in the ground state have almost the same energies (the largest separation is about 2 cm^{-1}), we notate the rotational branches according to the values of ΔN. In order to distinguish the transitions from F_1, F_2, and F_3 components in the ground state, we add 1, 2, and 3 as right subscript to ΔN, respectively.

Figure 7 shows the rotational assignment for the $3d\delta\ \Pi_g$ ($v' = 1$) $\leftarrow -X\ ^3\Sigma_g^-$ ($v'' = 0$) transition from which a rotational constant $B_1 = 1.72 \pm 0.01$ cm^{-1}, and an origin $v_1 = 87\ 563.0 \pm 1.0$ cm^{-1} were obtained. Rotational analysis of the $v' = 3$ band (Fig. 8) of the $3d\delta\ \Pi_g$ ($v' = 3$) $\leftarrow -X\ ^3\Sigma_g^-$ ($v'' = 0$) transition gave a rotational constant $B_3 = 1.68 \pm 0.01$ cm^{-1}, and an origin $v_3 = 91\ 197.0 \pm 1.0$ cm^{-1}. The rotational line positions for this transition are shown in Table IV. Most of the observed rotational lines fit to within 1 cm^{-1} of their least squares calculated positions. The $v' = 0$ and 2 levels of the $3d\delta$ state were not analyzed due to either weak signal or paucity of rotational lines.

For a $^3\Pi$ state, there are three spin–orbit components and each component shows a different rotational structure. In the case of a transition to the F_2 component of a $^3\Pi$ state, there occur all 15 rotational branches, i.e., N_3, O_2, O_3, P_1, P_2, P_1, Q_1, Q_2, Q_3, R_1, R_2, R_3, S_1, S_2, and T_1 branches. But for the F_1 component, there should occur M_3, N_2, and O_1 branches but no R_3, S_2, and T_1 branches. For the F_3 component, there should occur S_3, T_2, and U_1 branches but no N_3, O_2, and P_1 branches. In addition to these differences, some rotational structures with low rotational quantum numbers are also different from those of the F_2 component of the $^3\Pi$ state. As
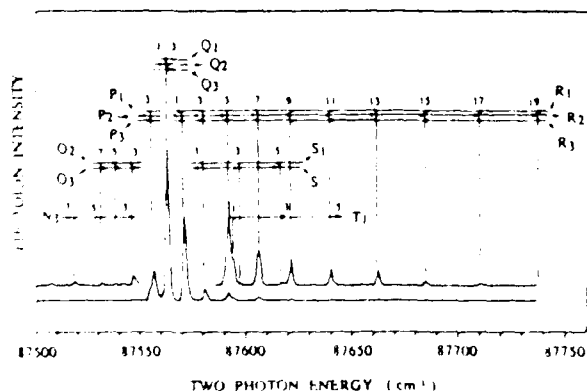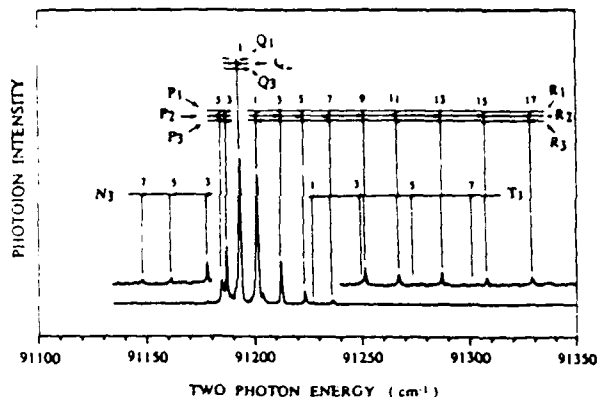
FIG. 8. Rotational structure and analysis of the $v' = 3$ band of the $3d\delta\ \Pi_g$ state [band (L) in Fig. 1(d)]. The dots indicate calculated positions of rotational lines.

shown in Figs. 7 and 8, we apparently observed all 15 branches which should occur only for the transition to the F_2 component of a $^3\Pi$ state. Thus we can plausibly assign this state to the F_2 component of the $3d\delta\ ^3\Pi_g$ state. However, we could find no convincing evidence for the other F_1 and F_3 components and the rotational structure of the transition to the F_2 component of a $^3\Pi$ state is the same as that of a $^1\Pi$ state since they have the same $\Omega = 1$ quantum number. Therefore there is still a possibility that this state could be a $^1\Pi$ state although the strong intensity of this band (see Fig. 1) argues somewhat against this assignment. However, as discussed earlier, the transition to the $3s\sigma\ ^1\Pi_g$ state shows stronger intensities than expected, and one might plausibly expect relatively strong intensities for transitions to the singlet states of the 4s–3d Rydberg complex. An REMPI experiment using the spin-allowed transition from the metastable $a\ ^1\Delta_g$ state of O_2 made by microwave discharge[11] will be very helpful for reliable assignment of this state.

Photoelectron spectra and ion state preparation

Simple application of the Franck–Condon principle to the single-photon ionization of well described single-configuration Rydberg states of molecules leads to the prediction that the vibrational quantum number of the ion core will be conserved almost exclusively. Photoionization of certain Rydberg states of some molecules such as NH_3, NO, and N_2 show such behavior.[16–18] However, there is a large and growing number of examples which show large deviations from this behavior. A general analysis of reasons for such apparently anomolous behavior has been given.[19] Among these reasons are the presence of shape resonances and autoionizing resonances in the ionization continua. The latter resonances may be core- or doubly excited resonances, or valence states which are either optically allowed or even forbidden but strongly autoionizing into the optically allowed continuum. Recently, strong $\Delta v \neq 0$ transitions in the photoelectron spectra of $3s\sigma\ ^3\Pi_g$ Rydberg states of O_2 have been ascribed to specific resonances.[12,20] However, many of the $3s\sigma$ Rydberg levels are strongly predissociated and significantly perturbed, while the 4s–3d and 5s–4d Rydberg states described in this work are not detectably perturbed and there

J. Chem. Phys., Vol. 89, No. 11, 1 December 1988

70

TABLE IV. Experimental and calculated rotational line positions (in cm^{-1}) and deviations ($\Delta = \nu_{calc} - \nu_{obs}$ in cm^{-1}) for the $3d\delta\ \Pi_g$ ($v' = 1$ and $v' = 3$) $\leftarrow X\ ^2\Sigma_g^-$ transitions.

$v' = 1$ ($B_1 = 1.72$)				$v' = 3$ ($B_3 = 1.68$)			
Obs.	Branch	Calc.	Δ	Obs.	Branch	Calc.	Δ
87 531.0	$O_2(7)$*	87 530.7	−0.3	91 184.8	$P_2(7)$	91 183.7	−1.1
87 538.2	$O_2(5)$	87 537.1	−1.1		$P_2(5)$	91 184.1	−0.7
87 546.2	$O_2(3)$	87 545.8	−0.4	91 187.1	$P_2(3)$	91 186.5	−0.6
87 555.8	$P_1(3)$	87 554.6	−1.2	91 188.9	$P_1(3)$	91 188.6	−0.3
	$P_3(3)$	87 554.7	−1.1		$P_3(3)$	91 188.5	−0.4
87 562.2	$Q_2(1)$	87 560.1	−2.1	91 193.2	$Q_2(1)$	91 194.1	0.9
	$Q_1(1)$	87 562.0	−0.2		$Q_1(1)$	91 196.0	2.8
	$Q_2(3)$	87 563.0	0.8				
87 570.2	$R_1(1)$	87 568.9	−1.3	91 201.4	$R_1(1)$	91 202.7	1.3
	$R_3(1)$	87 569.9	−0.3				
87 579.8	$R_1(3)$	87 578.7	−1.1	91 212.5	$R_1(3)$	91 211.9	−0.6
	$R_3(3)$	87 578.8	−1.0		$R_3(3)$	91 212.1	−0.4
	$S_1(1)$	87 579.2	−0.6				
87 591.0	$R_1(5)$	87 590.7	−0.3	91 223.2	$R_1(5)$	91 223.1	−0.1
	$R_3(5)$	87 590.7	−0.3		$R_3(5)$	91 223.1	−0.1
87 593.4	$T_1(1)$	87 593.0	−0.1	91 227.3	$T_1(1)$	91 227.2	−0.1
87 596.6	$S_1(3)$	87 595.9	−0.7				
87 605.5	$R_1(7)$	87 604.9	−0.6	91 236.0	$R_1(7)$	91 236.1	0.1
	$R_3(7)$	87 604.9	−0.6		$R_3(7)$	91 236.1	0.1
87 613.5	$S_1(5)$	87 614.7	1.2				
87 615.9	$T_1(3)$	87 616.6	0.7				
87 620.7	$R_1(9)$	87 621.4	0.7	91 251.5	$R_1(9)$	91 251.0	−0.5
	$R_3(9)$	87 621.3	0.6		$R_3(9)$	91 251.1	−0.4
87 639.1	$R_1(11)$	87 640.2	1.1	91 267.2	$R_1(11)$	91 268.1	0.9
	$R_3(11)$	87 640.1	1.1		$R_3(11)$	91 267.9	1.1
87 661.6	$R_1(13)$	87 661.3	−0.3	91 287.0	$R_1(13)$	91 286.9	−0.1
	$R_3(13)$	87 661.2	−0.4		$R_3(13)$	91 286.7	−0.3
87 684.1	$R_1(15)$	87 684.7	0.6	91 308.0	$R_1(15)$	91 307.9	−0.1
	$R_3(15)$	87 684.5	0.4		$R_3(15)$	91 307.7	−0.3
87 709.8	$R_1(17)$	87 710.4	0.6	91 329.0	$R_1(17)$	91 330.8	1.8
	$R_3(17)$	87 710.2	0.4		$R_3(17)$	91 330.6	1.6
87 738.0	$R_1(19)$	87 738.5	0.5				
	$R_3(19)$	87 738.2	0.2				

*Explanation of notation: The example of $O_2(7)$ corresponds to an O branch ($\Delta N = -2$) originating from the F_2 component ($N'' = 7$) of the ground state of O_2.

fore provide more ideal levels for the study of the effects of such resonances. One of the important goals of this research is to find Rydberg states whose photoionization produces nearly pure preparations of specific vibrational state of the O_2^+ ion. An initial report of this work has emphasized this aspect.[21]

Figure 4 shows the photoelectron spectra of band (L) which was tentatively assigned to the $3d\delta\ \Pi_g$ Rydberg state. As shown in this figure, all vibrational levels of this state show strong peaks for $v^+ = v'$ but very weak peaks for $v^+ \neq v'$. From the analyses of these spectra, we can estimate that over 80% of photoelectrons are produced by $\Delta v = 0$ (i.e., $v^+ = v'$) ionization. This $\Delta v = 0$ ionization corresponds to ejection of the Rydberg electron, with preservation of the electronic and vibrational state of the O_2^+ ion core. Thus resonance-enhanced multiphoton ionization via the $3d\delta\ \Pi_g$ Rydberg state can be a useful source for the production of the $v^+ = 0, 1, 2,$ and 3 levels of the O_2^+ ion in the $X\ ^2\Pi_g$ ground state.

In the single-color experiments of this work, the final photoionization step excites continua at considerably higher energies than in the case of the $3s\sigma$ Rydberg states. Also the

identity and relative amplitudes of various continua are expected to be different since most, if not all, of the Rydberg states have a large amount of d character. The photoelectron spectra, taken using the more intense peaks of Figs. 1 and 2, are shown in Figs. 3 and 4. Qualitatively, it is seen that although the $\Delta v = 0$ transition is (nearly ?) always the most intense one, very considerable intensity is observed for $\Delta v \neq 0$ transitions in most spectra. Photoelectrons corresponding to higher vibrational bands of the O_2^+ ion than shown in the spectra of Figs. 3 and 4 could not be observed due to a retarding potential of a few volts applied at the beginning of the photoelectron spectrometer flight tube. This was necessary in order to maintain vibrational resolution of the fairly energetic (≈ 4 eV), low v^+ photoelectrons.

Figure 9 shows the potential energy curve for the ground electronic state of the O_2^+ ion. Also shown are the potential energy curves for the valence states most likely responsible for the $\Delta v \neq 0$ transitions in the photoionization of the $3s\sigma$ Rydberg states.[17,20] It should be noted that above the potential energy curve of the O_2^+ ion, the $1\ ^1\Pi_u$ state becomes a shape resonance in the σ_u ionization continuum. The curves, which are taken from Guberman,[22] differ from
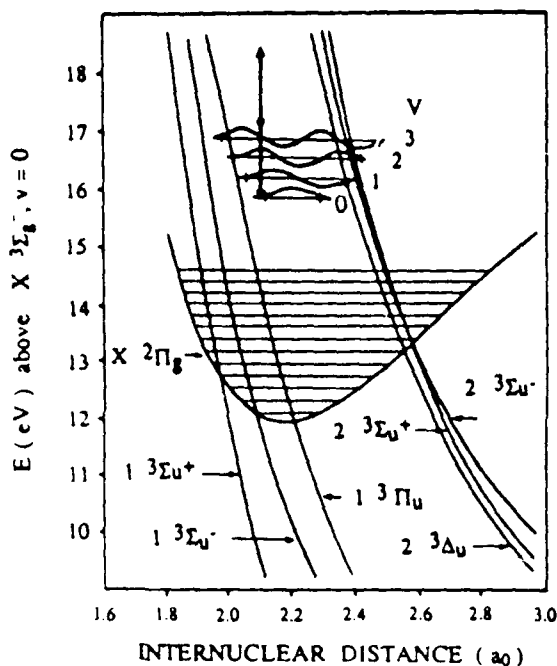
71

FIG. 9. Potential energy curves for the various O$_2$ valence states (including the 1 $^3\Pi_u$ shape resonance) which are expected to influence the photoelectron spectra of the Rydberg states. Also shown is the ground state O$_2^+$ potential energy curve. Horizontal lines (with schematic vibrational wave functions) indicate the energies reached by the photon ionizing the $v' = 0$-3 levels of the 4s–3d Rydberg states.

other theoretical calculations[23,24] by $< \approx 0.3$ eV. In the case of the 3sσ Rydberg states the final (continuum) energies (i.e., three-photon energies) were 12.22, 12.57, 12.92, and 13.26 eV for $v = 0$, 1, 2, and 3, respectively, and it is easily seen that, at these energies, the valence states shown, especially the 1 $^3\Pi_u$ (shape resonance) and 1 $^3\Sigma_u^-$ states, have very favorable Franck–Condon factors from a Rydberg state with a potential energy curve nearly identical with that of the O$_2^+$ ion. However, the transitions (≈ 15.88, 16.23, 16.57, and 16.90 eV for $v = 0$, 1, 2, and 3, respectively) from 4s–3d levels go to considerably higher energies as shown in Fig. 9. In this figure, the horizontal lines in the region ≈ 16–17 eV show the final energies reached from the 4s–3d Rydberg states with $v = 0$-3. These lines are drawn to span the classical (vertical) Franck–Condon region accessed by transition from a Rydberg state with potential energy curve identical with that of the ion and qualitative vibrational wave functions are shown.

It is apparent that, at least for the 4s–3d Rydberg states with lower values of v, the 1 $^3\Sigma_u^+$ and 1 $^3\Sigma_u^-$ states will be much less important than for the 3sσ Rydberg states. If the position of the shape resonance is actually shown by the 1 $^3\Pi_u$ curve, its effect for $v = 0$ might also be expected to be rather small. However, a calculation[25] of the cross section for O$_2$ 3s$\sigma \rightarrow k\sigma_u$ photoionization at the internuclear distance $R = 2.09 a_0$ shows the maximum due to the shape resonance to be at ≈ 7.2 eV with a width of ≈ 2.6 eV as indicated in the figure. The variation of the resonance position with internuclear distance should run roughly parallel to the

1 $^3\Pi_u$ curve shown. Thus, the theoretical calculations indicate that the σ_u shape resonance will probably affect the photoelectron spectra of all vibrational levels of the 4s–3d complex which have strong σ_u continua.

The 1 $^3\Sigma_u^-$ and 1 $^3\Sigma_u^+$ valence states should have much less effect on the 4s–3d photoelectron spectra than in the case of the 3sσ states. However, the photoionization of the 4s–3d states is beset by complications which do not affect the photoionization of the 3sσ states. There are a total of 62 valence states resulting from the ground configuration oxygen in ^3P, ^1D, and ^1S states and they all autoionize (i.e., go above the O$_2^+$ potential curve) at sufficiently small internuclear distance. Even if, as with Guberman,[22] we discard those which differ by more than two orbitals in addition to all singlet states (which may not be justified since some of our observed levels may have significant singlet character), ten states remain. Of these, the ones which pass through the vibrational wave functions of Fig. 8 are shown in that figure and can plausibly be expected to affect the photoelectron spectra. Furthermore, while core excitation of the 3sσ Rydberg states was shown to be very unlikely since it would require a spin–forbidden $a\,^4\Pi_u \leftarrow X\,^2\Pi_g$ transition, the photon energies used in exciting the 4s–3d Rydberg states are exactly in the range for the allowed core-excitation $A\,^2\Pi_u \leftarrow X\,^2\Pi_g$ which is a well known, although not very strong, transition (radiative lifetime $= 0.69\,\mu s, f = 0.001\,36$).[5] The effect of core excitation (i.e., excitation to 4s–3d Rydberg states with an O$_2^+$ $A\,^2\Pi_u$ core) will be negligibly weak for at least $v = 0$, due to a very small Franck–Condon factor ($\approx 2 \times 10^{-4}$) in addition to the low oscillator strength. Larger values of the Franck–Condon factor ($\approx 10^{-1}$–10^{-2}) for $v = 1$–3 make it possible that core excitation plays a significant part in promoting $\Delta v \neq 0$ transitions (since the decay of these core-excited states occurs by configuration interaction and is governed by the Franck–Condon factor between the core-excited Rydberg state and the ground state of the O$_2^+$ ion[26] with its very different potential energy curve), but the low oscillator strength makes it unlikely that the effect will play a dominant role. In order to contribute significantly, these bound core-excited autoionizing states must have appreciable widths so that the requirement for exact resonance is relaxed. They must also have sufficiently large autoionization efficiency relative to predissociation. Some of these states will be excited from the ground state of O$_2$ by a single photon and these questions can be addressed by examination of that spectrum. The single-photon ionization efficiency curve[27] in the relevant region from 720–785 Å shows a wealth of broad autoionization structure, some of which almost certainly belongs to the states of interest here. However, assignment is practically impossible at present due to overlap with stronger series converging to many vibrational levels of the $a\,^4\Pi_u$ and $b\,^4\Sigma_g^-$ states of the O$_2^+$ ion. This great complexity is graphically illustrated by the HeI photoelectron spectrum.[3]

Two general statements can be made about the REMPI photoelectron spectra. All vibrational levels of the band (L) progression (Fig. 4) show little intensity in the $\Delta v \neq 0$ transitions. The spectra of $v' = 0$ Rydberg states (see Fig. 3) are among those which have least intensity in $\Delta v \neq 0$ peaks, espe-

J. Chem. Phys., Vol. 89, No. 11, 1 December 1988

72

cially if one excludes progression (G) which probably overlaps the $v' = 1$ level of the $3d\sigma$ Rydberg state as mentioned earlier. The first observation can be rationalized by our tentative assignment of this progression : $4d\delta$ Rydberg state. In its photoionization there will be a propensity for $\Delta l = \pm 1$ and $\Delta \lambda = 0, \pm 1$. Therefore the σ_u continuum with its shape resonance will contribute only weakly to the total photoionization cross section and this source of $\Delta v \neq 0$ transitions will be absent. The second observation can be explained by noting that the core excitation will be negligible, as is noted above, and any effects due to the R dependence of the photoionization cross section (e.g., due to the shape resonance) is minimized by the small amplitude of the vibration. Quantitative explanation of the spectra will require detailed calculations such as those carried out by McKoy and his co-workers. However, in light of all the factors mentioned above which make the Franck–Condon principle invalid, the observed photoelectron spectra are not at all surprising.

Production of O⁺ Ions

In the present experiments, the structure in the wavelength dependence of the O⁺ intensity was qualitatively the same as that of the O_2^+ intensity. However, the ratio O^+/O_2^+ was found to vary considerably from one peak to another. Some representative data is shown in Fig. 10.

Two general mechanisms can be invoked to explain the data: (1) Oxygen atoms could be formed by predissociation of the resonant Rydberg states and the atoms then photoionized by nonresonant multiphoton ionization, or (2) the O_2^+ ions formed in the REMPI process may be subsequently photodissociated.

In the first mechanism, the variation of the O^+/O_2^+ ratio can be attributed to variation in the predissociation rate of the different states or, less plausibly, to variation in the branching ratio to different atomic states of O atoms (the two-photon energy is sufficient to yield either $^3P + {}^3P$ or $^3P + {}^1D$ atoms). Variation of predissociation rate could affect the O^+/O_2^+ ratio only if some of the rates were so low that predissociation is substantially incomplete in the time of the laser pulse duration. Strong $(2 + 1)$ REMPI production of the O⁺ ion from $^3P_{2,1,0}$ atoms formed by an as yet uniden-
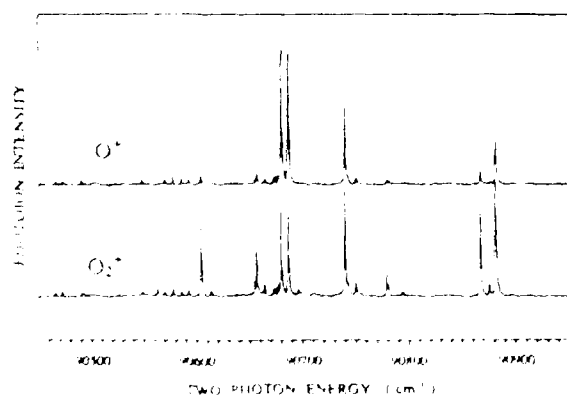
tified multiphoton dissociation process has been observed[28] at 225.7 nm, i.e., the region between $v' = 1$ and $v' = 2$ of the $4s$–$3d$ spectra of Fig. 1.

In the second mechanism, O_2^+ ions produced by REMPI may be photodissociated by a two-photon process. As mentioned earlier in connection with core excitation of the $4s$–$3d$ Rydberg states, the transition $A\,^2\Pi_u$–$X\,^2\Pi_g$ is known to occur in this region. However, in contrast to the excitation of Rydberg states, the lines of which can be very broad due to autoionization and predissociation, the lines in this case are very sharp (radiative lifetime $= 0.69$ μs, $f = 0.001\,36$)[5] and exact resonance with a $4s$–$3d$ Rydberg transition is unlikely. Nevertheless, the one-photon near-resonance condition could greatly enhance a two-photon dissociation process. We have measured the O^+/O_2^+ ratio in this region and photoelectron spectra show that we produce large amounts of O_2^+, $v^+ = 3$ ions. The $A\,^2\Pi_u$ $(v^+ = 17)$–$X\,^2\Pi_g$ $(v^+ = 3)$ transition should appear in this region. However, the resulting data of Fig. 10 do not give any support to this mechanism although the O^+/O_2^+ ratio appears to show other broad structure.

Evaluation of the mechanism could be advanced greatly by two-color experiments and by measurements of the kinetic energy of the O⁺ ions.

ACKNOWLEDGMENTS

[1] P. H. Krupenie, J. Phys. Chem. Ref. Data 1, 423 (1972).
[2] O. Edqvist, E. Lindholm, L. E. Selin, and L. Åsbrink, Phys. Scr. 1, 25 (1970).
[3] C. Y. Robert Wu, J. Quant. Spectrosc. Radiat. Transfer 37, 1 (1987).
[4] Y. Tanaka, J. Chem. Phys. 20, 1728 (1952).
[5] K. P. Huber and G. Herzberg, Molecular Spectra and Molecular Structure. Vol. IV, Constants of Diatomic Molecules (Van Nostrand–Reinhold, New York, 1979).
[6] D. C. Cartwright, W. J. Hunt, W. Williams, S. Trajmar, and W. A. Goddard III. Phys. Rev. A 8, 2436 (1973).
[7] T. A. York and J. Comer, J. Phys. B 16, 3627 (1983)
[8] A. Sur, C. V. Ramana, and S. D. Colson, J. Chem. Phys. 83, 904 (1985).
[9] A. Sur, C. V. Ramana, W. A. Chupka, and S. D. Colson, J. Chem. Phys. 84, 69 (1986).
[10] S. Katsumata, K. Sato, Y. Achiba, and K. Kimura, J. Electron Spectrosc. Relat. Phenom. 41, 325 (1986).
[11] R. D. Johnson III, G. R. Long, and J. W. Hudgens, J. Chem. Phys. 87, 1977 (1987).
[12] P. J. Miller, L. Li, W. A. Chupka, and S. D. Colson, J. Chem. Phys. 89, 3921 (1988).
[13] P. Kruit and F. H. Reed, J. Phys. E 16, 313 (1983).
[14] C. Jungen, J. Chem. Phys. 53, 4168 (1970).
[15] G. Herzberg, Molecular Spectra and Molecular Structure, Vol. I, Spectra of Diatomic Molecules (Van Nostrand–Reinhold, New York, 1950), p. 329.
[16] J. H. Glownia, S. D. Colson, J. C. Miller, and R. N. Compton, J. Chem. Phys. 77, 68 (1982)
[17] Y. Achiba, K. Sato, K. Shobatake, and K. Kimura, J. Chem. Phys. 78, 5474 (1983)
[18] S. T. Pratt, P. M. Dehmer, and J. L. Dehmer, J. Chem. Phys. 80, 1706 (1984)

FIG. 10. Relative intensities of the O⁺ and O_2^+ ions as a function of wavelength. Note the large variation of the O^+/O_2^+ ratio with wavelength.

73

[19]W. A. Chupka, J. Chem. Phys. 87, 1488 (1987).

[20]J. A. Stephens, M. Braunstein, and V. McKoy, J. Chem. Phys. 89, 3923 (1988).

[21]H. Park, P. J. Miller, W. A. Chupka, and S. D. Colson, J. Chem. Phys. 89, 3919 (1988).

[22]S. L. Guberman, in *Physics of Ion–Ion and Electron–Ion Collisions*, edited by F. Brouillard (Plenum, New York, 1983), pp. 167–200.

[23]R. P. Saxon and B. Liu, J. Chem. Phys. 67, 5432 (1977).

[24]H. Harvey Michels, in *Advances in Chemical Physics*, edited by J. Wm. McGowan (Wiley, New York, 1981), Vol. XLV.

[25]J. A. Stephens, M. Braunstein, and V. McKoy (unpublished results).

[26]A. L. Smith, Phil. Trans. R. Soc. London Ser. A 268, 169 (1970).

[27]P. M. Dehmer and W. A. Chupka, J. Chem. Phys. 62, 4525 (1975).

[28]H. Park (unpublished results).

J. Chem. Phys., Vol. 89, No. 11, 1 December 1988

7 4

Anomalous line shapes in delayed optical–optical double resonance studies of N_2[a)]

Leping Li and William A. Chupka

Sterling Chemistry Laboratory. Yale University, New Haven, Connecticut 06511

Stephen T. Pratt

Argonne National Laboratory, Argonne, Illinois 60439

Optical–optical double resonance (OODR) experiments using ionization detection on several short-lived vibronic levels of N_2 have revealed an unexpected phenomenon of considerable potential importance to this widely used technique. In these pulsed-laser experiments, the first (pump) laser populated the $a\ ^1\Pi_g, v' = 1$ state, which is sufficiently long lived ($\approx 100\ \mu s$) to allow measurement with either a simultaneous or time-delayed second (probe) laser. The probe laser was used to study transitions between the $a\ ^1\Pi_g, v = 1$ level and several vibrational levels of the $c_1\ ^1\Pi_u$ and $c_4'\ ^1\Sigma_u^+$ Rydberg states. When the two pulses were overlapped in time, normal double resonance peaks were observed as sharp or power-broadened Lorentzian line shapes, depending on the intensity of the probe pulse [see Figs. 1(a) and 1(b)]. When the high-power probe pulse was delayed by ≈ 13 ns, which ensured no significant temporal overlap with the pump pulse, those peaks that were readily power broadened, (specifically those corresponding to transitions
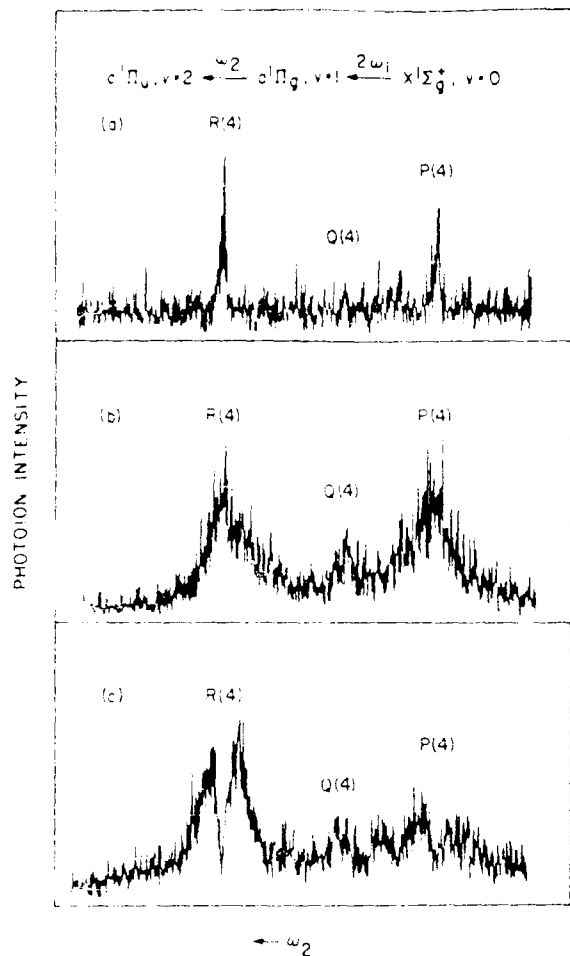
$$c^{1}\Pi_{u}, v\cdot 2 \xleftarrow{\omega 2} c^{1}\Pi_{g}, v\cdot 1 \xleftarrow{2\omega_{i}} x^{1}\Sigma_{g}^{+}, v\cdot 0$$

(a) R(4)

P(4)

Q(4)

(b) P(4) P(4)

Q(4)

(c) R(4)

P(4)

Q(4)

$\leftarrow \omega_2$

FIG. 1 Optical-optical double resonance peaks obtained by pumping the two-photon $S(2)$ transition to the $v = 1$ level of the $a^{1}\Pi_{g}$ state and probing the one-photon transition to the $v = 2$ level of the $c_3{}^{1}\Pi_u$ state of N_2. (a) Low probe laser power ($\approx 10\ \mu J$/pulse) and no delay between the two pulses. (b) High probe laser power ($\approx 100\ \mu J$/pulse) and no delay. (c) High probe laser power ($\approx 100\ \mu J$/pulse) but with 13 ns delay.

to $c_4{}'\,{}^{1}\Sigma_u^{+}$, $v = 0$ and $c_3{}^{1}\Pi_u\ v = 2$) showed a pronounced central dip that appeared to go to the baseline [see Fig. 1(c)]. In general, if a transition could not be power broadened, there was no change in peak shape when the probe pulse was delayed. One such example was the transition to the $c_4{}'\,{}^{1}\Sigma_u^{+}\ v = 2$ state. In addition, peaks corresponding to probe transitions to states with lifetimes long compared with the duration of the probe laser pulse do not exhibit such dips.

If, under strong dip conditions of Fig. 1(c), some 355 nm light was introduced simultaneously with the probe pulse, the dip decreased in magnitude. Increasing the intensity of the 355 nm pulse produced a further decrease in the relative size of the dip along with an enormous increase in the signal level. At high 355 nm pulse energies the normal, power-broadened peak shape was recovered.

The appearance of strong dip in Fig. 1(c) can be easily understood in terms of a kinetic model which has been proposed to explain a similar effect seen in the one-color resonant photoionization of electron-impact produced metastable atomic helium.[1] When the probe laser is resonant and

delayed in time, the rising edge of the laser pulse is strong enough to saturate the transition to the $c_3{}^{1}\Pi_u$, $v = 2$ state and yet is too weak to ionize this level at a significant rate. The $c_3{}^{1}\Pi_u$, $v = 2$ state decays to a nonionizing level extremely rapidly, and the entire population of the $a^{1}\Pi_g$, $v = 1$ state is depleted before the probe pulse becomes strong enough to ionize the $c_3{}^{1}\Pi_u$, $v = 2$ state efficiently. When the probe laser is off resonant, the early part of the pulse cannot "bleach away" the $a^{1}\Pi_g$, $v = 1$ state population, and the signal is due to the intense central (in time) part of the pulse that can photoionize the upper state at a rate faster than its spontaneous decay rate. When both lasers are overlapped in time, the loss of population via the short-lived $c_3{}^{1}\Pi_u$, $v = 2$ state still occurs during the pulse. However, the population of the pump state is constantly replenished by the temporally overlapped pump pulse, thus preventing complete bleaching.

The proposed mechanism requires that the upper state lifetime is significantly shorter than the probe pulse width. In addition, the probe transition on resonance must be so strong that it is readily power broadened (i.e., saturated) at such low laser intensity that the photoionization rate is considerably smaller than the decay rate of the upper state. In the case of N_2, radiative decay is the dominant decay channel, and the lifetimes of the $c_3{}^{1}\Pi_u$, and $c_4{}'\,{}^{1}\Sigma_u^{+}$ states are both about 1.0 ns.[2] The necessity of the second requirement is clearly illustrated by the fact that those peaks which could not be power broadened under the conditions described in Fig. 1(b) showed no change in peak shape when the probe pulse was delayed. This difference in behavior is due to the much smaller rate of the probe transition which in this case only occurs in the high intensity part of the probe laser pulse. However, the ionization rate during the intense part of the pulse is so high that the molecules have no time to decay before they are ionized. The mechanism is further supported by the effect of the overlapped 355 nm radiation. This much higher intensity pulse significantly increases the ionization rate, which then effectively competes with the rapid radiative decay of the $c_3{}^{1}\Pi_u$ or $c_4{}'\,{}^{1}\Sigma_u^{+}$ state. This is evidenced by the enormous increase of the overall signal as the dip is removed at high 355 nm pulse energies.

Although the necessary fast decay is radiative in the present case and in the helium experiment,[1] we point out that, unlike atoms, molecules can decay rapidly to very poorly ionizing states by a number of additional processes. Predissociation and other radiationless transitions (e.g., intersystem crossing and internal conversion) will be effective mechanisms if the bound–bound probe transition is very strong and the ionizing transition is relatively weak. Thus, this dip phenomenon is expected to occur in many other molecular systems. One case involving a state with previously unknown lifetime has already been observed for the NO molecule.[3] In that case, the decay has been shown to be predominantly predissociative. The observation of this phenomenon readily places an upper limit on the lifetime of the probe state. Such limits are often difficult to obtain using other techniques. Finally, it should be noted that, in general, the anomalous line shapes of ionization-detected OODR studies will not be observed in fluorescence-detected OODR

studies. However, dips in fluorescence from a pumped state due to double resonance and dips in ions due to stimulated emission can be observed and have been used as an important double-resonance technique.[4,5]

[1] H. Haberland, M. Oschwald, and J. T. Broad, J. Phys. B **20**, 3367 (1987).

[2] K. P. Huber and G. Herzberg, *Molecular Spectra and Molecular Structure, Vol. IV Constants of Diatomic Molecules* (Van Nostrand Reinhold, New York, 1979).

[3] R. J. Miller, L. Li, Y. Wang, W. A. Chupka, and S. D. Colson (submitted).

[4] D. E. Cooper, C. M. Klimcak, and J. E. Wessel, Phys. Rev. Lett. **46**, 324 (1981).

[5] T. Ebata, T. Imajo, N. Mikami, and M. Ito, Chem. Phys. Lett. **89**, 45 (1982).

Multiphoton ionization studies of NO: Spontaneous decay channels in the (4pπ)K ²Π(v = 2) Rydberg state

R. J. Miller,[a] Leping Li, Yumin Wang, William A. Chupka, and Steven D. Colson

Sterling Chemistry Laboratory, Yale University, New Haven, Connecticut 06511

Time-delayed optical double resonance multiphoton ionization (MPI) studies involving $(4p\pi)K\,^2\Pi(v=2) \leftarrow (3s\sigma)A\,^2\Sigma^+(v=1) \leftarrow\leftarrow X\,^2\Pi(v=0)$ NO show dramatic loss of the ionization signal amplitudes on a time scale that is very short relative to the lifetime of the A state. From direct comparisons of MPI and laser induced fluorescence (LIF) dip temporal profiles, it is concluded that loss of the signal amplitude results from inefficient ionization of the K state. MPI temporal profiles measured in a supersonic jet are identical with those measured in a cell indicating that collisional effects are not important. For delay times $\tau \gtrsim 20$ ns, ionization signals can be observed only at high probe laser intensities. The resultant spectra exhibit marked power broadening and a pronounced dip appears in the center of each of the power broadened resonances. The observed line shapes are rationalized in terms of the spatial and temporal distributions of the probe laser field in conjunction with a dynamical competition between photoionization and spontaneous decay channels in the K state. Such arguments lead to an upper bound on the $K\,^2\Pi(v=2)$ lifetime of ≈ 2 ns. The short lifetime of $K\,^2\Pi(v=2)$ is attributed to indirect heterogeneous predissociation through the $(4p\sigma)M\,^2\Sigma^+$ state and/or to homogeneous predissociation via the $a\,^4\Pi$ continuum.

I. INTRODUCTION

Optical–optical double resonance multiphoton ionization (OODR-MPI) spectroscopy has proven to be a powerful technique for the study of high Rydberg states of diatomic molecules.[1,2] The double resonance approach yields the necessary spectral simplification in regions of high density of states and photoionization detection provides extreme sensitivity and the ability to investigate nonradiative states. In contrast to spectral simplification achieved by rotational and vibrational cooling within a supersonic expansion, the double resonance method allows preparation of specific rovibronic levels over a wide range of internal energies. Systematic variation of the prepared state provides for the thorough examination of congested spectral regions and for the investigation of perturbations level by level.

In the case of nitric oxide, the $(3s\sigma)A\,^2\Sigma^+$ Rydberg state is a convenient and interesting intermediate state.[1,3,12] A chosen rovibronic level of the A state is populated by resonant two-photon excitation of the $X\,^2\Pi$ ground state by the pump laser. The probe laser is scanned through single-photon resonances with the higher Rydberg state of interest which is subsequently ionized by absorption of one or more additional photons from the total laser field. A plot of the photoionization current as a function of probe laser frequency gives a rotationally resolved excitation spectrum of the higher Rydberg state. Such experiments have provided the first observations of several Rydberg–Rydberg transitions[3] and have helped to elucidate complex Rydberg valence multistate interactions.[5,6,13,14]

While OODR-MPI experiments are typically conducted with the pump and probe laser pulses overlapped in time, the discrete intermediacy of the A state in the absorption

process has been rigorously established in cell experiments using a time delay between the pump and probe pulses.[8–10] Indeed, the $E\,^2\Sigma^+(v'=1) \leftarrow A\,^2\Sigma^+(v''=0)$ and $S\,^2\Sigma^+(v'=0) \leftarrow A\,^2\Sigma^+(v''=1)$ transitions have been used[8] to study the time dependence of rotational relaxation within $A\,^2\Sigma^+(v=0,1;J=3.5-21.5)$ induced by collisions with NO, Ar, N_2, and C_3H_8.

In preparation for optical–radio frequency–optical triple resonance experiments designed to establish the utility of photoionization detection methods in the measurement of fine structure and magnetic hyperfine structure parameters of excited electronic states, a 30 ns delay was introduced between the pump and probe laser pulses.[15] With this delay, spectra involving $K\,^2\Pi(v'=2) \leftarrow A\,^2\Sigma^+(v''=1)$ were observed to change dramatically! The initial experiments were conducted on $N=3$ of the $A(v=1)$ state. Under the delayed conditions the amplitude of the MPI spectrum was drastically reduced. The $N=6$ and 9 levels of the $A(v=1)$ state were also investigated. At these higher rotational levels, $K\,^2\Pi(v=2)$ is perturbed by $F\,^2\Delta(v=3)$ such that both $K\,^2\Pi(v'=2) \leftarrow A\,^2\Sigma^+(v''=1,N''=6,9)$ and $F\,^2\Delta(v'=3) \leftarrow A\,^2\Sigma^+(v''=1,N''=6,9)$ transitions are observable. Under the delayed conditions all signals involving $K\,^2\Pi(v'=2)$ were again greatly reduced in amplitude; the $F\,^2\Delta(v'=3) \leftarrow A\,^2\Sigma^+(v''=1,N''=9)$ signals remained sharp and strong. These results cannot be rationalized by a significant loss of the A state population during the delay interval. Such a conjecture is inconsistent with the known lifetime of this state,[9,11] with the results of Ito and co-workers[10] described above, and with the observations that the $F\,^2\Delta(3,1)$ signal amplitudes were undiminished. The latter result also argues against any rationalization, such as adiabatic following in the pump transition, that depends upon substantive differences in the extent to which the A state is populated in delayed and undelayed experiments.

---

[a] Current address: Battelle Pacific Northwest Laboratories, Richland, Washington 99352

A series of experiments have recently been conducted in an effort to arrive at some satisfactory understanding of these observations. These experiments were designed to independently study the $K \leftarrow A(2,1)$ transition and photoionization of the K state by utilizing laser induced fluorescence (LIF), dip and MPI detection schemes, and by examining experimental variables such as pressure and collisions, time delay, and laser intensity. Effects associated with the probe laser intensity have proven especially enlightening; they constitute the central theme of this paper. Particular attention is addressed to one spectral dips observed in time-delayed optical double resonance MPI spectra obtained at high probe laser intensity and to the photophysical processes and the dynamical properties of the $K^2\Pi(v=2)$ state that are responsible for the observed phenomena.

II. EXPERIMENTAL

Experiments were conducted both in a cell configured for MPI and LIF detection, and in a molecular beam apparatus employing time-of-flight mass spectrometric detection of photoions.

The cell was constructed around a 4.5 in. ultrahigh vacuum six-way cross. The eight baffling arms bore several suprasil windows were ... these served to ... and define the optical axis of the apparatus. Photoionization and fluorescence detectors were mounted on adjacent faces of the cube at right angles to the optical axis.

The photoionization detector was of the coaxial kind after that of Ferrell. It consisted of a central detection electrode (0.0015 in. ϕ stainless steel wire) mounted within a stainless steel cylindrical shield (1 in. ϕ, 2 in. long). The ends of the shield were covered with stainless steel screen. A radial section (0.6 × 1.0 in.) of the cylinder was removed such that charged particles generated at the laser interaction region (≈0.75 in. from the outer conductor) could be accelerated to the detection electrode. Typically, the center electrode was biased, using batteries, to approximately −280 V dc for the detection of photoelectrons. Signals were capacitively coupled to a Keithley 427 current amplifier for subsequent digitization. Under normal operating conditions no bias was applied to the shield.

Unresolved fluorescence from the low vibrational levels of the A state was detected by an Hamamatsu 2078 solar blind photomultiplier tube (or Acton Research 220-B-1D bandpass filter ...) could be inserted as necessary in the tube housing. Time-resolved LIF signals ... without preamplification.

During experiments to ...

The general features of ...

mer, the grounded tungsten grid was removed, the flight tube was maintained at 5×10^{-7} Torr, and the detector was a Thorn EMI 9642/2B electron multiplier. In the current experiments, pure NO, at a stagnation pressure of 30 psig, was expanded continuously through a 12.5 μm nozzle into the main vacuum chamber which was maintained at 10^{-5} Torr. The laser interaction region was approximately 5 mm downstream from the nozzle.

The laser system consisted of two independent, tunable dye laser systems. The pump laser, that used to populate the A state, was a Lambda Physik 2002 dye laser (Coumarin 440/CH$_3$OH) excited by a Questek 2240 excimer laser operated on XeCl (308 nm). The probe laser, that used to stimulate the $K \leftarrow A(2,1)$ transitions, was a Quanta-Ray PDL-1 dye laser (Coumarin 450/CH$_3$OH) excited by the third harmonic (355 nm) from a Quanta-Ray DCR-2A Nd:YAG laser which was operated in the long pulse (≈ 8 ns) mode. In this configuration, the temporal relationship of the pump and probe dye laser pulses could be varied at will (see below) without affecting the spatial overlap of the beams.

The pump laser delivered pulse energies of ≈ 5 mJ. This beam was attenuated as necessary using a Glan–Taylor polarizer and was focused onto the interaction region using a 250 mm nominal focal length lens. Probe laser pulses of 1 mJ energy were used and this beam was not focused except as noted otherwise. In all experiments the linearly polarized pump and probe laser beams counterpropagated through the interaction region with their electric field vectors oriented at right angles to one another.

In certain of the molecular beam experiments, one additional laser beam (532 nm) was used to directly ionize the K state population. This beam was derived from a Quanta-Ray DCR-11 Nd:YAG laser and, when used, counterpropagated with respect to the pump laser beam.

All timing sequences were controlled by a Stanford Research Systems DG535 delay/pulse generator interfaced to an LSI 11/23 computer. During time scans, the delay was incremented in 2 ns intervals. Data was acquired using a Tektronix 7612D dual channel digitizer fitted with 7A16 series vertical amplifiers.

III. RESULTS

Figure 1 summarizes the various stimulated and spontaneous transitions used in the experiments. Figure 2A illustrates a one-photon $K^2\Pi(v=2) \leftarrow A^2\Sigma^+(v=1,N=3)$ MPI excitation spectrum obtained in the cell at a pressure of 1 Torr of NO with the laser pulses overlapped in time as well as in space. The pump laser was tuned to resonance with the ... rotational branch of the two-photon ... such that only the F_1 spin component of ... was populated. This spectrum is consistent with previously reported spectra and rotational branch assignments taken directly from the literature. Figure 2B depicts a spectrum recorded under identical experimental conditions except that the probe laser pulse was delayed by ... relative to the pump laser pulse.

With the probe laser fixed on resonance with a given ... in the $K \leftarrow A(2,1)$ spectrum, temporal ... by monitoring the decay of the A state ...
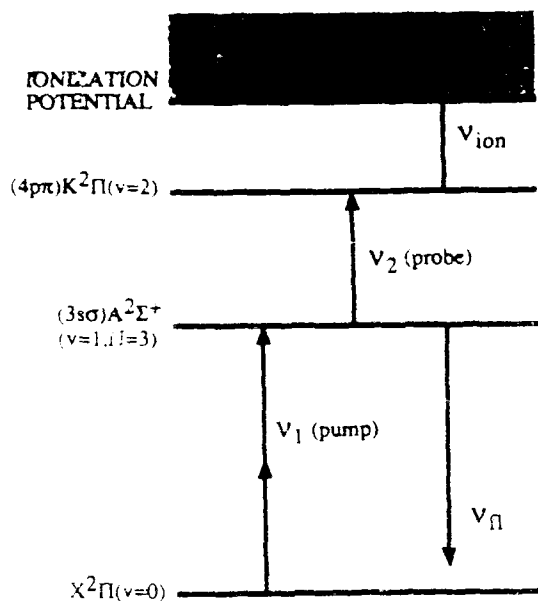
FIG. 1. Schematic energy level diagram summarizing the stimulated and spontaneous transitions used in the experiments

FIG. 3. Decay curves illustrating the effect on the A state fluorescence induced by probing $P_{11}(J^{\ast} = 3.5)$ of $K(v' = 2) \leftarrow A(v'' = 1, N^{\ast} = 3)$ at two different delay times. The solid curve represents the best fit of a convolution of a Gaussian impulse function and a single exponential decay function to data obtained at negative delays. The set of data points depicts the fluorescence profile obtained with $\tau = 20$ ns. Pump: $O_{12}(J^{\ast} = 5.5)$ of $A(v' = 1, N' = 3) \leftarrow X(v'' = 0)$.

fluorescence and the amplitude of the MPI signal as a function of delay time τ between the pump and probe laser pulses. Figure 3 illustrates the effect on the decay of the A state fluorescence induced by probing $P_{11}(J^{\ast} = 3.5)$ of $K^2\Pi(v' = 2) \leftarrow A^2\Sigma^+(v'' = 1, N^{\ast} = 3)$ at negative and at positive delay times. (Negative time is defined by a condition in which the probe laser pulse precedes the pump laser pulse.) Figure 4 depicts temporal profiles of the LIF and
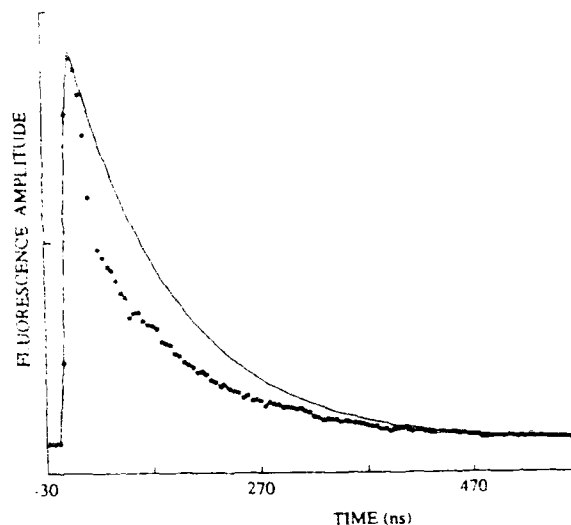
MPI responses: the initial portion of a fluorescence decay curve (Fig. 3, $\tau = 20$ ns) is directly compared to an MPI temporal profile obtained by scanning the delay time in 2 ns increments. Each rotational branch of the $K \leftarrow A(2,1)$ spectrum was examined in turn and each manifested comparable temporal dependencies.
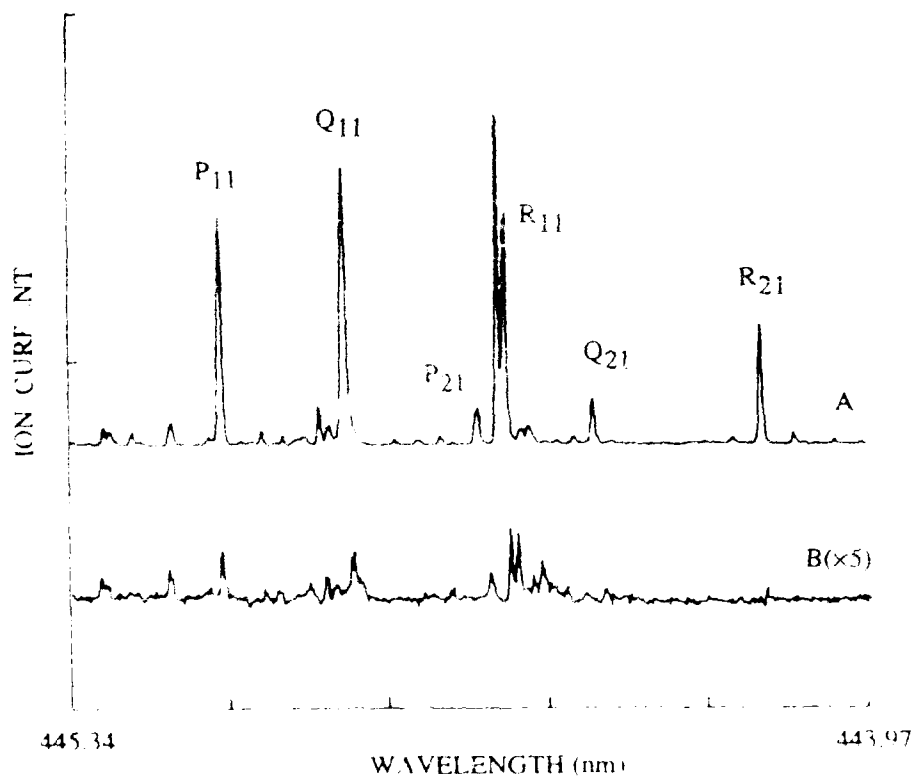
A series of experiments was then conducted in the mo-

FIG. 2. Optical–optical double resonance MPI spectra illustrating the effect of a time delay τ between the pump and probe laser pulses. A: $\tau = 0$. B: $\tau = 30$ ns. Spectra were measured in the cell at 1 Torr pure NO. Pump: $O_{12}(J^{\ast} = 5.5)$ of $A(v' = 1, N' = 3) \leftarrow X(v'' = 0)$. Probe: $K(v' = 2) \leftarrow A(v'' = 1, N^{\ast} = 3)$.

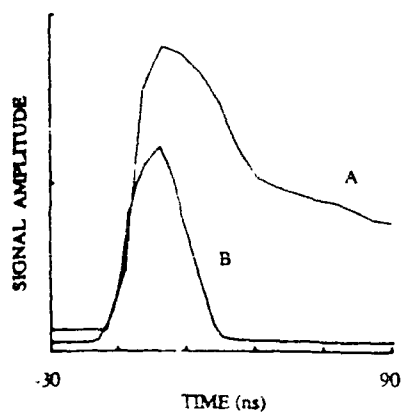J. Chem. Phys., Vol. 90, No. 2, 15 January 1989

80

FIG. 4. Temporal dependencies of the LiF and MPI responses measured in cell experiments at 1 Torr pure NO. A. Fluorescence decay, $\tau = 20$ ns (Fig. 3). B: MPI. Pump: $O_{12}(J'' = 5.5)$ of $A(v' = 1, N' = 3) \leftarrow X(v'' = 0)$. Probe: $P_{11}(J'' = 3.5)$ of $K(v' = 2) \leftarrow A(v'' = 1, N'' = 3)$.

lecular beam apparatus. MPI temporal profiles measured under the collision-free conditions of a supersonic jet expansion were indistinguishable from those measured in the cell (Fig. 4B). Figure 5A shows an OODR-MPI spectrum obtained in the beam apparatus with the laser pulses overlapped in time and in space. In this case, the pump laser was tuned to resonance with the $P_{12} + O_{22}(J'' = 4.5)$ rotational branches of the two-photon $A \leftarrow \leftarrow X(1,0)$ band such that both the F_1 and F_2 spin components of $A(v = 1, N = 3)$ were populated; as in all prior experiments, the probe laser beam was not focused. This spectrum is again consistent with previously reported spectra.[3] The spectrum reproduced in Fig. 5B was recorded under identical experimental conditions except that the intensity of the probe laser pulse was increased by focusing the beam onto the interaction region using a 300 mm nominal focal length lens. With the probe laser beam focused, introduction of a delay time $\tau = 20$ ns afforded the spectrum illustrated in Figure 6A. Note the pronounced dip in the center of each of the power broadened $K \leftarrow A(2,1)$ resonances. Figure 6B shows the spectrum observed when ionizing the K state population using an intense, 532 nm pulse that was overlapped in time with the delayed, probe laser pulse.

IV. DISCUSSION

Figure 2 illustrates the dramatic loss in the signal amplitudes found in optical–optical double resonance multiphoton ionization experiments involving $K^2\Pi(v' = 2) \leftarrow A^2\Sigma^+(v'' = 1)$ when the probe laser pulse is delayed by $\tau > 20$ ns relative to the pump laser pulse. It was conceivable that such observations could be associated with an anomalously fast decay of the A state population, with a diminished ability to stimulate the $K \leftarrow A(2,1)$ transitions, or with inefficient ionization of the K state by the probe laser field. Each of these potentialities was considered in turn.

With the probe laser pulse preceding the pump laser pulse, the A state fluorescence follows a single exponential decay curve (Fig. 3) giving a radiative lifetime for the $A(v = 1)$ state of 115 ± 5 ns at 1 Torr pure NO. This result is in excellent agreement with expectations based upon independent measurements of the zero-pressure radiative life-

time[16,17] and of the rate coefficient for quenching of $A(v = 1)$ by ground state nitric oxide.[16,17,20] Loss of the OODR-MPI signal clearly occurs on a time scale that is very short relative to decay of the A state population.

The dip in the $A(v = 1)$ fluorescence induced by exciting the various rotational branches of $K \leftarrow A(2,1)$ at $\tau = 20$ ns (Fig. 3) establishes that under the conditions of these experiments the A state population can indeed be bleached. Such fluorescence dips are readily detected at delays $\tau > 50$ ns. Direct comparison of a dipped fluorescence profile and the temporal dependence of the MPI response (Fig. 4) demonstrates unambiguously that the $K \leftarrow A(2,1)$ transition can be easily saturated at delay times that are long compared to loss of the ionization signal. Inspection of Fig. 4B indicates that the MPI temporal profile is nothing more than the convolution of the pump and probe pulse widths. It is concluded that ionization of the K state by the probe laser field is highly inefficient.

Given this conclusion and assuming that the cross section for the one-photon, bound–continuum transition is a slowly varying function of frequency over the domain of the pump and probe fields ($v_1 = 23\,183$ cm^{-1}, $v_2 = 22\,455$ to $22\,520$ cm^{-1}), one must physically rationalize the precipitous drop in the MPI signal amplitudes as the laser pulses just separate in time. Viewed from a different perspective, it is equivalent to consider why the spectra become so strong when the laser pulses are overlapped in time. Although the lifetime of the K state is unknown, these observations are consistent with the hypothesis that the K state undergoes rapid decay, via spontaneous or collisionally induced processes, provided either that the presence of the pump laser pulse serves to replenish the K state population, or that the higher intensity of the pump laser field merely affords an ionization rate that is sufficient to compete successfully with the decay process. The facts that pumping of the $A \leftarrow \leftarrow X(1,0)$ transition was maintained well below saturation while the $K \leftarrow A(2,1)$ transition was saturated (Fig. 4A) argue strongly against the former condition. Based upon the above hypothesis, it was therefore expected that by increasing the intensity of the probe laser field the photoionization rate would become more competitive with the decay rate thereby enhancing the MPI spectral amplitudes observed at delay times greater than the laser pulse widths.

Figure 5 illustrates the effect of probe laser intensity on the MPI spectrum measured in the molecular beam apparatus with the pump and probe laser pulses overlapped in time. At high probe laser intensity (Fig. 5B) the $K \leftarrow A(2,1)$ signals exhibit substantial power broadening and several additional spectral features appear. These new features, labeled with an asterisk in the figure, are tentatively assigned to one-photon transitions to the $(3d\delta)F^2\Delta(v = 3)$ Rydberg state. These $F \leftarrow A(3,1)$ transitions presumably result from $K^2\Pi(v = 2) \sim F^2\Delta(v = 3) \sim B^2\Pi(v = 29,30) \sim B'^2\Delta(v = 8,9)$ perturbations which are known[3] to occur at values of $J > 6.5$. At high probe laser intensity, signals resulting from ionization of the K state levels are now readily observed at delay times $\tau > 50$ ns. In all cases, a pronounced dip occurs in the center of each of the power broadened $K \leftarrow A(2,1)$ resonances (Fig. 6A).
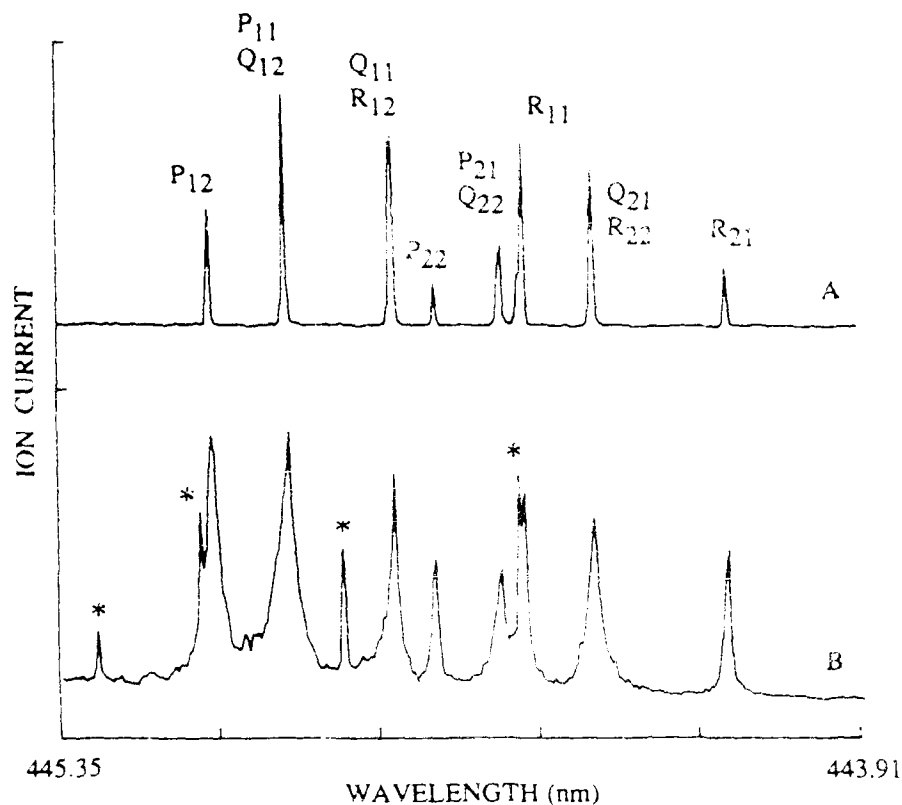
J. Chem. Phys., Vol. 90, No. 2, 15 January 1989

81

FIG. 5. Optical–optical double resonance MPI spectra showing the effect of probe laser intensity at $\tau = 0$. A: Low intensity. B: High intensity. Spectra were measured in the molecular beam apparatus. Pump $P_{12} + O_{12}(J'' = 4.5)$ of $A(v' = 1, N' = 3) \leftarrow X(v'' = 0)$. An asterisk indicates signals tentatively assigned to $F^2\Delta(v' = 3) \leftarrow A^2\Sigma^+(v'' = 1, N'' = 3)$ as discussed in the text.

A. Ionization dips

Analogous dips in the ionization yield as a function of laser frequency have been recently observed in multiphoton ionization investigations of the 2 ^1S metastable state of helium,[21] of dense magnesium vapors,[22] of the E,F $^1\Sigma_g^+$ ($v_E = 0$) state of molecular hydrogen,[23] and of the a $^1\Pi_g$ ($v = 1$) metastable state of molecular nitrogen.[24] Each of these systems share the common feature that the ionization process is resonantly enhanced through an intermediate state that is subject to rapid decay. The mechanism by which a particular intermediate state decays may vary widely. For
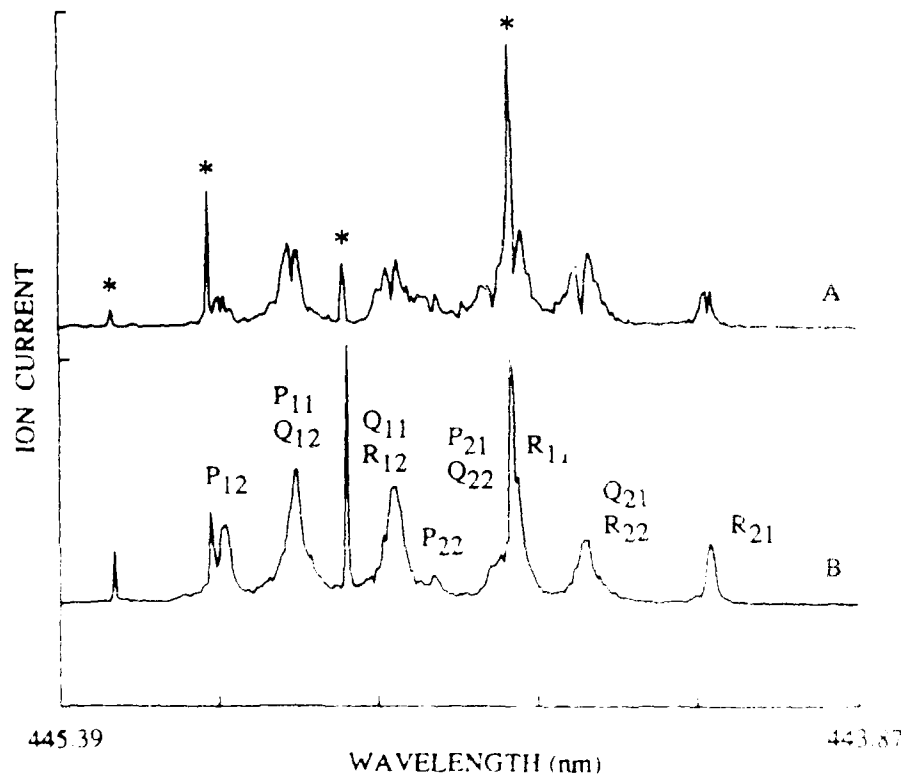

FIG. 6. Time-delayed ($\tau = 20$ ns) optical–optical double resonance MPI spectra illustrating the effects of ionization of the $K(v = 2)$ state population by different laser fields. A: Probe laser at high intensity. B: Intense 532 nm excitation simultaneous with the high intensity probe laser pulse. Spectra were measured in the molecular beam apparatus. Pump: $P_{12} + O_{12}(J'' = 4.5)$ of $A(v' = 1, N' = 3) \leftarrow X(v'' = 0)$. An asterisk indicates signals tentatively assigned to $F^2\Delta(v' = 3) \leftarrow A^2\Sigma^+(v'' = 1, N'' = 3)$ as discussed in the text.

J. Chem. Phys., Vol. 90, No. 2, 15 January 1989

82

example, the $3\,^1P$ state of He and the $c_1\,^1\Pi_u\,(v=2)$ and $c_4'\,^1\Sigma_u^+\,(v=0)$ Rydberg levels of N_2 undergo radiative decay,[21,24] while the $4p\pi\,^1\Pi_u\,(v=1)$ state of H_2 undergoes predissociation.[23] In the case of dense magnesium vapors, the $3s3p\,^1P$ state is involved in a collisional process leading to the rapid formation of the $A\,^1\Sigma_u^+$ state of magnesium dimer which subsequently predissociates to atomic levels that are not ionized.[22] Whatever the mechanism, the rate of decay of the intermediate level must be comparable to its rate of photoionization.

Recall that dips in the centers of power broadened ionization signals are observed when the resonant intermediate state (the K state in the current experiments) is populated by and ionized by the same laser pulse. Under such conditions the observed line shapes can be qualitatively understood in terms of the temporal and spatial distributions of the driving laser field in conjunction with a dynamical competition between the photoionization and pertinent decay channels.[21] Two conditions must be satisfied for the observation of such line shapes. The first condition is that the rate of decay must be greater than or approximately equal to the inverse of the rise time of the laser field. The second condition is that, at the resonance condition, the cross section for the bound–bound transition to the intermediate state must be much greater than the cross section for the bound–continuum transition leading to photoions. At the resonance condition the ratio of the cross sections is therefore such that the rising edge of the laser field readily saturates the intermediate level long before the field intensity is sufficient to ionize that level. Given the first condition specified above, this situation allows ample time for the intermediate level to decay before it can be ionized. The result is a low ion yield, or dip, at the resonant frequency of the bound–bound transition. As the laser is detuned from the resonance condition, the cross section governing population of the intermediate level decreases rapidly while the cross section for ionization remains essentially constant: the ratio of the cross sections quickly approaches unity. The intermediate level is now populated only when the field intensity approaches its maximum, becoming sufficiently high to power or broaden the transition to compensate for the detuning. At such high intensities the rate of ionization competes successfully with the rate of decay. The result is wings that reflect normal power broadened line shapes.

The effects of the spatial distribution of the laser field are closely associated with those of the temporal distribution. At the resonant frequency, the volume element surrounding the focal point in which the field intensity is adequate to populate the intermediate level increases as the field amplitude increases with time. In this expanding volume element, the field always becomes intense enough to populate the intermediate level well before it becomes intense enough to ionize that population. Once again there is ample time for the population to decay before it can be ionized. Thus the region of space about the focal point contributes directly to the low ion yield observed at the resonant frequency of the bound–bound transition. As the laser is detuned from resonance, the field intensity required to populate the intermediate level rises rapidly and the effectual interaction region

shrinks accordingly. A more rigorous description of these effects that is based upon two dressed states coupled to a continuum and that satisfactorily reproduces the observed line shapes has been presented by Haberland, Oschwald, and Broad.[21]

This rationalization of the line shapes is predicated on the facts that any real laser pulse has a finite rise time, and that the rate of photoionization is a function of the time dependent field intensity, whereas the rate of decay is independent of that intensity. Such an explanation yields the obvious prediction that if a second laser field of sufficient intensity is used to drive the ionization process, then the dips will vanish leaving only the power broadened ionization profiles. Such an experiment has been conducted in the case of the $K(v=2)$ state of NO using a very intense, 532 nm pulse overlapped in time with the probe laser pulse. Figure 6B clearly demonstrates that under these experimental conditions no dips are observed in the ionization profiles.

Photoionization excitation spectra exhibiting dips in the centers of the power broadened $K \leftarrow A(2,1)$ resonances and the disappearance of these dips in the presence of a second, more intense ionization field strongly support the conclusion that the $K(v=2)$ state of NO is subject to rapid decay. Estimates of the rise time of the probe laser pulse lead to an upper bound on the $K\,^2\Pi(v=2)$ lifetime of $\simeq 2$ ns.

B. Decay channels

The mechanism by which the $K(v=2)$ state decays remains to be identified. Note that the only decay channels that need be considered are ones leading to low energy atomic or molecular states that cannot be ionized under the conditions of these experiments. The possible channels include collisional deactivation, radiative decay, and predissociation. The observations that the MPI temporal dependencies measured in a supersonic jet expansion are identical to those measured in the cell and that the dips in the ionization profiles occur in molecular beam experiments preclude the importance of collisional deactivation of the K state population.

No report of emission from the K state of NO has been found in the literature. However, an estimate of the radiative lifetime of this state can be made because the lifetime of a member of an $(nl\lambda)$ Rydberg progression is, to good approximation, directly proportional to the effective principal quantum number n^* raised to the third power.[25] The radiative lifetime of the $(4p\pi)K\,^2\Pi$ Rydberg state can therefore be estimated from the experimentally measured radiative lifetime of the $(3p\pi)C\,^2\Pi$ Rydberg state. For rotational levels below the threshold for predissociation ($J<3.5$), the lifetime[26-28] of $C(v=0)$ is 32 ± 5 ns. Using the quantum defects reported by Miescher and Huber,[29] one calculates the radiative lifetime of the K state to be $\simeq 100$ ns. The short lifetime of the $K(v=2)$ level cannot be attributed to radiative decay.

This conclusion is supported by experimental evidence. Consider the dipped fluorescence decay profile illustrated in Fig. 3. Were the K state to undergo rapid radiative decay, it would be reasonable to expect that a significant fraction of

J. Chem. Phys., Vol. 90, No. 2, 15 January 1989

83

the K state population would decay to the low vibrational levels of the A state.[30] The subsequent emissions from the A state levels would certainly be detected as a secondary maximum in the fluorescence profile appearing just after the dip induced by excitation of the K state. No such secondary maxima are observed. In fact, following the dip, the fluorescence decay profiles do not deviate from a single exponential decay function having a time constant that is identical, within experimental uncertainty, to the lifetime of the originally pumped $A(v = 1)$ state.

By default, the short lifetime of the $(4p\pi)K\,^2\Pi(v = 2)$ level must be ascribed to predissociation. Each member of the $(np\pi)$ Rydberg series is perturbed by the $B\,^2\Pi$ valence state[14] such that those vibronic levels lying above the dissociation limit of the B state to $N(^2D) + O(^3P)$ at $\approx 71\,630$ cm^{-1} are strongly predissociated.[34] The $K(v = 2)$ level lies well below this dissociation limit at $69\,019$ cm^{-1} and therefore does not undergo direct predissociation via the B state continuum. While coupling of the $K(v = 2)$ and $B(v = 29,30)$ vibronic levels[3,14,35] makes possible the existence of an indirect predissociation channel, this potential explanation is deemed unlikely because firm evidence for predissociation of the bound levels of the B state is lacking. The weakness of the $K(v = 2)$ couplings to the vibronic levels of the $L\,^2\Pi$ valence state[3,14] argues against any significant indirect predissociation channel involving this valence state. Deliberation of the potential energy curves[14,36-38] of the electronic states of NO yields no reasonable candidates for predissociation of $K(v = 2)$ by spin–conserving homogeneous or by direct heterogeneous mechanisms.

Miescher and co-workers[35,39] have shown that the $(4p\pi)K\,^2\Pi$ and $(4p\sigma)M\,^2\Sigma^+$ states of NO constitute a p complex satisfying the Van Vleck hypothesis of "pure precession."[40-42] This hypothesis assumes the "unique perturber" approximation[42,43] such that the Λ doubling of the $(np\pi)^2\Pi$ state is a direct manifestation of the heterogeneous perturbation of that state by the $(np\sigma)^2\Sigma$ member of the complex. This situation is of significance because the $M\,^2\Sigma^+$ levels are known to be strongly predissociated through the repulsive $A'\,^2\Sigma^+$ state.[35,39] The applicability of the hypothesis of pure precession means that the effects of indirect heterogeneous predissociation of the $K\,^2\Pi$ levels can be evaluated in terms of a simple system of two weakly interacting states. Furthermore, the analysis requires knowledge of a minimal number of observables: the $M \leftarrow X(2,0)$ linewidth in absorption, the rotational constant, and the energy separation of the $K(v = 2)$ and $M(v = 2)$ levels.

Consider a system of two eigenstates $|\xi\rangle$ and $|\zeta\rangle$ corresponding to the $(np\pi)$ and $(np\sigma)$ members of the p complex. The widths Γ (in cm^{-1}) of the two levels are related by[44]

$$\Gamma_\xi = (c_{\xi\zeta})^2\Gamma_\zeta, \tag{1}$$

where the coefficient $c_{\xi\zeta}$ describes mixing of the eigenstates. Perturbation theory expresses this mixing coefficient as

$$c_{\xi\zeta} = H_{\xi\zeta}/\Delta E_{\xi\zeta}, \tag{2}$$

where $H_{\xi\zeta}$ is the matrix element characterizing the interaction and $\Delta E_{\xi\zeta}$ is the energy separation between the two discrete eigenstates. The weighting term in Eq. (1) can there-

fore be written explicitly in terms of the Λ doubling $\Delta \nu_{cJ}(J)$ such that

$$\Gamma_\xi = \frac{\Delta \nu_{cJ}(J)}{\Delta E_{\xi\zeta}}\Gamma_\zeta. \tag{3}$$

For Hund's case (a), the hypothesis of pure precession gives

$$\Delta \nu_{cJ}(J) = qJ(J + 1), \tag{4}$$

where the Λ doubling parameter q is defined by

$$q = \frac{2B_v^2l(l + 1)}{\Delta E_{\xi\zeta}} \tag{5}$$

in which B_v is the rotational constant and l is the orbital angular momentum quantum number. Using $B_v = 2$ cm^{-1}, $l = 1$ and $\Delta E = 373$ cm^{-1}, Eq. (5) yields $q = 0.043$ cm^{-1} ($q_{obs} = 0.035^{39}$). In absorption, the $M(v = 2)$ level of $^{14}N^{16}O$ is found to be diffuse,[39,45] lacking rotational structure, with $\Gamma_{M(v=2)} \approx 5$ to 10 cm^{-1}. For the range of $K(v = 2)$ rotational levels ($J = 1.5$ to 4.5) probed in these experiments, substitution of Eq. (4) into Eq. (3) affords $\Gamma_{K(v=2)} \approx 2$ to 30×10^{-3} cm^{-1}. These level widths correspond to predissociation lifetimes,[46] given by $(2\pi c\Gamma)^{-1}$, of the order of 2 to 0.2 ns.

While this indirect heterogeneous predissociation mechanism predicts lifetimes that are consistent with the experimental observations, it must be noted that this channel can account for only half of the observed dips: the $M\,^2\Sigma^+$ state can couple only to the Π^+ component of the K state. For example, this channel can rationalize the dip found in the $Q_{21} + R_{22}$ line of the $K \leftarrow A(2,1)$ MPI spectrum, but not that found in the $Q_{11} + R_{12}$ line (Fig. 6A). No $^2\Sigma^-$ state is available to provide an energetically feasible, analogous predissociation channel for the Π^- component of $K(v = 2)$.

Some additional predissociation channel must also be operative. The only remaining possibility is direct homogeneous predissociation via the continuum of the $a\,^4\Pi$ valence state. Weak predissociation of the $(3p\pi)C\,^2\Pi$ levels is attributed to the $a\,^4\Pi$ state.[26,31] Thus, as in the discussion of the radiative lifetime above, consideration of the predissociative properties of the C state allows estimates of the predissociative properties of the K state.

The onset of predissociation in the $(3p\pi)C\,^2\Pi$ state occurs at $v = 0, J \approx 3.5$. At higher J, $C(v = 0)$ predissociates at a measured rate[26,28,31] of $\approx 10^9$ s^{-1}. For $C(v = 1)$, a lifetime of <0.3 ns has been reported.[47] In absorption, the vibrational levels ($v = 0$ to 6) of the C state are sharp at a spectral resolution of ≈ 0.1 cm^{-1}; yet emission from the $v \geqslant 1$ levels is not observed.[26] [A low resolution emission spectrum of $C(v = 1)$ has been recently reported in an experiment using dispersed synchroton radiation as the excitation source.[48]] This balance between sharp absorption features and unobservable emissions implies that the predissociation lifetimes of all of these vibrational levels of the $C\,^2\Pi$ state fall within the range of 0.5 to 5×10^{-10} s. The electronic part of the perturbation matrix element characterizing predissociation scales as $(n^*)^{-3/2}$. The potential energy curve of the $^4\Pi$ state is, however, not known with sufficient accuracy to allow reliable calculation of Franck–Condon integrals. Assuming that the Franck–Condon factors for the $K\,^2\Pi$–$a\,^4\Pi$

J. Chem. Phys., Vol. 90, No. 2, 15 January 1989

84

action are comparable to those for the $C^2\Pi$-$a^4\Pi$ interaction, then the lifetime will scale approximately as $(n^*)^3$. Thus, the predissociation lifetimes of the lower vibrational levels of the $K^2\Pi$ state are expected to fall within the range of 0.15 to 1.5 ns. Predissociation of $K^2\Pi(v=2)$ NO via the $a^4\Pi$ state predicts lifetimes that are consistent with the experimental observations. This direct homogeneous channel can account for the dip observed in each line of the K-$X(2,1)$ MPI spectrum.

V. CONCLUSIONS

The unusual line shapes observed in resonantly enhanced ionization spectra involving $K^2\Pi(v=2)$-$A^2\Sigma^+(v'=1)$ NO are interpreted in terms of a dynamical competition between photoionization and spontaneous decay of the $K(v=2)$ intermediate level. The expectation that such line shapes are a manifestation of the response time of the laser field leads to an upper bound on the $K(v=2)$ lifetime of $\lesssim 2$ ns. From a careful examination of the potential decay channels based upon fundamental physical principles, it is concluded that the short lifetime of NO $K^2\Pi(v=2)$ is the result of indirect heterogeneous predissociation through the $(4p\sigma)M^2\Sigma^+$ state and/or of direct homogeneous predissociation via the $a^4\Pi$ continuum.

As the methods of optical–optical double resonance multiphoton ionization spectroscopy are extended to investigations of the high Rydberg states of an increasing number of atoms and molecules, the laser phenomenon exemplified here may prove to be of general utility in uncovering the existence of dynamical processes that are not otherwise easily recognized.

ACKNOWLEDGMENTS

1 (1983).

2 Annu. Rev. Phys. Chem. 32, 139 (1981).

3 W. A. Chupka, S. D. Colson, D. Gauyacq, Ph. Avouris, and J. J. Wynne, J. Phys. Chem. 90, 1086 (1986).

4 W. A. Chupka, S. D. Colson, D. Gauyacq, Ph. Avouris, and J. J. Wynne, J. Chem. Phys. 78, 3625 (1983).

5 Y. Anezaki, T. Ebata, N. Mikami, and M. Ito, Chem. Phys. 97, 153 (1985).

6 Y. Anezaki, T. Ebata, N. Mikami, and M. Ito, Chem. Phys. 89, 103 (1984).

7 T. Ebata, Y. Anezaki, M. Fujii, N. Mikami, and M. Ito, J. Phys. Chem. 87, 4773 (1983).

8 T. Ebata, Y. Anezaki, M. Fujii, N. Mikami, and M. Ito, Chem. Phys. 84, 151 (1984).

9 T. Ebata, N. Mikami, and M. Ito, J. Chem. Phys. 78, 1132 (1983).

10 T. Ebata, T. Imajo, N. Mikami, and M. Ito, Chem. Phys. Lett. 89, 45 (1982).

11 T. Ebata, H. Abe, N. Mikami, and M. Ito, Chem. Phys. Lett. 86, 445 (1982).

12 S. C. Wallace and K. K. Innes, J. Chem. Phys. 72, 4805 (1980).

13 K. Dressler and E. Miescher, J. Chem. Phys. 75, 4310 (1981).

14 R. Gallusser and K. Dressler, J. Chem. Phys. 76, 4311 (1982).

15 R. J. Miller, D. T. Biernacki, and S. D. Colson (unpublished results).

16 H. Zacharias, J. B. Halpern, and K. H. Welge, Chem. Phys. Lett. 43, 41 (1976).

17 J. F. Burris, T. J. McGee, and J. Barnes, Chem. Phys. Lett. 121, 371 (1985).

18 W. R. Ferrell, Ph.D. thesis, University of Tennessee, 1985.

19 A. M. Woodward, W. A. Chupka, and S. D. Colson, J. Phys. Chem. 88, 4567 (1984).

20 M. Asscher and Y. Haas, J. Chem. Phys. 76, 2115 (1982).

21 H. Haberland, M. Oschwald, and J. T. Broad, J. Phys. B 20, 3367 (1987).

22 J.-Y. Zhang, H.-T. Zhou, Q.-R. Li, J. Yang, J.-Z. Zhao, and Y.-X. Nie, J. Phys. B 21, 589 (1988).

23 D. Normand and J. Morellec (personal communication).

24 L. Li, W. A. Chupka, and S. D. Pratt, J. Chem. Phys. 90, 606 (1989).

25 H. A. Bethe and E. E. Salpeter, *Quantum Mechanics of One- and Two-Electron Atoms* (Plenum, New York, 1977), p. 269.

26 J. Brzozowski, P. Erman, and M. Lyyra, Phys. Scr. 14, 290 (1976).

27 H. Rottke and H. Zacharias, J. Chem. Phys. 83, 4831 (1985).

28 K. Tsukiyama, T. Munakata, M. Tsukakoshi, and T. Kasuya, Chem. Phys. 121, 55 (1988).

29 E. Miescher and K. P. Huber, Int. Rev. Sci. Phys. Chem. Ser. 2 3, 37 (1976).

30 This assertion is based upon consideration of the observed fluorescence branching ratio (≈ 0.7) of the C state to the A and X states (Refs. 31–33). To the extent that the radiative rates for the various emissive transitions scale as $(n^*)^{-3}$, the fluorescence branching ratio of the K state will be approximately equal to that of the C state. Thus $\approx 40\%$ of the K state population would decay to the A state.

31 A. B. Callear and M. J. Pilling, Trans. Faraday Soc. 66, 1618 (1970).

32 W. Groth, D. Kley, and U. Schurath, J. Quant. Spectrosc. Radiat. Transfer 11, 1475 (1971).

33 H. Scheingraber and C. R. Vidal, J. Opt. Soc. Am. B 2, 343 (1985).

34 A. Giusti-Suzor and Ch. Jungen, J. Chem. Phys. 80, 986 (1984).

35 A. Lagerqvist and E. Miescher, Can. J. Phys. 44, 1525 (1966).

36 F. R. Gilmore, J. Quant. Spectrosc. Radiat. Transfer 5, 369 (1965).

37 H. H. Michels, Adv. Chem. Phys. 45, 225 (1981).

38 K. Dressler (unpublished results).

39 K. Dressler and E. Miescher, Astrophys. J. 141, 1266 (1965).

40 J. H. Van Vleck, Phys. Rev. 33, 467 (1929).

41 R. S. Mulliken and A. Christy, Phys. Rev. 38, 87 (1931).

42 H. Lefebvre-Brion and R. W. Field, *Perturbations in the Spectra of Diatomic Molecules* (Academic, Orlando, 1986), pp. 226–231.

43 R. N. Zare, A. L. Schmeltekopf, W. J. Harrop, and D. L. Albritton, J. Mol. Spectrosc. 46, 37 (1973).

44 Reference 42, pp. 375–378.

45 E. Miescher and F. Alberti, J. Phys. Chem. Ref. Data 5, 309 (1976).

46 Reference 42, p. 341.

47 O. B. d'Azy, R. L. Delgado, and A. Tramer, Chem. Phys. 9, 327 (1975).

48 Y. LeDuff, M. Chergui, and E. Boursey, Chem. Phys. Lett. 123, 445 (1986).

85

Origin of Slow Electron Generation in the 1+1 Photoionization Process via the $(3s\sigma)A^2\Sigma^+(v=0)$ State of NO Molecules

William A. Chupka and Leping Li

Sterling Chemistry Laboratory, Yale University

New Haven, Connecticut 06511

In recent years many measurements have been made of photoelectron spectra produced by multiphoton ionization of NO with its Rydberg states as the resonant intermediate. Since potential curves of unperterbed Rydberg states with a specific ion core are very nearly identical with those of the bare ion, a $\Delta v=0$ selection rule is generally expected to hold for their photoionization. Violation have been found which can be attributed to perturbation of the Rydberg state. In cases for which the Rydberg state is photoionized by two photons, violations have been shown to be due to accidental resonances at the penultimate photon energy. However, one strong violation has been found which involves single-photon ioniation of an unperturbed Rydberg state, namely the $(3s\sigma)A^2\Sigma^+$, $v=0$ state of NO. The photoelectron spectrum has been measured by Miller and Compton[1] and by Viswanathan, Jebreta and Reilly[2].

The obtained 1+1 photoelectron spectra via $A^2\Sigma^+(v=0)$ state show a dominant peak corresponding to the expected $\Delta v=0$ peak producing NO^+ in the $v_+=0$ level. In addition, a roughly comparable peak was observed which corresponded to production of NO^+ ion with $v_+=6$ together with electrons of ≈ 10 meV of kinetic energy. Furthermore, Viswavatnan et al. observed that the fast ($\Delta v=0$) electrons had an angular distribution which peaked in the direction of photon polarization and was very weak at right angles, i.e. approximately a $\cos^2\theta$ distribution expected for single-photon ionization of an s electron (if intermediate state alignment effect is negligible). In contrast the slow electrons had a nearly isotropic angular distribution which was observed in both 2+2 as well as 1+1 ionization schemes[1,2]. Viswanathan et al. also showed that even though the rotational structure of the A+X transition of room temperature NO extended over ≈ 2.0nm, the anomalous slow electrons were produced only over a much narrower wavelength region of about 0.3nm. They considered these observations as providing "compelling evidence that a resonant autoionizing state is involved in producing the $v_+=6$ ions". However, no attempt has been made to

identify such a state. It is the purpose of this paper to identify the state and show that it's decay characteristics can explain the observations.

We now present evidence that the $8p\sigma$, $v=7$ Rydberg state is responsible for the observed slow electrons in the 1+1 REMPI process via the $3s\sigma$, $v=0$ state. The position of this level has not been reported but can be estimated accurately in the following manner. The $8p\sigma$, $v=2$ level has been reported[3] to be at 77,333 cm^{-1}. (It has also been seen in the single-photon ionization spectrum of jet-cooled NO[4]). For such a high principle quantum number, the vibrational intervals will be given accurately (except for small perturbations) by the intervals for the ion. These intervals are also given in Table 5.2 of ref.3. The energy interval between $v_+=2$ and $v_+=7$ is given as 11,069 cm^{-1} which, when added to 77,333 cm^{-1}, gives the position of $8p\sigma$,$v=7$ as 88,402 cm^{-1}. This value, divided by 2, corresponds to a one-photon wavelength of 226.24nm. The wavelength given in references 1 and 2 is 226.2nm.

While the close agreement is gratifying, we must consider other possibilities as well. We have followed the above prescription for all s,p,d and f Rydberg states reported in ref.3 and find no other Rydberg state with $^1\Sigma^+$ core which is close enough in energy to account for the slow electron generation at 226.2nm.

Another possibility that should be considered is core-excitation to the $3s\sigma$ Rydberg state of the series converging to the $a^3\Sigma^+$ state of the NO^+ ion. Some structure which might be attributed to this state has been observed by Reese and Rosenstock[5]. However, the energy corresponding to two 226.2nm photons falls in a valley between observed structure. Also the core excitation is spin-forbidden, and the resulting autoionization by configuration interaction will yield a broad[6] photoelectron vibrational distribution totally unlike that observed. Thus this possibility can be excluded.

Three more factors must be addressed successfully in order to support the above identification: (1) The autoionization must favor strongly the production of the $v_+=6$ state of the ion; (2) the intensity of the slow electron peak must be explained in light of the very small Franck-Condon factor for the $3s\sigma,v=0 \rightarrow 8p\sigma,v=7$ transition; (3) the nearly isotropic angular distribution must be explained. We address these in turn.

It is not sufficient to ascribe glibly the production of $v_+=6$ ions to vibrational autoionization with its strong $\Delta v=-1$ propensity rule. The reason for caution derives from the fact that the $np\pi$ Rydbergs are well known to be predissociated strongly and to be subject to predissociation-induced autoionization[7] to which the $\Delta v=-1$ propensity rule does not apply. The degree of predissociation of the higher autoionizing $np\sigma$ states is not known, but will surely become great at sufficiently high values of n and N (total angular momentum excluding eletron and nuclear spins) due to ℓ-uncoupling and consequent mixing with the $np\pi$ state of the same n and v. These ℓ-uncoupled levels will then decrease in autoionization efficiency and be subject to predissociation-induced autoionization with increasing fraction of $\Delta v \neq 0$ transitions.

We fi estimate the mixing of $8p\sigma$ with $8p\pi$ due to ℓ-uncoupling. Since these states well satisfy the conditions of "pure precession"[8] we calculate the Λ-doubling parameter $q = 2B^2\ell(\ell+1)/v_{\Sigma\Pi} = 0.4$ cm^{-1} using the value $v_{\Sigma,\Pi} = 40$ cm^{-1} from Table 2.3 of ref.3. We then estimate the contribution, $\Delta\Gamma_{8p\sigma}$, to the decay width of the $8p\sigma$ state due to the perturbation by the $8p\pi$ state using a simple two-state perturbation treatment as:

$$\Delta\Gamma_{8p\sigma} = [v_{\Sigma,\Pi}qN(N+1) + q^2N^2(N+1)^2]v_{\Sigma,\Pi}^{-2}\Gamma_{8p\pi} \quad . \quad (1)$$

The ratio $\Delta\Gamma_{8p\sigma}/\Gamma_{8p\pi}$ is given in Table I from which it is seen that strong mixing occurs for $N>3$. This is supported by the observed line spacing and widths shown in Fig.1 which is a section

89

of the single photon ionization spectrum of rotationally cold NO.[4] It is readily seen that the N=2 peak of the 8pσ, v=2 state is significantly broadened by interaction with the nearby 8pπ, v=2 state (the same situation should hold for the 8pσ, v=8 state as well). In contrast, the 9sσ, v=2 peaks show no sign of broadening since there is no strong interaction with a predissociating state. We note that a careful examination of this figure shows that the effective rotational constant, B, is slightly larger than that of the ion for the 8pσ state due to the λ-doubling, while that of the 9sσ state is somewhat smaller, due to interaction with the 6dσ state.[9] For larger values of N we can expect increasing rate of predissociation, strongly decreasing autoionization efficiency and the weak emergence of $\Delta v \neq 0$ in addition to the $\Delta v \neq -1$ transitions. However, we note that the slow electron phenomenon is due to the lowest values of N since the experiment of Miller and Compton[1] was carried out on supersonic jet-cooled NO molecules nearly exclusively in the lowest rotational state and the experiments of Viswaratnan et al.[2] were carried out at the same wavelength region near 226.2nm. Therefore we need not be concerned with predissociation by mixing with the 8pπ state.

The 8pσ state may be homogeneously predissociated and thus may be subject to predissociation-induced autoionization. Although the 8pσ state is probably significantly predissociated, we show that the amount of predissociation-induced autoionization is negligible compared with purely vibrational autoionization. First we estimate the rate of vibrational autoionization of the 8pσ, v=7 state. For this purpose we need the value of $d\delta_\sigma/dR$, i.e. the derivative of the npσ quantum defect as a function of internuclear distance. Giusti-Suzor and Jungen[7] have estimated the value of this quantity for the npπ states and given $d\delta_\pi/dR = -0.14$ (a.u.)$^{-1}$. We can be certain that the value for the npσ states will be significantly larger than this value due to the fact that in going from separated atoms to united atom, the principal quantum number changes by unity for npσ but remains unchanged for npπ (see Fig

187, p.329 of ref.8). In the case of H_2[10,11] it is larger by a factor of ≈ 5. We note that direct estimation of this quantity using equation (29) of ref.7 together with the tabulated[12] value of the rotational constant, B_e, for the $(3p\sigma)D^2\Sigma^+$ state of NO would yield an incorrectly small value for $d\delta_\sigma/dR$, since this state is strongly perturbed by the A' valence state giving it a rotational constant anomalously near that of the ion. The appropriate deperturbed value is presently not available. We also note that the value of $d\delta_\sigma/dR$ for H_2 is ≈ 0.18 (a.u.)$^{-1}$ (or 0.34 A^{-1}) and we do not expect it to be much larger for NO. Therefore we use a value of 0.15 (a.u.)$^{-1}$ or 0.30 A^{-1}, which cannot be in error by more than a factor of about one and a half.

The rate of vibrational autoionization may be calculated by formulas given in references 10 and 11,

$$\Gamma_\lambda = 4\pi R_y \, (n^*)^{-3} \, (\varsigma_\lambda{}^{vv'})^2 \qquad cm^{-1} \qquad , \tag{2}$$

where

$$\varsigma_\lambda{}^{vv'} = \langle \psi_v | R - R_e^+ | \psi \rangle \, \frac{d\delta_\lambda}{dR} \qquad .$$

for a purely harmonic oscillator

$$\varsigma_\lambda{}^{vv'} = \sqrt{\frac{h}{8\pi^2\mu c\omega}} \, \sqrt{v} \, \frac{d\delta_\lambda}{dR} \quad ,$$

for $\Delta v = -1$, i.e. where state v decays to the continuum $v-1$. The expression in Eq. (2) simplifies to

$$\Gamma_\lambda = 2.32 \times 10^7 \, \frac{v}{(n)^3 \nu_e \, ,cm^{-1}} \, \left(\frac{d\delta_\lambda}{dR} \, (A^{-1})\right)^2 \, cm^{-1} \, , \tag{3}$$

where M_R is the reduced mass in atomic mass units (e.g. 7.467 for NO) and the quantum defect is ≈ 0.66 for $np\sigma$ and ≈ 0.75 for $np\pi$.[13]

Using Eq.(3), we calculate the vibrational autoionization width to be 2.1 cm^{-1} for 8pσ, v=7. It is also of interest to calculate the vibrational autoionization width for the 8pσ v=2 state which has been observed in absorption[14] as well as in single photon ionization of a jet-cooled NO molecular beam[4]. Using Eq.(3) and the parameters given above we calculate $\Gamma \approx 0.6$ cm^{-1}. The observed width has been given as ≈ 1 cm^{-1} (see Table 3 of ref.14) and this is in agreement with the peak widths shown in Fig.1. Therefore we conclude that a significant fraction of the width is due to vibrational autoionization.

We now estimate the extent of predissociation of the 8pσm v=2 state. We can make a crude estimate by comparing the integrated intensity of the 8pσ, v=2 peaks from the Fig.1 with the intensity of the kpσ, v=2 continuum (i.e. the continuum to which the npσ, v=2 series converges), since they are related by the condition of continuity of oscillator strength. The intensity of the kpσ, v=2 continuum may be estimated as follows. The continuum shown in Fig.1 consists of v=0 and v=1 continua of all partial waves. From Franck-Condon factors for photoionization (see p.28 of ref.15), the v=2 (all partial waves) is about 0.56 of the sum of v=0 and 1 continua (i.e. the continuum of Fig.1). Furthermore, the kpσ absorption cross section relative to the total absorption cross section for all partial waves for high Rydberg states (and hence adjoining continuum) is estimated to be 21% (Table V of ref.7). Thus the intensity of the kpσ, v=2 continuum is estimated to be $\approx 0.56 \times 0.21 = 0.12$ of the continuum of Fig.1. If the 8pσ, v=2 peaks of Fig.1 represented 100% autoionization (i.e. corresponded exactly with absorption) their integrated intensity should be approximately equal to the hypothetical intensity of the kpσ, v=2 continuum integrated from n=7.5 to n=8.5. The latter integration was derived from Fig.1 of ref.4 using the factor 0.12 estimated above. This

procedure yields the estimate that the $8p\sigma$, $v=2$ band of Fig.1 is low in intensity by a factor of four or so, i.e. the autoionization efficiency is $\approx 25\%$ and the predissociation rate is ≈ 3 times greater than that of autoionization, Thus yielding a total width of about $4\times0.6=2.4$ cm^{-1} with an error of about a factor of two, still in reasonable agreement with the crude estimates of ≈ 1 cm^{-1}. The same procedure applied to the $9p\sigma$, $v=2$ and $10p\sigma$, $v=2$ states (data of Fig.1 of ref.4) yields autoionization efficiencies of about 10% and 25%, respectively.

It is also of importance to compare the characteristics of the $8p\pi$, $v=2$ and $8p\sigma$, $v=2$ bands of Figure 1. From experimental absorption spectra (see Table V of ref.7) the ratio of relative absorption cross sections, $\sigma(p\pi)/\sigma(p\sigma)$, is estimated to be $\approx 45/21$ $=2.1$. A comparison of the integrated intensities of the bands of Fig.1 yields the ratio $8p\pi/8p\sigma \approx 0.15$. Therefore we estimate that the autoionization efficiency of the $8p\pi$, $v=2$ state is only $\approx 0.25\times0.15 \approx 0.04$. From similar examination of $np\pi$ states which can autoionize with $\Delta v=-1$, we conclude that the autoionization efficiency is generally ≈ 0.1 or less, i.e. the "survival factor" for predissociation is $> 90\%$. Most of this autoionization is predissociation induced and will be spread over the entire photoelectron spectrum. We now show that only a minor part of photoelectron spectrum produced by autoionization of $np\sigma$, $v=7$ will be due to predissociation-induced autoionization.

While the electronic contribution to the rate of autoionization and predissociation both scale as $(n^*)^{-3}$, the Franck-Condon factor for predissociation has no simple behavior with either n or v. A review of reported widths of $np\sigma$ states with $n>4$ and $v=0 - 5$ shows them to be in the range of 1 to 3 cm^{-1} and we can assume that the predissociation width of $np\sigma$, $v=7$ will be in that range, if no other predissociating state becomes effective. However, as can be seen from Eq.(3) the vibrational autoionization rate increases linearly with v, so that the autoionization width

calculated above is 2.1 cm^{-1}. Therefore we estimate that predissociation and autionization rates are comparable giving a total decay width of $\approx$ 4 cm^{-4}. The predissociation can be expected to yield < 10 % predissociation-induced autoionization spread over the photoelectron spectrum (v_+=0 to 6) while the vibrational autoionization is expected to yield > 90 % yield of slow electrons and v_+=6 ions. Thus the v_+=1 - 5 photoelectron peaks are expected to be at most several percent of the intensity of the v_+=6 (slow electron) peak. The experimental results are in accord with this estimate.

The remaining aspect to be considered is the magnitude of the very small Franck-Condon factor to be expected for the A, v=0 $\rightarrow$ 8po, v=7 transition. We can readily estimate the order of magnitude required to explain the intensity of the slow-electrons relative to the fast ones. First we estimate this relative intensity. The most reliable data are those of Viswanathan et al.[2] who used a time-of-flight photoelectron spectrometer. We integrate the peaks shown in their Fig.3D which shows the spectrum taken with laser polarization parallel to the electron flight direction and with an accelerating potential of -9 Volts. This insures practically complete collection of slow electrons and nearly complete collection of fast ones, as is indicated by the fact that the fast "turn-around" peak has an area very nearly equal to that of the forward fast peak in spite of the fact that the former will have considerably lower collection efficiency due to loss of electrons with considerable perpendicular component of velocity. We find the ratio slow/fast to be $\approx$0.20 which is certainly an upper limit and should not be in error by more than 20 % or so.

However, the experimental conditions of Miller and Compton are closer to ours, i.e. they used rotationally cold NO while Viswanathan et al. used room temperature NO and the latter data may include transitions from higher rotational states which would be more strongly predissociated, thus lowering this ratio from the

94

value ≈1.0 obtained from the data of 2 for this ratio.

We now estimate the relative cross sections for direct ionization of the 3sσ state and for electronic excitation (i.e. without Franck-Condon) of the 8pσ state with decay width, as discussed above, of ≈4 cm^{-1}. The oscillator strength of the transition D,3pσ → A,3sσ was measured by Wray[16] to be 0.18 and calculated by Gallusser and Dressler[17] to be 0.30. We take it to be 0.25. Using the well-known $(n^*)^{-3}$-dependence of oscillator strength, we obtain the oscillator strength of the transition A,3sσ → 8pσ to be f ≈ $0.25(2.737/7.66)^3$ = 0.011. We then calculate the average cross-section for absorption over the 4 cm^{-1} broad line by [18]

$$ \sigma = \frac{\pi e^2 h}{mc} \frac{df}{dE} = 1.098 10^{-16} \text{ cm}^2\text{eV} \frac{df}{dE} . \qquad (4) $$

We take df/dE = $0.011/(5.0 \times 10^{-4}$ eV) ≈ 22 (eV)$^{-1}$, and get σ ≈ $1.098 \times 10^{-16} \times 22$ ≈ 2.4×10^{-25} cm^2 for absorption and about half that for ionization. This cross section is approximately $10^2 - 10^3$ times greater than that expected for direct photoionization of the A state. Thus a Franck-Condon factor of the order of 10^{-3} or somewhat greater would suffice to explain the intensity of the low-energy electrons.

A Franck-Condon factor on the order of 10^{-3} requires some justification. The molecular parameters of the A,3sσ state are virtually identical with those of the ion (ω_e = 2374.3 and 2376.4 cm^{-1} respectively; B_e = 1.9965 and 1.99727 cm^{-1} respectively) so that the Franck-Condon factor between v=0 and 7 is many orders of magnitude smaller than 10^{-3}. However, the simple Franck-Condon approximation is certainly not appropriate in this case, as we now show.

If we assume that the Born-Oppenheimer approximation is valid (an

assumption to be discussed later), the transition amplitude for a particular vibrational channel $v_i \to v_f$ is given by[14]

$$D(v_f, v_i) = \int \chi_{v_f}(R)^+ D(R) \chi_{v_i}(R) \, dR , \qquad (5)$$

where $\chi(R)$ is a vibrational wave function and $D(R)$ is the R-dependent dipole amplitude where R is the internuclear distance. The Franck-Condon approximation consists of assuming that $D(R)$ is independent of R. While this approximation is often fairly accurate for vibrational transition probabilities which are significant fractions of the total electronic transition probability, it should always be suspect for such small values ($\leq 10^{-3}$) as we consider here (and also for large values of both vibrational quantum numbers for which the wave functions extend over a considerable range of internuclear distance).

Of particular relevance to the present discussion is the set of potential curves shown in Fig.2. All the curves but one (the A' curve labelled "Michels") are adapted from Fig.1 of a paper by Bardsley[20] on dissociatiove recombination of electrons with NO^+ ions. The curve for NO^- is accurately known from extensive vibration-rotation spectra.[21] The remaining curves are those of excited valence states of NO. All but A' are bound states with observed vibrational levels. The B and B'states are particularly accurately characterized, the L and I states somewhat less so.[21] However, the position of the purely repulsive A' state is inferred[22] only from its presumed perturbation and predissociation of other states and is very uncertain. Its location will have a very significant effect on photoelectron spectra and we argue here that it is situated about 3 eV higher than given in Bardsley's paper and is more likely located near the curve labelled A'(Michels).

The A' state is unique among the valence states shown in another respect. It's configuration[23] $\cdots(3\sigma_g)^2(1\pi_u^*)^4 3\sigma_u^*$ differs from those of the Rydberg states (and adjoining continuum), $\cdots(3\sigma_g)^2(1\pi_u^*)^4(n\ell\lambda)$, by one orbital only (The u and g symmetries are approximate only). Therefore above the NO^+ curve it exists only as a shape resonance[24] in the σ^* continuum. It is in fact the same orbital responsible for the well known shape resonances in N_2[25], CO[26] and O_2[27-29].

The position of this shape resonance at the equilibrium internuclear distance of NO in its ground state has been calculated by Smith et al.[30] and probably observed experimentally by Southworth et al.[31] and both determinations are shown by the vertical bars in Fig.2. This position for the shape resonance is supported by the calculated potential curves of Michels[23]. His calculated curves for the B, B', L and I valence states are in good agreement with the curves of Gallusser and Dressler used by Bardsley, and shown in Fig.2, except for the A' state which he calculates to be about 3 eV higher. In Fig.2, we show Michel's A'state curves as measured from his plotted curves slightly extrapolated. The error in transferring this curve from his small scale figure is less then ±0.5 eV. Nevertheless it is seen to be in good agreement with the calculation of Smith et al. and the data of Southworth et al., and in gross disagreement with the curve used by Bardsley.

There are several important consequences of moving the A' curve to the position calculated by Michels. Firstly, the cross section for dissociative recombination of the ≈ 2 state of NO^+ as calculated by Bardsley seems too large by a factor of ≈ 2 (see his Table 1). Secondly, the higher position of the shape resonance explains why the 1+1 photoelectron spectrum of Viswanathan et al. at wavelengths in the region of 226 nm, except for the very narrow resonance at 226.2 nm, shows no detectable $\Delta v \neq 0$ transitions and on the narrow resonance shows only $\Delta v = 0$ and $\Delta v = 6$ peaks, as

does the spectrum of Miller and Compton. The two photon energy is about 11.0 eV which would place it near the center of the shape resonance according to Bardsley's curve. This would result in sifnificant intensity of $\Delta v \neq 0$ transitions but cannot be directly responsible for the relatively intense slow ($\Delta v = 0$) peak. This follows from the theory[24] which has been successful in predicting vibrational distributions resulting from the effects of shape resonances. Since these resonances are generally much broader tan vibrational spacings, it is appropriate to use an adiabatic approximation which consists of using equation(5) with a R-dependent transition moment. The variation of this moment over the relevant range of R is usually sufficiently slow that a Taylor series expansion about the equilibrium value of R is justified, with the first few terms of most significance. If harmonic oscillator wave functions are used, it is easily seen that transitions with $\Delta v = n$ come only *from terms of the power n and greater*. An example of an unusually strong effect of a shape resonance is that of O_2. The accurate calculations of Stephens et al.[29] for $\Delta v \neq 0$ processes show a monotonic decrease in intensity as $|\Delta v|$ increases from zero. No such transitions are seen in either experiments[1,2], strongly supporting the absence of the A' shape resonance at the lower energy.

While the A' shape resonance is very probably too high in energy to play a direct part in the photoionization process considered here, it can play an indirect part since it certainly affects the potential curves of high-n Rydberg states in the region of R where it drops below the NO^+ curve (see Fig 1 of ref.[19]), thereby affecting Franck-Condon factors by breaking the near-orthogonality of the Rydberg and ion vibrational wave functions for high values of v in the neighborhood of 7. (It could also lead to small snifts in energy levels as well, of course, making our excellent agreement with the calculated position of the 8pσ, v=7 level fortuitous)

Another source of an enhanced Franck-Condon factor for v=7 is the presence of the other valence states of Fig.2, especially the I and B states. While the transition moment for their excitation from the A,3sσ state is very small since the transition is configurationally forbidden (which would require a "two-electron jump"), they will be effective (see p.1490 of ref.19) since they interact with the σ and π ionization continua respectively with fixed-nuclei widths of 0.048 eV and 0.074 eV, respectively.[20,22] At a fixed internuclear distance those states would manifest themselves as Fano-type resonances with q≈0 ("window-resonances") in the ionization continua with which they interact, the position of the resonance being R-dependent. Since the autoionization widths of those resonances are much smaller than vibrational intervals, they will lead predominantly to predissociation and a minor fraction of autoionization spread over all energetically allowed vibrational levels of the photoelectron spectrum as in the case of H_2.[19,32] The predissociation will also lead to population of any high n and v Rydberg states whose decay widths include the photon energy used, specifically the 8pσ,v=7 state but also any other state of lower n and higher v in this energy range. All such states will decay by vibrational autoionization (in addition to predissociation) predominantly with Δv= minimum, yielding the slow electron peak.

The quantification of the effective Franck-Condon factor for the production of the v_+=6 "slow electron" peak is not readily accomplished and this remains the only weak part of our explanation. Nevertheless the above considerations at least make plausible the required factor of ≈10^{-3}.

The nearly isotropic angular distribution of the slow electrons remains to be rationalized. The fast electrons have a nearly $\cos^2\theta$ distribution as is expected for photoionization of the 3sσ electron into a p partial wave nearly exclusively (i.e. the asymmetry parameter[34], β≈2). Any type of resonance in which the outgoing

electron is temporarily trapped so that it makes many "collisions" with the ion core will lead to enhanced angular momentum exchange. In our case this will lead to decrease of the value of β toward the isotropic value of $\beta=0$. This general trend has been confirmed theoretically and experimentally many times.[24]

While the angular distribution of electrons detached from a p orbital in a negative ion should be isotropic[33] at threshold due to suppression of the d-wave relative to the s-wave by an angular momentum barrier,[18] such a barrier does not exist for pure Coulomb field. However, a shielded Coulomb field as in a many electron atom or molecule can have such an effective barrier and direct photoionization of a p electron or photoionization via an intermediate resonance in which core-scattering can lead to s-waves, one can expect the dominance of s-waves at threshold and hence an isotropic distribution. This is nicely illustrated by a calculation by Berry[34] (see his Fig.5) which shows the s-wave dominating overwhelmingly for the first 0.7 eV above threshold in a model calculation of vibrational autoionization by dipole and quadrupole interaction leading to s,p and d outgoing waves from an initially bound p electron. It is of interest to examine the scattering process by which the $8p\sigma$ electron is scattered into an s-wave so efficiently. Normally this requires a large variation of ion core dipole moment as a function of internuclear distance R. The dipole moment of NO^+ has been calculated[35] (referred to the center of mass) to be 0.72 Debye at R_e and to vary approximately linearly with internuclear distance with $dD/dR \approx 3.4$ Debye/A. It is interesting to note that in Berry's calculation, he used a value $dD/dR=1.4$ Debye/A and found the autoionization rate of s partial wave is about 80 times larger than that of the d partial waves near threshold energies (less than 0.7eV). Therefore the very large value of 3.4 Debye/A of NO^+ not only rationalize "ℓ-mixing" in the resonant autoionization state but also suggest that a significant part of the vibrational autoionization may be attributed to the long range interaction between $8p\sigma$ Rydberg electron and the

oscillating dipole moment of NO^+ ion core.

Acknowledgements

References

1) J.C.Miller and R.N.Compton, J. Chem. Phys. 84, 675(1986).

2) K.S.Viswanathan, E.Sekreta and J.P.Reilly, J. Phys. Chem. 90, 5658(1986).

3) E.Miescher and K.P.Huber in "Spectroscopy" Phys. Chem. Series Two, Vol.3 (ed. A.D. Buckingham and D.A. Ramsay, Butterworths) Table 2.3, p.49

4) P.J.Miller, P.Chen and W.A.Chupka, Chem. Phys. Lett. 120, 217(1985).

5) R.M.Reese and H.M.Rosenstocks, J. Chem. Phys. 44, 2007(1966).

6) A.L.Smith, Phil. Tran·. Roy. Soc. Lond. A 268, 169(1970).

7) A.Giusti-Suzor and Ch.Jungen, J. Chem. Phys. 80, 986(1984).

8) G.Herzberg, Spectra of Diatomic Molecules, (Van Nostrand-Reinhold, Princeton, New Jersey, 1950)pp.226 - 229.

9) E.Miescher, Can. J. Phys. 54, 2074(1976). See Fig.9

10) G.Herzberg and Ch.Jungen, J. Mol. Spectroscopy 41, 425(1972).

11) P.M.Dehmer and W.A.Chupka, J. Chem. Phys. 65, 2243(1976).

12) K.P.Huber and G.Herzberg, Constants of Diatomic Molecules,(Van Nostrand Reinhold, New York, 1979).

13) T.Ebata, Y.Anezaki, M.Fujii, N.Midami and M.Ito, J. Phys. Chem. 87, 4773(1983).

14) E.Miescher and F.Alberti, J. Phys. Chem. Ref. Data, 5, 309(1976), Table 3.

15) K.Kimura, S.Katsumata, Y.Achiba, T.Yamazake and S.Iwata, Handbook of HeI Photoelectron Spectra of Fundamental Organic Molecules,(Halsted Press, N.Y. 1981).

16) K.L.Wray, J. Quant. Spectrosc. Radiat. Transfer 9, 255(1969).

17) R.Gallusser and K.Dressler, AZMP 22, 792(1971).

18) U.Faro and J.W.Cooper, Rev. Mod. Phys. 40, 441(1968),Eq.2.14.

19) W.A.Chupka, J. Chem. Phys., 87, 1488(1987) and references therein.

20) J.N.Bardsley, Planet. Sace Sci. 31, 667(1983).

21) References contained in the book by Huber and Herzberg of Ref.8.

22) R.R.Gallusser dissertation No.5759, Eidgenössisck Technische Hochschule Zurich; R.R.Gullusser and K.Dressler, J. Chem. Phys. 76, 4311(1982).

23) H.H.Michels in Advances in Chemical Physics, Vol.XLV, Part 2 (1981), Chapter 3.

24) An excellent discussion of shape (and other) resonances is given ty J.L.Dehmer, A.C.Parr and S.H.Southworth in Handbook on Synchrotron Radiation, Vol. II, edited by G.V.Marr (North-Holland, Amsterdam, 1986), A short description in connection with photoionization of Rydberg states is given in ref.19.

25) J.L.Dehmer and D.Dill, Phys. Rev. Lett. 35, 213(1975).

26) R.Stockbauer, B.E.Cole, D.L.Ederer, J.B.West, A.C.Parr and J.L.Dehmer, Phys. Rev. Lett. 93, 757(1979).

27) A.Gerwer, C.Asaro, B.V.McKoy and P.W. Langhoff, J. Chem. Phys. 72, 713(1980).

28) P.J.Miller, L.Li, W.A.Chupka and S.D.Colson, J. Chem. Phys. (submitted to J. Chem. Phys.).

29) J.A. Stephens, M.Braunstein and V.McKoy, J. Chem. Phys. (submitted to J. Chem. Phys.).

30) M.E.Smith, R.R.Lucchese and V.McKoy, J. Chem. Phys. 79, 1360(1983).

31) S.H.Southworth, A.C.Parr, J.E.Hardis and J.L.Dehmer, J. Chem. Phys. 87, 5125(1987).

32) A.P.Hickman, Phys. Rev. Lett. 59, 1553(1987).

33) J.Cooper and R.N.Zare, J. Chem. Phys. 48, 942(1968).

34) R.S.Berry, J. Chem. Phys. 45, 1228(1966).

35) V.McKoy, private communication.

Figure Captions

Fig.1 - One photon ionization spectrum of cold NO showing N=0, 1 and 2 lines of 8pσ, v=2 and the strongly predissociated 8pπ, v=2. Note evidence of interaction by pure precession leading to visible broadening of the N=2 line.

Fig.2 - Potential curves of excited valence states of NO and of the ground state NO^+ ion. Note that the A' state becomes a shape resonance above the NO^+ curve. Experimental evidence suggests that the higher energy A' curve is the correct one.
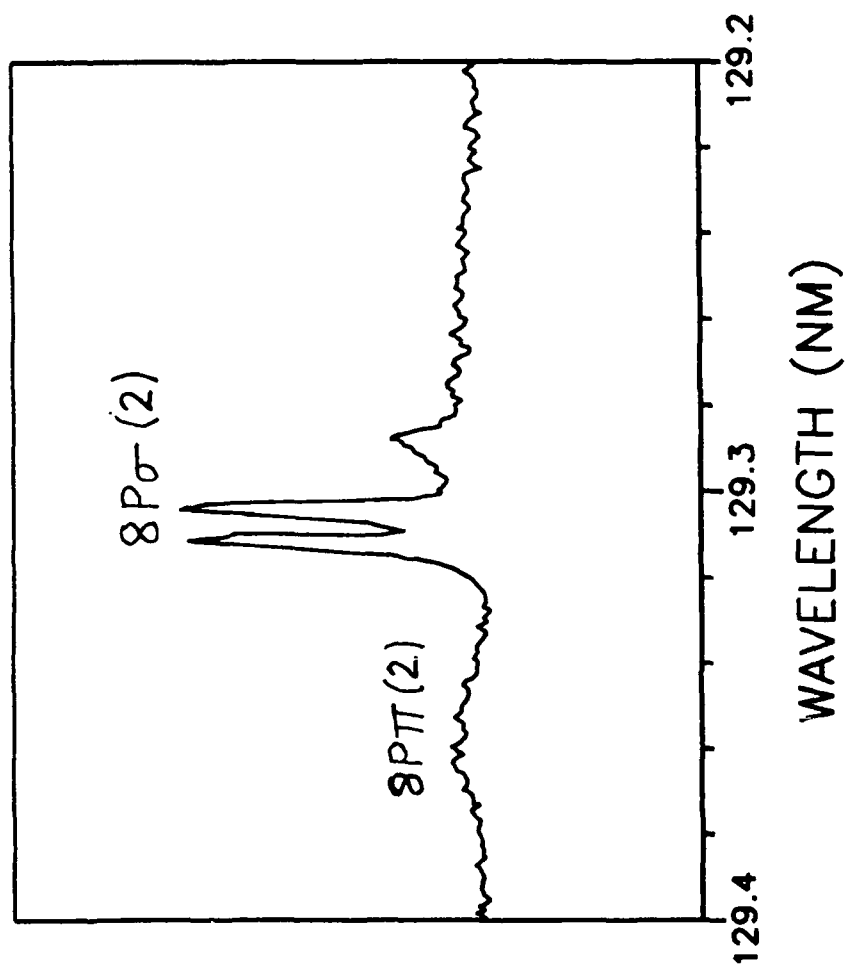
WAVELENGTH (NM)

$F_{IG}.1$

Photoionization efficiency curve of nitric oxide.
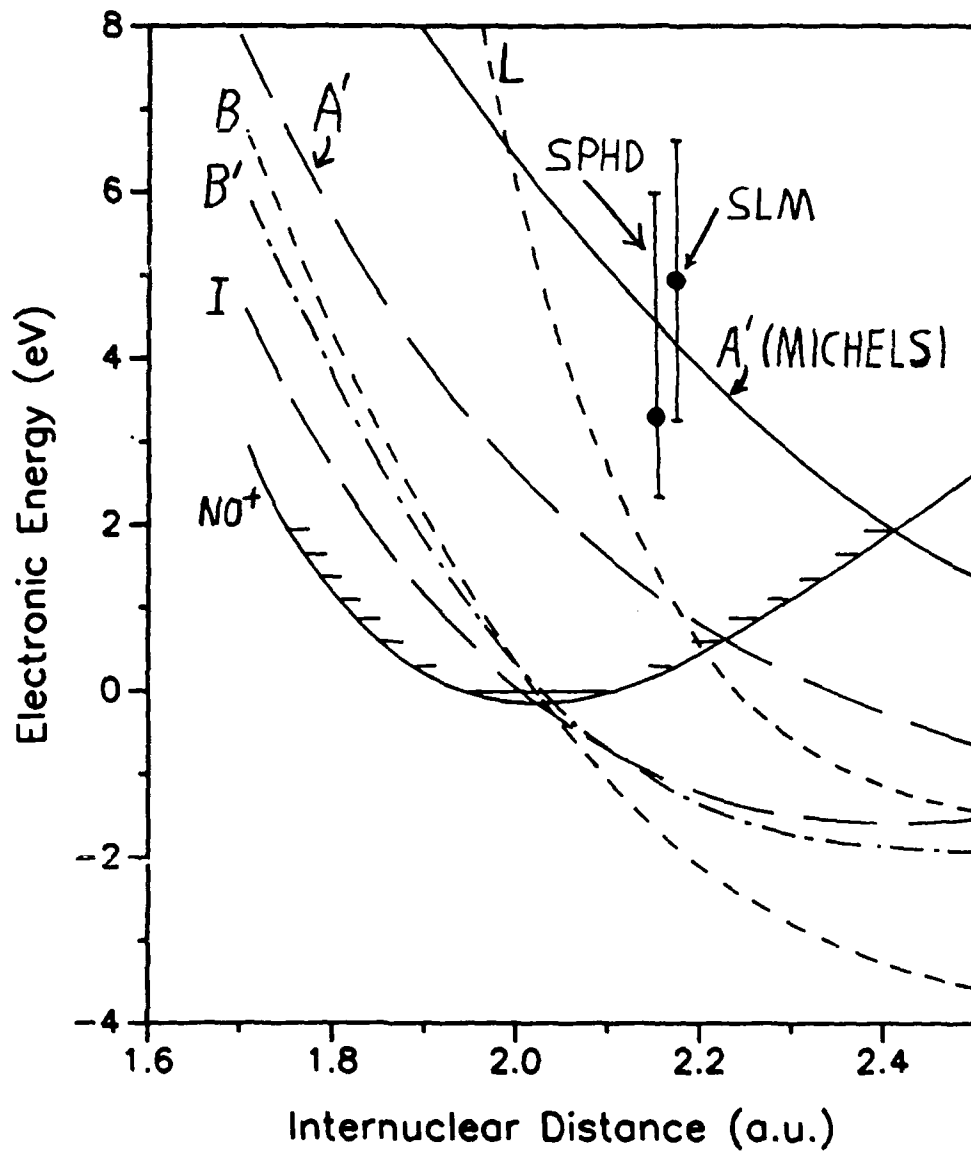
FIG. 2

Photoelectron Spectrum of the E state of O_2

William A. Chupka and Leping Li

Sterling Chemistry Laboratory, Yale University

New Haven, Connecticut 06511

Abstract

It is argued that the photoelectron spectrum of the mixed Rydberg-valence E state of O_2 as measured by Miller et al [J. Chem. Phys. **88**, 2972(1988)] is better described by the method given in that paper than by the calculational method given recently by Wang et al [J. Chem. Phys. **89**, 4654(1988)], since the latter method treats the overall three-photon process as coherent whereas experimental evidence indicates that the last step, in this and most other cases, is uncoupled from the excitation process.

Photoionization and photoelectron spectroscopy of Rydberg states has proved to be a valuable tool for investigating the properties of the Rydberg states and their photoionization continua as well as for the preparation of ions in specific rovibronic states. The simple application of the Franck-Condon principle to the photoionization of unperturbed single-configuration Rydberg states yields the prediction that the vibronic state of the ion core will be preserved and a number of such cases are known experimentally. However a growing number of cases exist for which strong violations of this propensity rule occur. An analysis of reasons for such violations has been given in terms of unusual features in the ionization continua, such as shape and core-excited resonances. It has also been shown[1] that the photoelectron spectrum can also be a sensitive indication of perturbations of the Rydberg state. Recently an extreme case of such a perturbation has been studied for the O_2 molecule[2]. The $E^3\Sigma_u^-$ state has been described as formed by the very strongly avoided crossing of the $B^3\Sigma_u^-$ valence state (upper state of the Schumann-Runge bands) with the $3p\pi$ $^3\Sigma_u^-$ Rydberg state. The three-photon resonant, four-photon ionization spectrum of the v=0 level of this state shows that the peak corresponding to the formation of the v=0 state of the ion is a minor one comprising ≈10% of the total intensity. The observed photoelectron distribution was qualitatively explained by an approximate method which considered the overlap integrals of the v=0 vibrational wave function of the calculated adiabatic E state potential curve and those of the ion, weighted by the fraction of Rydberg character of the E state as a function of internuclear distance, since photoionization of the valence state is configurationally forbidden. Recently Wang et al[4,5] have obtained both adiabatic and diabatic potential curves for the E and B states by modelling the observed photoabsorption cross-section to high precision using a coupled Schrodinger equation method[6] and by comparing calculated with measured isotope effects. They consider their potential curves to be superior to previously calculated ones which are similar but have significant differences. Using

108

their potential curves they calculated[4] the photoelectron spectrum in two ways. The first method, suggested by Miller et al[2] and which Wang et al consider too crude an approximation, used the $v=0$ vibrational wave function of the uncoupled adiabatic $E^3\Sigma_u^-$ potential. The second, which they consider far more appropriate, used the Rydberg solution of the diabatic coupled Schrodinger equations in the overlap integral with ion vibrational wave functions. Both methods reproduce the general trend of the observed spectrum but the method of Wang et al produced somewhat better overall agreement with experiment.

While the latter method would be appropriate for certain experiments and represents an important step toward the proper treatment of the MPI experiments, it is suggested here that it suffers from an approximation which makes it less valid than the first method for the experiment in question. The method of Wang et al depends on the assumption that the overall multiphoton ionization process is coherent, i.e. that the amplitude for production of a specific final state, f, of the ionization continuum from the initial state i, is proportional to the usual[7] fourth rank tensor element

$$\Sigma_{j,k} \langle f|\mu|\phi\rangle\langle\phi|\mu|k\rangle\langle k|\mu|j\rangle\langle j|\mu|i\rangle$$

with appropriate photon permutations and energy denominators, where ϕ is the function of Wang et al and all other states i,j,k, and f are stationary states. However, for experiments of the type of Miller et al, all experimental evidence[8] indicates that the ionization step is not coherent, i.e. a real population of the resonant stationary state is created and then photoionizated over a time determined by the photoionization cross section of the resonant state and the laser intensity and describable by a rate equation. In fact researchers[9-11] have successfully used rate equations to model the competition between predissociation and photoionization in order to determine relative predissociation rates from MPI rotational line intensities. The narrow rotational structure observed in such experiments attests to the long life of

the resonant state in the laser field.

All this previous experience suggests that, for the experiment in question, the non-stationary function of Wang et al should be propagated in time and its formation, decay and photoionization integrated over the laser pulse. This is not simple and is complicated by the fact that the temporal and spatial structure of the laser pulse is not well-controlled. However, some semi-quantitative estimates can be made from the Rydberg-valence interaction energy and the known properties of the $v=0$ level of the E state. In the absorption spectrum of $^{16}O_2$ the band is diffuse[12], while for $^{18}O_2$ the rotational structure[13] is well resolved with line widths $\leq$ 1cm^{-1}. Thus the line widths for $^{16}O_2$ are very unlikely to be much broader than $\approx$ 5cm^{-1} corresponding to a lifetime of 10^{-12} second. The non-stateionary state of Wang et al will evolve in a time of the order of femtoseconds to approximately the $v=0$ wave function of the adiabatic E state potential and a small amplitude of dissociative part, the whole then decaying according to the predissociation rate of about 10^{12} sec^{-1} (the photoionization rate is estimated to be $\approx$ 3x10^{10} sec^{-1}, laser pulse length $\approx$10 nsec, energy $\approx$1mJ, focal diameter $\approx$100μ, cross section $\approx$10^{-17} cm^2). Subsequent photoionization of this state corresponds to the method one.

Thus, while the method of Wang et al is certainly appropriate for modelling the absorption spectrum of O_2 and could be appropriate for processes proceeding coherently via this absorption such as (off-resonant) Raman scattering, it is of questionable suitability for the photoionization experiment of Miller et al unless extended as described above. However it may be possible to perform experiments which might approach the conditions required by their method. An experiment using a (few) femtosecond pulse, whose Fourier transform spans the E-B interaction region would be appropriate but very difficult at present. The effective experimental time might be shortened by operating sufficiently far

off resonance as in fluorescence emission spectroscopic experiments[14] but photoionization intensities are too weak under such conditions with present laser powers, and greatly increased laser powers could introduce other effects. Since the coherent four-photon process will have some finite amplitude, it would be interesting to attempt an approach toward conditions mentioned above (e.g. by use of pico- or sub pico-second lasers) in order to assess its possible importance and elucidate this poorly-studied aspect of resonant MPI.

Finally, one may ask why, if the diabatic coupled method is less appropriate than the adiabatic one, does it produce somewhat better agreement with experimental data in this case. Several reasons are plausible. The calculated photoelectron intensities are very sensitive to the position and shape of the adiabatic E potential curve and a small shift could change the order of agreement. An R (internuclear distance) dependence of the photoionization cross section, of the kind found in the ungerade ionization continuum of gerade Rydberg states of O_2, could have an equivalent effect. While the presently relevant gerade continuum has received little theoretical attention, the calculations of Guberman show that a number of autoionizing gerade valence states exist in the relevant region although they do not give strengths of interaction with Rydberg states or continua. Nevertheless it is clear that very close quantitative agreement cannot be expected, nor used reliably to assess the validity of calculational methods, if these and other[17] properties of the continua are ignored.
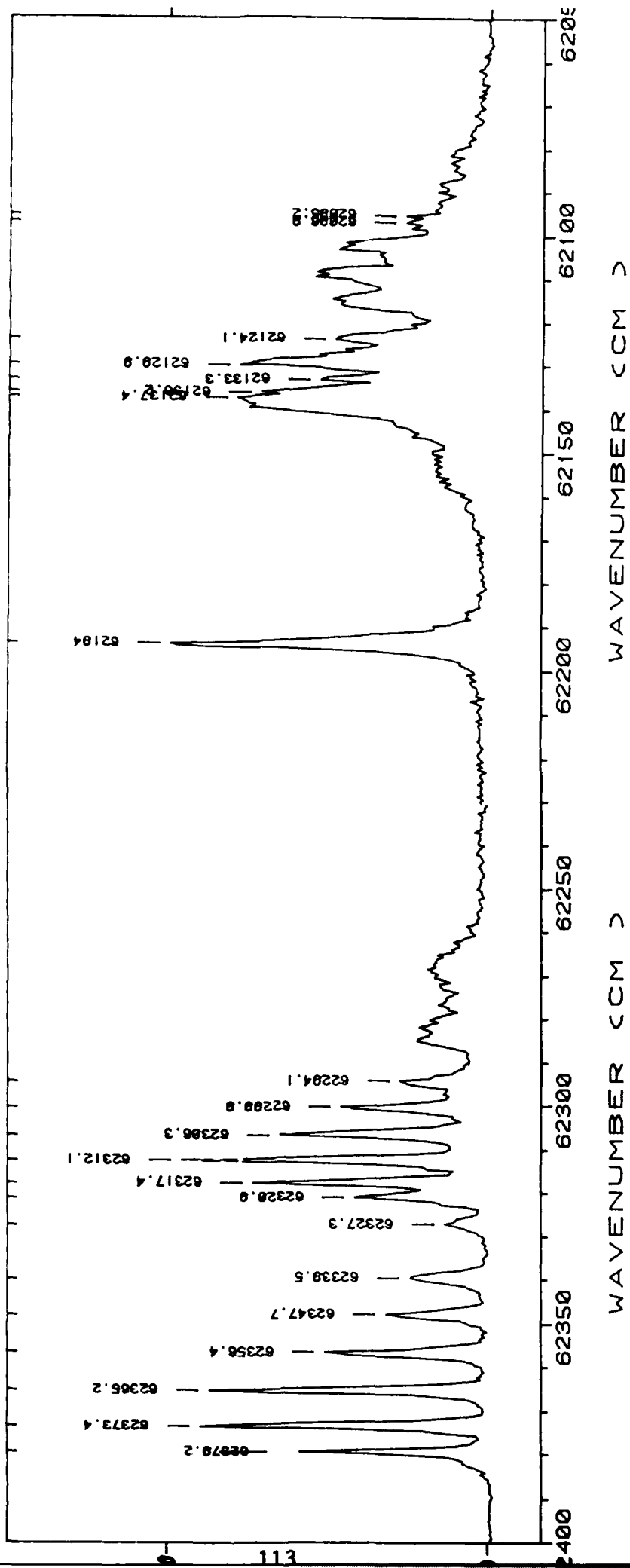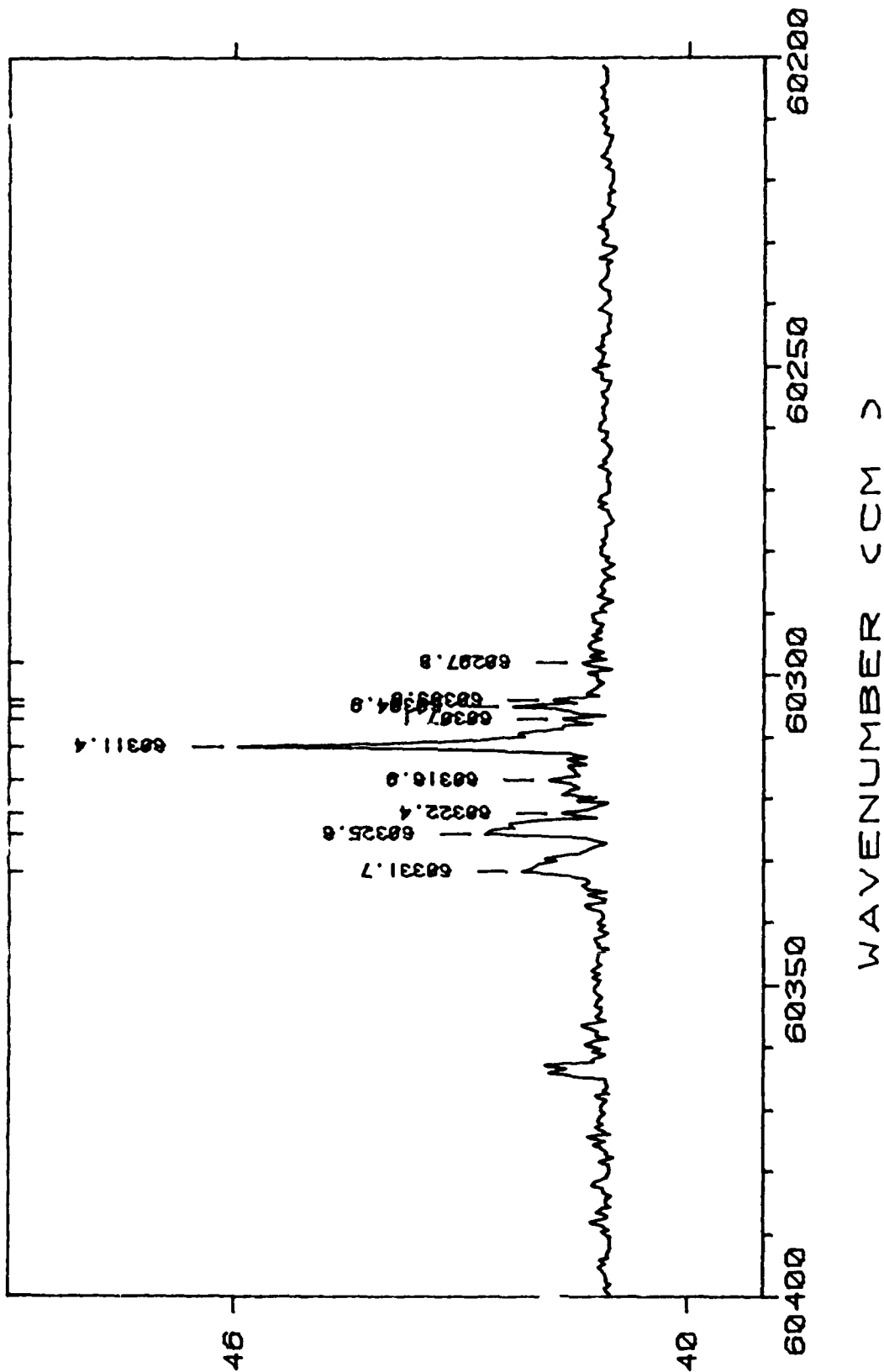
Acknowledgement

References

1) M.G. White, M. Seaver, W.A. Chupka and S.D. Colson, Phys. Rev. Lett. **49**, 28(1982).

2) P.J. Miller, L. Li, W.A. Chupka and S.D. Colson, J. Chem. Phys. **88**, 2972(1988).

3) R.J. Buenker, S.D. Peyerimhoff and M. Peric, Chem. Phys. Lett. **42**, 383(1976).

4) J. Wang, A.J. Blake and L. Torop, J. Chem. Phys. **89**, 4654(1988).

5) J. Wang, A.J. Blake, D.G. McCoy and L. Torop, JQSRT (in press, 1988).

6) L. Torop, D.G. McCoy, A.J. Blake, J. Wang and T. Scholz, JQSRT **38**, 9(1987).

7) See for example R.N. Dixon, J.M. Bayley and M.N.R. Ashfold, Chem. Phys. **84**, 21(1984).

8) P.M. Johnson and C.E. Otis, Ann. Rev. Phys. Chem. **32**, 139(1981).

9) M.N.R. Ashfold and R.N. Dixon, Chem. Phys. Lett. **93**, 5(1982).

10) M.N.R. Ashfold, J.M. Bayley and R.N. Dixon, Chem. Phys. **84**, 35(1984).

11) M.N.R. Ashfold, J.M. Bayley, R.N. Dixon and J.D. Prince, Ber. Bunsenges. Phys. Chem. **89**, 254(1985).

12) M. Ogawa, K.R. Yamawaki, A. Hashizusne and Y. Tanaka, J. Mol. Spectry. **55**, 425(1975).

13) M. Ogawa, Can. J. Phys. **53**, 2703(1975).

14) D. Imre, J.L. Kinsey, A. Sinka and J. Krenos, J. Phys. Chem. **88**, 3956(1984). Note that here also as resonance is approached the effective lifetime of the resonant state increases and at no excition wavelength is there a distinction between fluorescence and Raman scattering.

15) P.J. Miller, L. Li, W.A. Chupka and S.D. Colson, J. Chem. Phys. **89**, 3921(1988).

16) J.A. Stephen, M. Braunstein and V. McKoy, J. Chem. Phys. **89**, 3923(1988).

17) W.A. Chupka, J. Chem. Phys. **87**, 1488(1987).
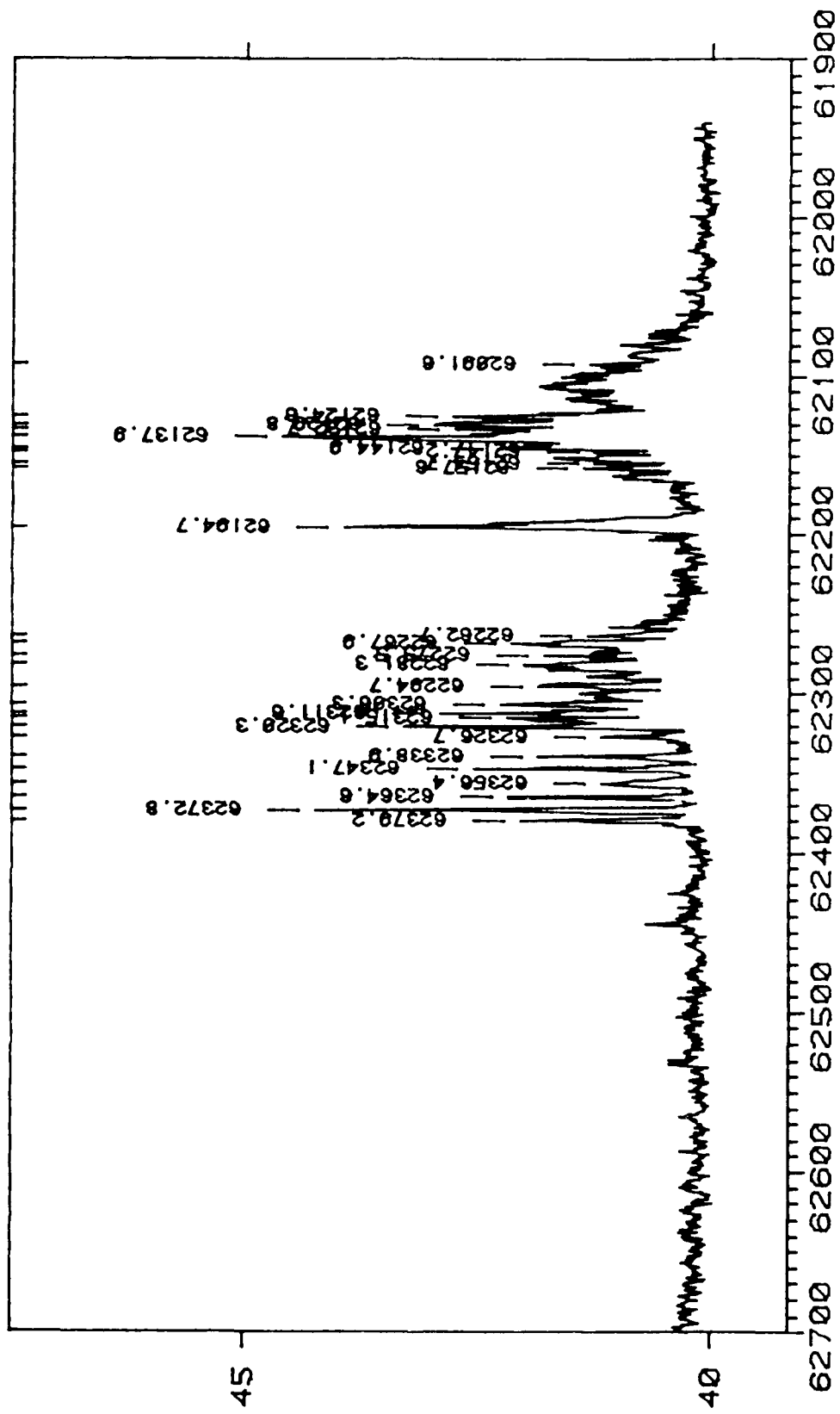
The (2+1) MPI spectrum of the $(v', 0)$ $3s\sigma^1\Pi_g \leftarrow {}^1\Delta_g$ transition of O_2

C17

C13

60297.8
60303.8
60304.8
60307.1
60311.4
60316.8
60322.4
60325.6
60331.7

WAVENUMBER <CM >

46

40

60400   60350   60300   60250   60200

114

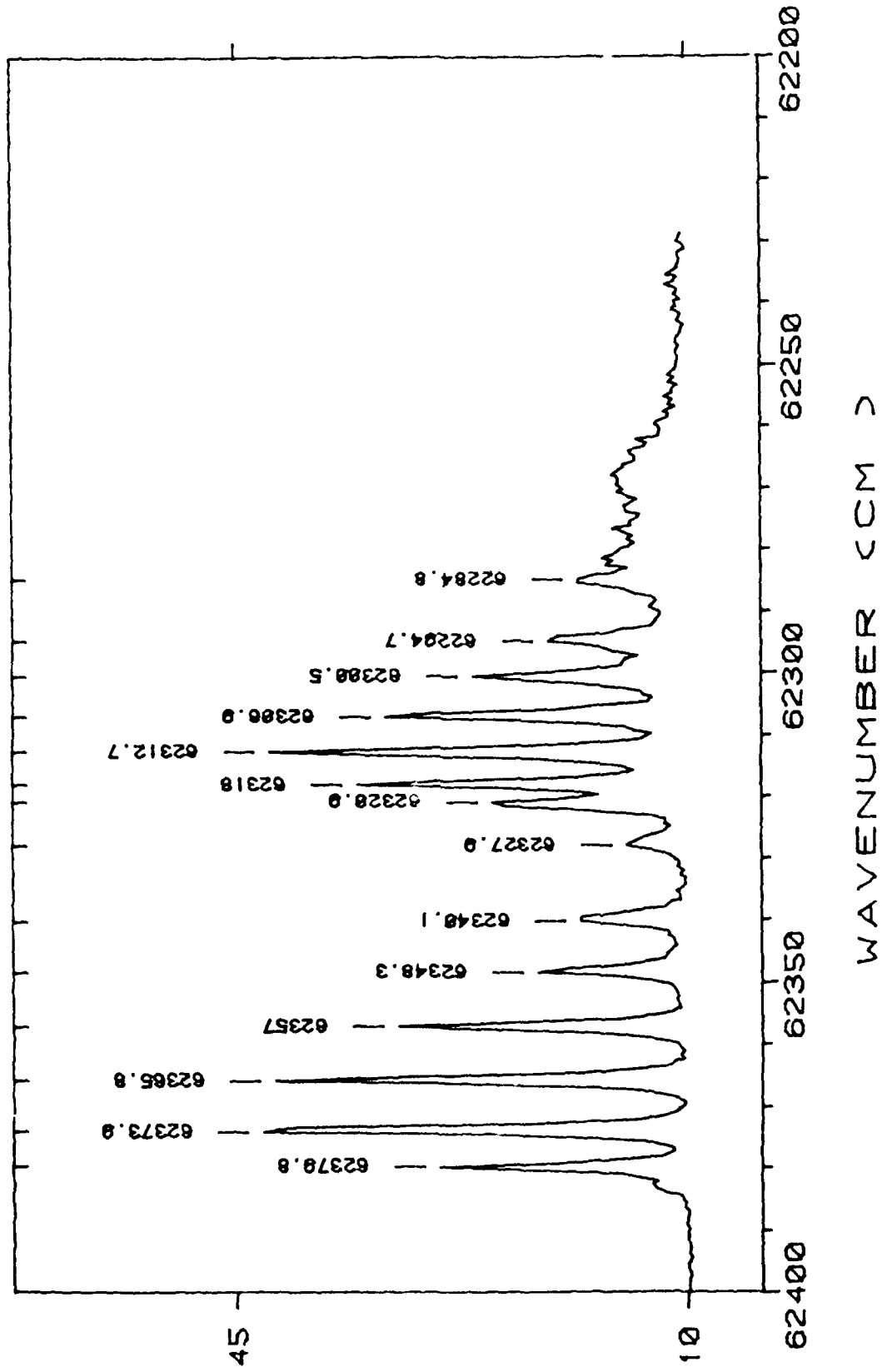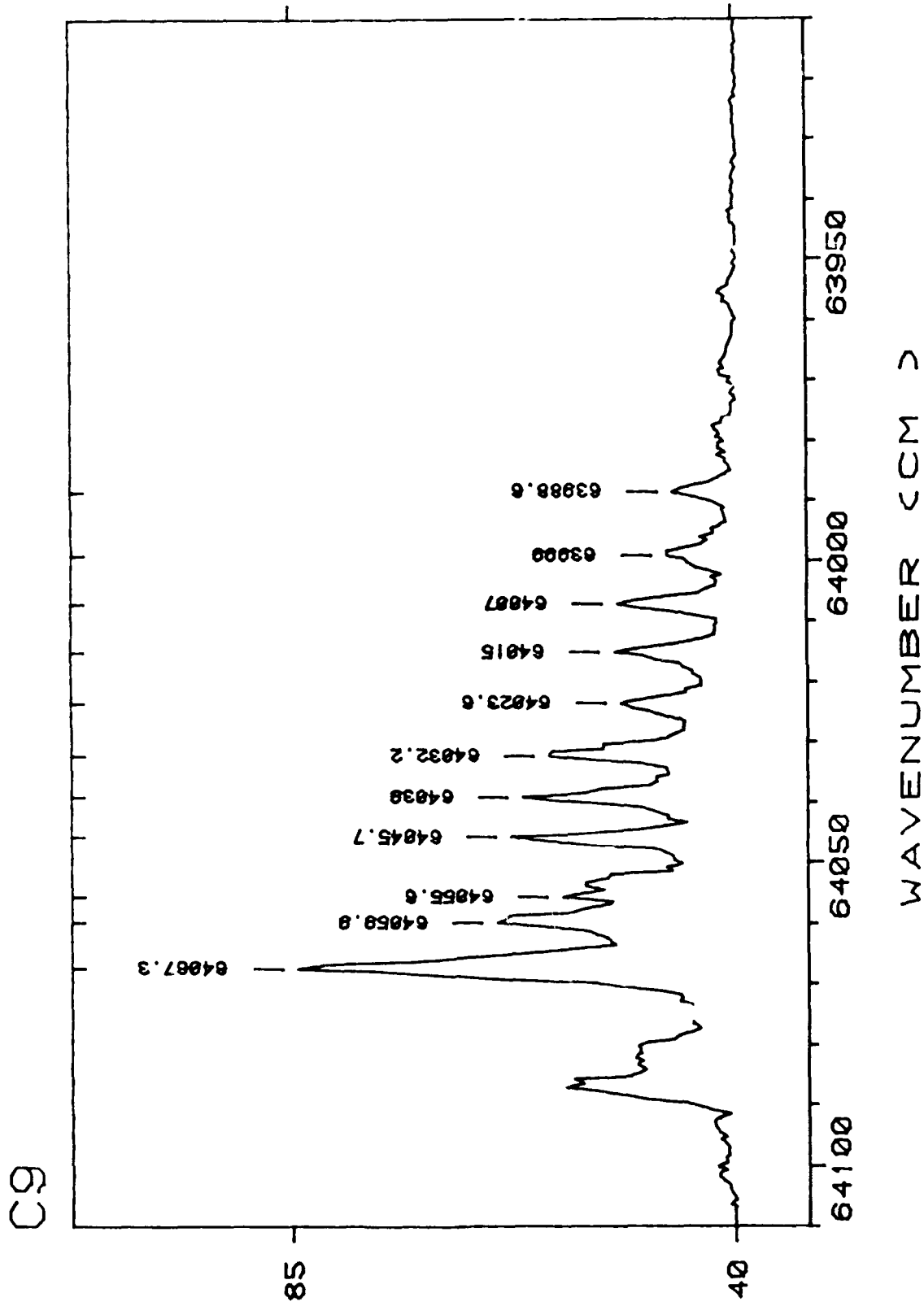WAVENUMBER (CM⁻)

C10

C18

WAVENUMBER (CM⁻)

C9

WAVENUMBER (CM⁻¹)

<u>Detection and Identification of O Atoms formed</u>

<u>by Multiphoton Dissociation of O_2</u>

Ground state ($^3P_{2,1,0}$) oxygen atoms were detected as products of a multiphoton dissociation process initiated by a single color pulsed laser beam in the wavelength region around 225-226 nm. The detection process used a 2-photon resonant, 3-photon ionization process (with mass resolution of product ions) illustrated by the following scheme :

$$O(2p^4\ ^3P) \rightarrow \rightarrow O^*(2p^33p\ ^3P) \rightarrow O^+(2p^3\ ^4S) + e^-$$
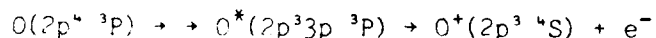
A figure (Fig.1) showing the resonant MPI spectrum of the three fine structure (spin-orbit) components of the ^3P ground state of the oxygen atom is attached. The total fine structure splitting in the resonant (upper) state is only 0.7 cm^{-1} and is unresolved in the figure. These results illustrate the high sensitivity for detection of ground state oxygen atoms attainable by MPI methods.

It is of some interest to determine the mechanism of formation of the ground state oxygen atoms. The complete absence of molecular oxygen ions in the same mass spectrum showed that they did not result from photodissociation of molecular ions. Instead the process must initially involve photodissociation of molecular oxygen by either one or two photons (higher order processes can be neglected at the laser powers used). The photons have about 5.5 eV energy compared to the dissociation energy of 5.1 eV for molecular oxygen so that a single

photon process is energetically possible. However the absorption cross section in this region of the spectrum is extremely small ($\sim 4.6 \times 10^{-24}$ cm^2)[1,2] and at our laser powers we estimate crudely that the possibility of a two-photon dissociation process must also be considered.

In order to distinguish between one- and two-photon processes, a measurement was made of the kinetic energy of the O^+ ion. While, in a two-photon process, not all the excess energy above the dissociation limit is necessarily available as kinetic energy since the undetected oxygen atom can be either ^3P, ^1D or ^1S states, the four possible kinetic energies are sufficiently different to allow us to distinguish among the various possibilities. The kinetic energy measurement was made by measuring the time-of-flight of O^+ ions as a function of the electric field strength in the region of ion formation. The results, which are somewhat tentative since the ion source configuration was far from optimum for this purpose, support a two-photon dissociation process forming two ground state (^3P) atoms.

Possible states which can be excited by two photon absorption from the ground $^3\Sigma_g^-$ state of O_2 can be obtained from potential energy curves calculated by Guberman[3] and others. The 1 $^3\Pi_g$ state of Guberman's Fig.6 or, less likely, the 1 $^1\Pi_g$ state of the same figure are the most plausible candidates.

Extension of such measurements as these give promise of exploring very highly excited states, forbidden in one-photon absorption, which may play

a part in other photophysical process in oxygen, such as e.g., the dissociative recombination processes treated by Guberman and others.

MPI methods for detecting ^1D and ^1S oxygen atoms have been planned, but not carried out due to termination of this contract.

reference

[1] M.Ogawa, J.Chem.Phys. **54**, 2550 (1971)

[2] This weak transition is ascribed by Huber and Herzberg, "Constants of Diatomic Molecules" (Van Nostrand Reinhold, New York, 1979) to the transition $A\ ^3\Sigma_u^+ \leftarrow X\ ^3\Sigma_g^-$ which is highly forbidden.   See their footnote e on p.496.

[3] S.L.Guberman in Physics of Ion-Ion and Electron-Ion Collisions (ed. F.Brouillard, Plenum, New York, 1983).

(2+1) MPI ATOMIC OXYGEN

WAVELENGTH (NM)
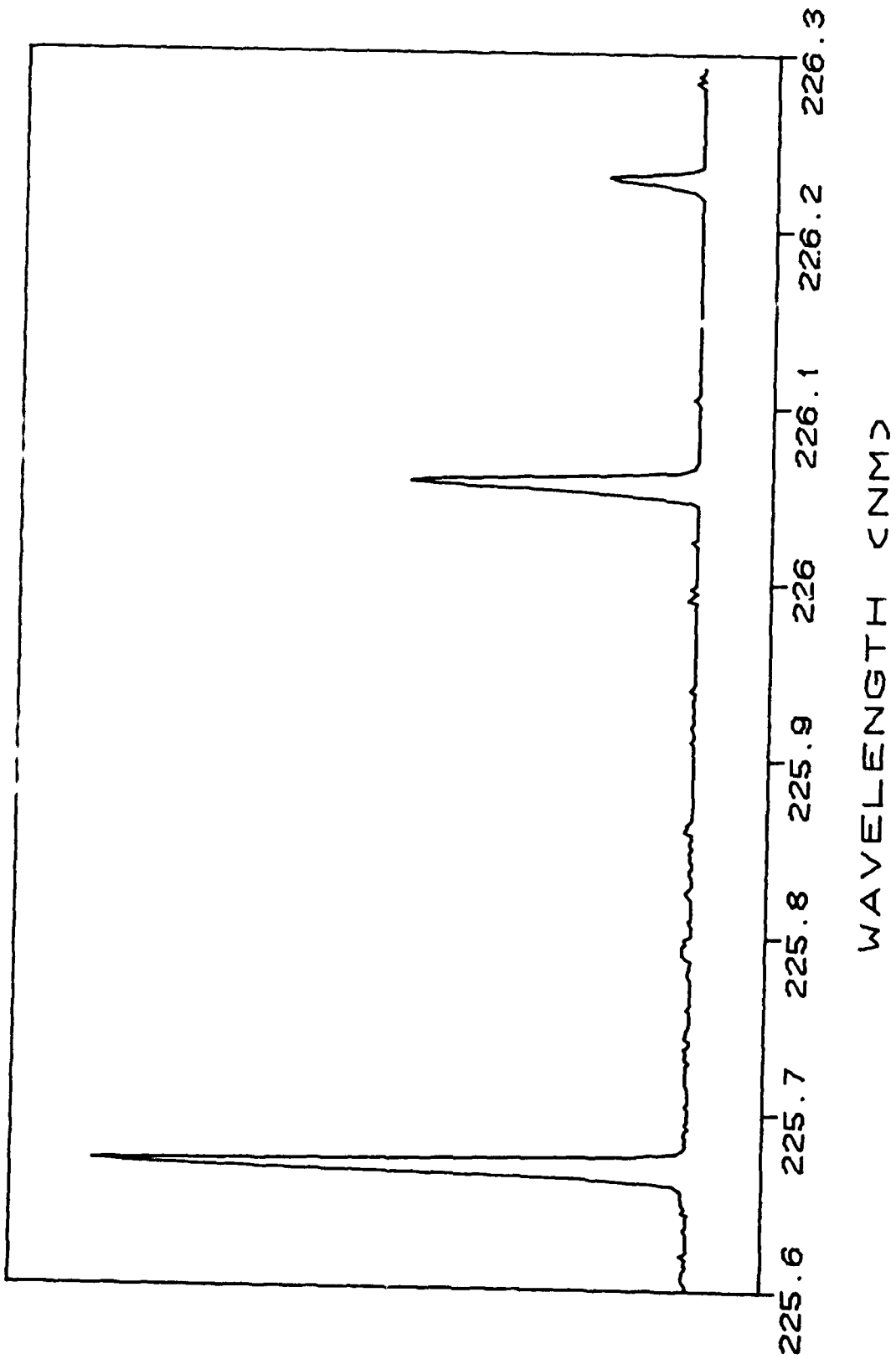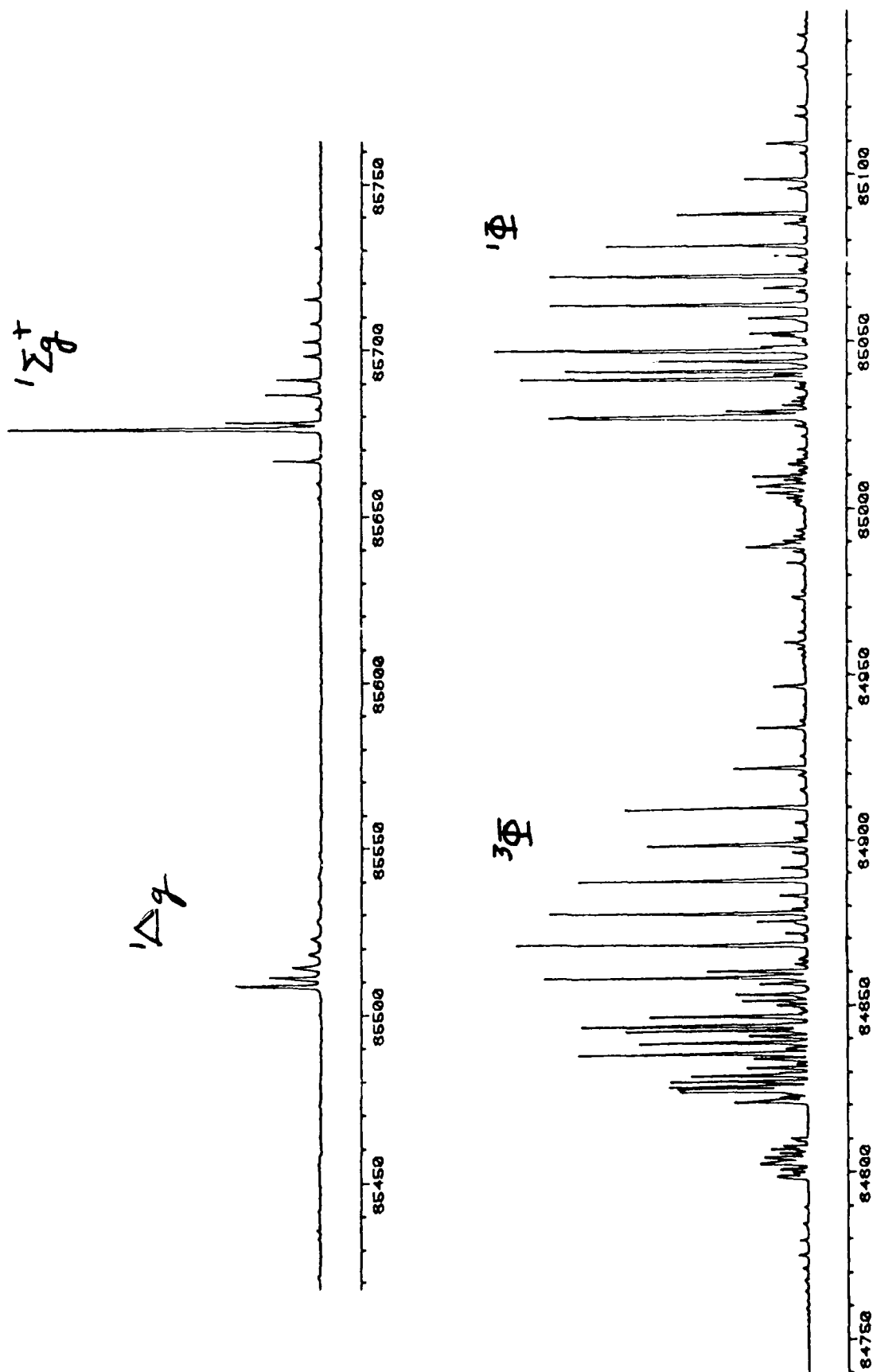
The (2+1) MPI spectra of the v'=0 bands of 3d(π,δ) $^1\Lambda_g$, $^1\Sigma^+$g, $^1\Phi_{3g}$ and $^3\Phi_{3g}$ states of O_2 excited from the metastable a$^1\Delta_g$ (v''=0) state.

123